Organic matter incorporation into sea ice and potential matter release into the nearshore zone of the southern Beaufort Sea, Canada

Kristoffer Nils Laux

A thesis presented for the degree of

MASTER OF SCIENCE

Geology

Freie Universiät Berlin

Germany

Date of Submission: 29.09.2020

Supervisors: Dr. Michael Fritz - Alfred-Wegener-Institut Centre for Polar and Marine Research (AWI), Potsdam

Bennet Juhls - Freie Universität Berlin

Reviewers: Prof. Dr. Liane Benning - Freie Universität Berlin / Helmholtz Centre Potsdam - German Research Centre for Geosciences (GFZ)

Prof. Dr. Hugues Lantuit - Universität Potsdam / Alfred-Wegener-Institut Centre for Polar and Marine Research (AWI), Potsdam

"Wir sehen in der Natur nie etwas als Einzelnheit, sondern wir sehen alles in Verbindung mit etwas anderem, das vor ihm, neben ihm, hinter ihm, unter ihm und über ihm sich befindet."

Johann Wolfgang von Goethe

Zusammenfassung

Die globale Erwärmung, die hauptsächlich durch menschliche Einflüsse verursacht wird, hat in den letzten Jahrzehnten stark zugenommen. Während die Erddurchschnittstemperatur im Zeitraum des gesamten letzten Jahrhunderts um etwa 0.8°C gestiegen ist, hat die Erwärmung allein in den letzten 30 Jahren um 0.6°C zugenommen (GISTEMP, 2016; Lenssen *et al.*, 2019). Die Arktis hat sich mehr als doppelt so schnell erwärmt wie der globale Durchschnitt (Serreze *et al.*, 2009; Screen and Simmonds, 2010). Diese beschleunigte Erwärmung hat dramatische Auswirkungen auf eine Vielzahl von Bereichen, einschließlich des Auftauens und Wiedergefrierens von Permafrostböden. Die Landfläche der nördlichen Hemisphere ist mit etwa 23 Millionen km^2 zu fast ein Viertel von Permafrost beeinflusst. Wenn der Permafrost auftaut, vertieft sich die aktive Schicht und die jährliche Auftauphase der Permafrostböden wird länger. Infolge des Auftauens wird die damit verbundene Bodenwassermobilität und die Erosionsrate erhöht und dadurch mehr Sedimente und gelöster organischer Kohlenstoff (DOC) in Seen, Flüssen, Grundwasserflüssen und Küstengewässern mobilisiert werden.
Meereiskerne und Wasser aus der darunter liegenden Wassersäule, wurden aus dem Küstengebiet des südkanadischen Schelfes der Beaufort-See nahe der Insel Herschel - Qikiqtaruk entnommen, um den möglichen Einbau organischer Stoffe, sowie die Freisetzung durch Winter-landfestes Meereis zu untersuchen. Meereis- und Wasserproben wurden an zwei sich kreuzenden Transekten entnommen, bevor die Schmelzsaison im Frühjahr 2019 begann. Analysen von gelöstem organischem Kohlenstoff (DOC), farbiger gelöster organischer Substanz (CDOM), Salzgehalt, stabile Wasserisotopenverhältnisse sowie suspendierter Partikel (SPM) wurden durchgeführt, um Informationen darüber zu erhalten, wie und wieviel organisches Material während der Meereisbildung im Winter aufgenommen und während des Abschmelzens im Frühjahr freigesetzt wird.
Die gemessenen DOC-, CDOM- sowie SPM-Konzentration, sind im Vergleich zu Meereismessungen anderer Studien relativ niedrig. Isotopen- und Salzgehaltsmessungen zeigen an der Südseite von Transekt 1, dass die Süßwasser- und Flusseinflüsse im Winter abnehmen, was bedeutet, dass die Süßwasserquelle im Laufe des Winters versiegt und dadurch der Fluss als Quelle der organischen Substanz (OM) nahe liegt. Die Ergebnisse zeigen auch eine signifikante höhere SPM-Konzentrationen in manchen küstennahen Bereichen.
Die aus dieser Studie gewonnnen Daten zeigen, wie empfindlich die Regionen der Arktis und ihre Material- und Kohlenstoffflüsse auf steigende Temperaturen reagieren, und deuten darauf hin, dass die Küstenerosion schon in Teilen der Wintersaison stattfinden kann.

Abstract

Global warming, mainly caused by human influences, has become much more severe in recent decades. While the average temperature of the Earth has increased of about 0.8°C over the time period of the entire last century, the temperature has increased by 0.6°C over only the past 30 years (GISTEMP, 2016; Lenssen *et al.*, 2019). The Arctic region has warmed more than twice as fast as the global average (Serreze *et al.*, 2009; Screen and Simmonds, 2010). This accelerated heating has dramatic effects on a wide range of fields including the thawing and re-freezing processes of permafrost soils. Almost a quarter of the land area of the northern hemisphere is influenced by permafrost at around 23 million km^2. When the permafrost thaws, the active layer deepens and the annual thawing phase of the permafrost soils becomes longer. A result of the thawing is the associated soil water mobility and an increased rate of erosion, causing more sediment and dissolved organic carbon (DOC) to be deposited in lakes, rivers, groundwater fluxes and coastal waters.

In this work, sea ice cores and water from the water column below were sampled from the coastal area in the southern Canadian shelf of the Beaufort Sea, near Herschel Island - Qikiqtaruk, in order to investigate the possible incorporation of organic substances and the release from winter land-fast ice. The samples were collected from two intersecting transects, before the beginning of the melting season in spring 2019. Analyses of DOC, colored dissolved organic matter (CDOM), salinity, water isotope ratios as well as suspended particulate matter (SPM) were made, to gain information on how organic matter has been incorporated and released during the winter freeze up and through the season.

The measured DOC-, CDOM- and SPM-concentrations are relatively low compared to sea ice concentrations measured in other studies. Isotopes and salinity measurements show decreasing freshwater and river influences at the south side of transect 1 through the winter, meaning that the freshwater source petered out through the course of winter and through that giving indication of the river as the organic matter source. Results also showed a significantly higher SPM concentrations at the near shore north side of transect 1 and the west near shore side of transect 2.

The data obtained from this study show how sensitive the regions of the Arctic and their material- and carbon-fluxes react to rising temperatures and suggest that coastal erosion can occur already as early as part of the winter season.

Selbstständigkeitserklärung

Hiermit versichere ich, dass ich die vorliegende Arbeit selbstständig verfasst und keine anderen als die angegebenen Quellen und Hilfsmittel benutzt habe; alle Ausführungen, die anderen Schriften wörtlich oder sinngemäß entnommen wurden, kenntlich gemacht sind und die Arbeit in gleicher oder ähnlicher Fassung noch nicht Bestandteil einer Studien- oder Prüfungsleistung war.

Berlin, September 28, 2020 .....

Contents

List of Figures

List of Tables

List of Abbreviations

AO Arctic Ocean. 4, 7, 8, 14

AORB Arctic Ocean river basins. 4

AWI Alfred-Wegener-Institut. vi, 10–12

CDOM colored dissolved organic matter. ii, 11–15, 25, 47, 52

DOC dissolved organic carbon. ii, 11–13, 22, 25, 35, 47–49, 52

DOM dissolved organic matter. 1, 13, 15, 25, 47, 48, 53

GFZ German Research Center for Geosciences. 14

GMWL global meteoric water line. 29, 30, 46

LIS Laurentide Ice Sheet. 6, 8

OC organic carbon. 4

POC particulate organic carbon. 48

SPM suspended particulate matter. ii, 2, 11, 12, 35, 49, 52

SUVA specific ultra violet Absorbance. 15, 16, 48

TOC total organic carbon. 22

UV ultra violet. 13, 15

V-SMOW Vienna standard mean ocean water. 16

Chapter 1

Introduction

1.1 Scientific background

The oceans of the earth contain roughly the same amount of carbon, in the form of dissolved organic matter (DOM), as is present in our atmosphere in the form of carbon dioxide (CO_2) (Hansell and Carlson, 2001). The mass of carbon found within the soils of the earth is higher than the masses of carbon in our atmosphere and in the entire living biomasses combined (Ciais *et al.*, 2014). The main sources of terrigenous organic matter (OM) to the oceans are rivers, groundwater discharges, coastal erosion, sea ice inputs and aeolian material fluxes (Stein *et al.*, 2004; Raymond *et al.*, 1999). When global temperatures rise, profound geological effects can be triggered and the organic matter supply to the seas increase through a stronger river flux input, as well as eroding coastlines through thawing of permafrost (Fritz *et al.*, 2017; Schuur *et al.*, 2015; Freeman *et al.*, 2001; Freeman *et al.*, 2004; Frey and Smith, 2005). Since permafrost soil can only exist under temperature conditions which are below the freezing point, its existence is particularly endangered by rising air temperatures and changing climatic conditions and the eventual release of more greenhouse gases is expected (Christiansen *et al.*, 2010; Vieira *et al.*, 2010).

With the trend of rising temperatures over the past decades (Hansen *et al.*, 2010), connected with greenhouse gases (Petit *et al.*, 1999), humans bringing their emission each year to new level highs (Friedlingstein *et al.*, 2019), the projections for the future not look very good (Meehl *et al.*, 2007; Collins *et al.*, 2013; Slater *et al.*, 2020). The prospects are especially bad for vulnerable regions of the Arctic and Antarctica (Serreze *et al.*, 2007; Maslanik *et al.*, 2007; J. Comiso *et al.*, 2007; Schaefer *et al.*, 2014), which store a tremendous amount of carbon within their regions of permafrost. Recent studies calculated the global stock of soil organic carbon only within the permafrost to be around 1325 Pg (Köchy *et al.*, 2015). For comparison, it is estimated that since 1850, with the beginning of the industrial revolution, about 440 $\pm$ 20 Pg C was produced by humans and entered the atmosphere (Friedlingstein *et al.*, 2019).

Next to those regions of high elevations, the temperature within the atmosphere has not increased faster anywhere than in the polar regions (Pepin *et al.*, 2015) and nowhere else can the results of the global warming be observed more obviously than at the polar regions with visible

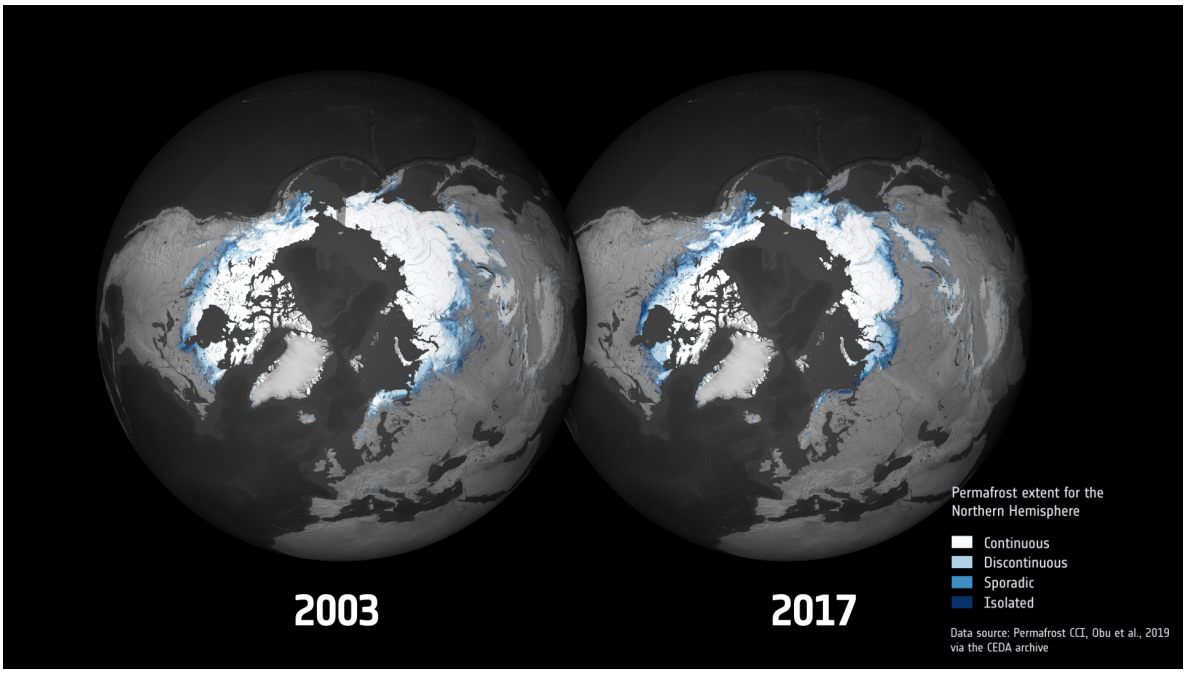

Figure 1.1: Permafrost extent in 2003 compared to 2017. Continuous permafrost is defined as a continuous area with frozen material beneath the land surface, except for large bodies of water. None-continuous permafrost is broken up into separate areas and can either be discontinuous, isolated or sporadic. It is considered isolated if less than 10% of the surface has permafrost below, while sporadic means 10%-50% of the surface has permafrost below, while discontinuous is considered 50%-90%. From: Permafrost CCI, Obu et al, 2019 via the CEDA archive

thawing and vanishing of the permafrost, only withing the last decades (Fig.: 1.1).
Even if one assumes that the earth does not warm more than 2°C by 2100, the impact on permafrost would be catastrophic, with an estimated 40% loss (Chadburn *et al.*, 2017).
Along with thawing other processes are likely to go hand in hand or be initiated, which will then further accelerate climate change. It can for example be assumed that, as a result of the thawing, microorganisms will increasingly begin to decompose the carbon that was previously stored in the permafrost soil and thereby release large quantities of the greenhouse gases, carbon dioxide and methane, into the atmosphere (Schaefer *et al.*, 2014; Schuur *et al.*, 2015). This in turn will affect other areas, such as the eco and hydro systems but also those of infrastructure (Bowden, 2010; Larsen and Fondahl, 2015; Radosavljevic *et al.*, 2016; Hjort *et al.*, 2018).
For many years now the Arctic, the ice and the carbon cycle has gained the focus of researchers from all fields (Stein *et al.*, 2004) providing a better understanding and view on these highly important regions and matter.
There have been many improvements made in the field on gaining data by remote sensing from satellite pictures. For example, this is used to estimate the DOC concentration and fluxes in the waters for certain regions or oceans, by analysing the colored part of the dissolved organic matter, also known as CDOM (Matsuoka *et al.*, 2017), providing e.g. insights about the source, the physiochemical as well as biological processes (Matsuoka *et al.*, 2012). Others have used remote sensing technology to measure suspended particulate matter (SPM) concentrations within the waters (Li *et al.*, 2015; Fettweis and Nechad, 2011), for tracking turbid river plumes or to

study the horizontal distribution, sinks and sources of SPM (Sathyendranath, 2000).
Isotopic data, on the other hand, yield important information about the origin and sources of different waters or can also be used for the reconstruction and determination of the paleoclimate (Dansgaard, 1964; Meyer *et al.*, 2002). When combining isotopic analysis with other hydrochemical properties, including CDOM and DOC, a more detailed and specific analysis on the origin and characteristics of ice and/or water samples can be achieved (Fritz *et al.*, 2011; Juhls *et al.*, 2020).
When it comes to in situ measurements, the focus of the research and expeditions for the polar regions has been narrowed down to those month of the year which make the region accessible to scientists. Due to the natural barriers given in the winter such as ice, cold temperatures and darkness (R. Macdonald *et al.*, 1999), a sort of biased look through those brief warmer months has been created. The quantification of carbon fluxes from thawing permafrost, melting ground ice and coastal erosion and here in particular the role of winter sea ice in terms of incorporating, transporting and releasing carbon and particulates has still not been researched well enough to fully understand the carbon cycle and budget for this region (R. Macdonald *et al.*, 1998; Fritz *et al.*, 2015).

1.2 Aims & objectives

The aim of this thesis is to quantify the organic material in winter landfast ice with regard to the concentration and distribution within the ice cores regionally spanned over the two transects, and to analyze it with regard to its origin and potential release.
For this purpose, ice cores and the associated water samples from the water column below are examined for DOC, CDOM, salinity, water isotopes and the SPM entry. Not only are respective concentrations within the various ice cores quantified and analyzed, but also the concentrations in the regional distribution over the two transects are compared.
In advance, the following hypothesis was put forward:

Organic material from the thawing permafrost soils and the eroding coasts also accumulates in first year sea ice over the course of winter.

Chapter 2

Study Area

2.1 The Arctic Ocean and the Beaufort Sea

The study area with its two transects is located on the Canadian continental shelf along the Yukon Coast of the southern Beaufort Sea and is therefore part of the Arctic Ocean (AO) (Fig. 2.1).

The Arctic Ocean is connected to the Atlantic Ocean over a length of 1500 km and to the Pacific Ocean over a length of 85 km, via the Bering Strait. It holds an area of about 14×10^6 km^2, which is almost the same size as Antarctica and with that, the AO is the smallest of the five major oceans on Earth.

Although the AO contains only 1% of the worlds ocean water, it receives 11% of the global runoff (Shiklomanov, 1993). Due to its position as the so called "Arctic Ocean River Basin" (AORB) (Lewis *et al.*, 2000), it becomes a major player within the global water cycle.

The AO consists of the world's largest shelf seas (Barents, Kara, Laptev, East Siberian, Chukchi, Beaufort and Lincoln Sea), which make up as much as 52.7 % of the entire area of the Arctic Ocean (Stein *et al.*, 2004).

The continental shelf of the Beaufort Sea, compared to the others of the AO, is rather narrow (Fig. 2.1). Only close to the Mackenzie River mouth does it widen up to 145 km (Fig. 2.2). These shelf regions of the Beaufort sea are subject to strong seasonal changes, during the summer being almost ice-free while they are almost entirely covered with ice in winter. The cold surface water layer of the Mackenzie Shelf has been found to have a low density compared to other shelf regions, due to the mixing with River runoff, sea ice melt and the influence of the low saline Pacific waters (Rudels *et al.*, 1996).

Close to the coast the depth of the Beaufort Sea does not exceed more than 60 m, compared to the further offshore regions in the north, where the depth increases rapidly up to a few kilometers, forming the massive "Canada Abyssal Plain" (Fig. 2.2).

The most important sources of freshwater and terrigenous OC, to the shelf seas and the AO, are large river and ground water discharges, coastal erosion, sea ice inputs and aeolian material fluxes (Rachold *et al.*, 2004). The top five rivers in terms of annual volumetric water discharge to the AO are: Yenisei, Lena, Ob, Mackenzie and Yukon River respectively. The Yenisei, Lena

Figure 2.1: The Arctic Ocean on a global view with top five biggest Arctic rivers on water discharge. Red map marker sets study area at Yukon coast within Beaufourt Sea. (Modified after © Geographic Guide - Maps of World)

and Ob are located on the Russian continental shelf in Siberia, flowing into Kara- and Laptev Sea and the Mackenzie and Yukon River are located on the north American continental shelf flowing into the Beaufort and Bering Sea, respectively (Tab.: 2.1) (Fig. 2.1).
The mouth of the Mackenzie River in Northwest Territory (Canada) is on average 130 km away from the area from which the samples for this work were taken. (Fig. 2.2). It is the fourth largest river in terms of water discharge and has the highest sediment discharge to the Arctic Ocean (Rachold *et al.*, 2004) (Tab.: 2.1).
The Beaufort Sea and the Mackenzie Delta host many small islands, and only a few bigger ones significantly extend out of the landscape towards the west of the delta, such as Herschel Island or "Qikiqtaruk", meaning "it is island" in the Inuvialuit language.

2.2 Shoreline and sea ice characteristics

34% of the world's coasts consist of permafrost or are directly influenced by it (Lantuit *et al.*, 2012). Permafrost soil is a soil, sediment or rock that remains at temperatures below the freezing point for at least two continues years. Permafrost terrain comprises a seasonally thawed active layer underlain by perennially frozen ground. It can vary in thickness and depths under the earth's surface (Brown and Kupsch, 1974; Van Everdingen, 2005) and is therefore differentiated

River	Water Discharge ($km^3\ yr^{-1}$)	DOC ($10^9\ g\ yr^{-1}$)	Sediment ($t/km^2/yr$)
Yenisei	673	4645	1.9
Lena	588	5681	8.5
Ob	427	4119	6.4
Mackenzie	316	1377	74
Yukon	208	1472	72

Table 2.1: Water, DOC and sediment discharges of the top five rivers floating into the Arctic Ocean. After: R. M. Holmes *et al.*, 2002; McClelland *et al.*, 2016; R. M. Holmes *et al.*, 2012

into different standard classifications:

- continuous permafrost (90 to 100% of the subsoil in a region is frozen)
- discontinuous permafrost (more than 50% of the subsoil of a region is frozen)
- sporadic permafrost (patchy distribution of the frozen subsoil)

(Weise, 1983; French and Williams, 1976; Romanovsky *et al.*, 2007).
Rampton, 1982 described the Yukon Coastal Plain, which is the extension of the Beaufort continental shelf between the Mackenzie Delta and the Alaskan border, as an area mainly consisting of a thick layer of continues permafrost. It consists of Tertiary sandstones and shale, which are covered by a thin layer of uncosolidated sediments (Fritz *et al.*, 2012) covered by the Laurentide Ice Sheet (LIS) during the Late Wisconsin.
In line with the Yukon coast, the coast of the study area is described as consisting of 65% unlithified and 35% lithified with low cliffs (1 to 50 m) and mainly unconsolidated, frozen fine sand sediments (Lantuit *et al.*, 2012). When these coasts are interacting with arctic marine as well as periglacial processes, they become an extremely dynamic and erosional environment (Harper, 1990; R. Macdonald *et al.*, 1998) with erosion rates calculated of up to 2 m $year^{-1}$ (Lantuit *et al.*, 2012).
Within the area of this study are throughout the year and seasons, different kinds of sea ice being created, pushed in towards the coast and being released again offshore, to be partly subject of summer melt.
In general two different kinds of sea ice and zones of the nearshore sea ice environment can be distinguished. From coast to sea those are:

- Landfast ice, a largely undeformed sea ice that is "fastened" / attached to the coastline, or to the sea floor (bedfast ice) and attaining a maximum thickness of about 2 m and a maximum extension offshore to the approximate 20-m isobath, with the stamukhi-zone (Reimnitz *et al.*, 1978) being the natural last barrier before the polynya. With temperatures dropping at around late October, landfast ice grows either in place from the sea

Figure 2.2: Seafloor map of the Beaufort - Red map marker shows study area. (Modified after "THE INTERNATIONAL BATHYMETRIC CHART OF THE ARCTIC OCEAN" (IBCAO))

water or by accumulation of drift or pack ice from the sea at the shore. Throughout the season this type of ice does not move, until melting begins.

- The stamukhi, a pebble ice field formed by ice convergence and collision of the offshore pack ice, extends downward, forming an inverted 'dam' of rubble ice plates (Fig. 2.3). Beyond the stamukhi comes usually an area of flaw polynya.
- Flaw polynya is an open water area which can have a great extent or only be a narrow shear zone, before the area of pack ice.
- Seasonal and polar pack ice is the second type of sea ice. In contrast to the landfast ice it freely drifts on the AO (D. L. Forbes, 1981; W. Weeks, 2010).

2.3 Study site - From Herschel Island to Kay Point

The two transects at which the ice cores were drilled and the underlying water samples were taken span between Herschel Island (Qikiqtaruk), (69°35' N, 139°5' W) and Kay Point, (69°27' N, 138°5' W) (Fig. 3.1), a bay area located around 130 km west of the mouth of the Mackenzie River and 90 km east of the U.S. border to Alaska.
The Mackenzie River is the main fresh water and sediment source of the Canadian Beaufort

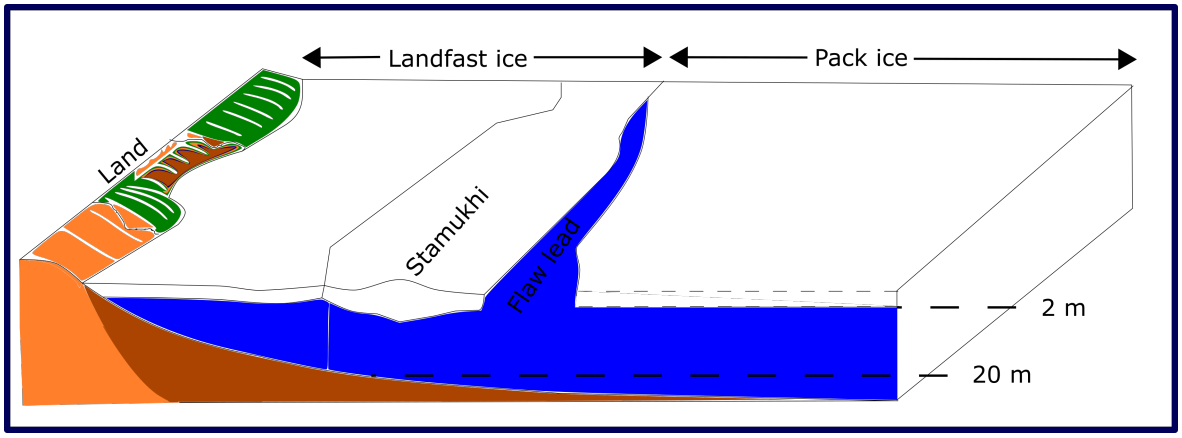

Figure 2.3: Land- and Pack ice environments. Landfast ice anchors at the shore until summer break up. Stamukhi marks the border or outer rim of the landfast ice. In contrast to the landfast ice, the pack ice is free floating and, depending on in which region it is in, can last for several years.

Shelf (O'brien *et al.*, 2006; R. M. Holmes *et al.*, 2002) and as can be seen from Table 2.1, the Mackenzie River is, despite a lower water discharge in comparison to the other major rivers, an undisputed very large contributer of organic matter and suspended sediments for the AO and for large parts of the Beaufort Sea (Fichot *et al.*, 2013). Thus, even though its mouth is at a greater distance, the Mackenzie River has a potential influence on the study area (R. Macdonald *et al.*, 1998). However, this is very different from year to year and especially season to season. The discharge peaks in June/July and falls sharply in winter (Woo and Thorne, 2003; Nghiem *et al.*, 2014). However starting in mid to end of May, an already warmer water arrives at the river's delta and begins to break up the sea ice within a few weeks (Mulligan *et al.*, 2010).
In addition to Herschel Island and Kay Point, the bay is confined by the coastline of the Yukon coast and seaward by a narrow submerged ridge called Herschel Sill, which extends southeast from the eastern tip of Herschel Island until Kay Point and is a natural shallow bathymetric obstacle for water circulation in the basin and for fast ice development (Fig.: 2.4).
Near Kay Point the Babbage River flows into Phillips Bay (Fig.: 2.4), which is an Arctic River with a length of around 185 km, a catchment area of about 4750 km^2 and an approximate water discharge of 11.3 m^3s^{-1}. The Babbage River carries source materials with a wide geological time spectrum, between Precambrian metaclastics over Palaeozoic and Mesozoic clastics and carbonates, until Quaternary glacial and non-glacial materials (D. Forbes, 1983).
Next to the Babbage River there are also other smaller rivers and creeks which flow into the study area, such as the Spring River and Roland creek (Fig.: 2.4), but like the Babbage River they run dry during the winter and have peak again during the month of snow melt (D. L. Forbes, 1981).
The bathymetry between Herschel Island and Kay Point ranges between 5-10 m at Thetis and Phillips Bay and up to 80 m at Herschel Basin (Fig. 2.4), the basin as well as the aforementioned ridge right next to it (Herschel Sill) formed during the late Wisconsin period (21 to 11.3 cal ka BP) by dredging and carving of the LIS, on the dry-fallen shelf (Mackay, 1959; Fritz *et al.*,

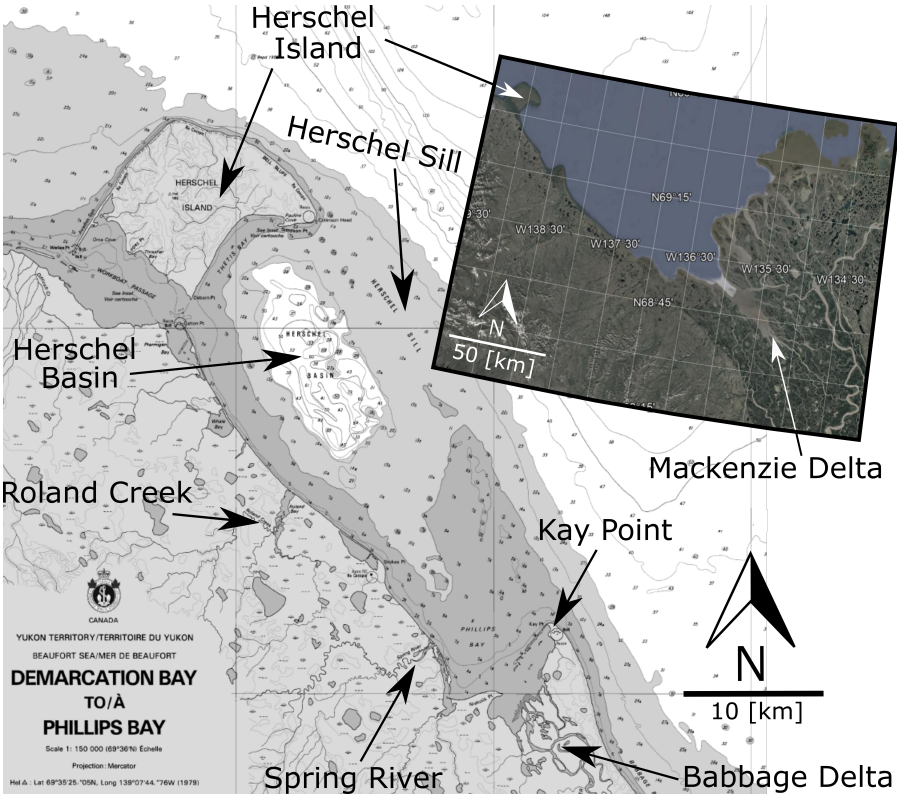

Figure 2.4: Large image: Bathymetric map of the study area (Modified after: Federal publications Inc: Nautical charts of the Beaufort Sea, 1998-2016); Small map (inset) showing study area and Mackenzie River Delta (Modified after: Google Earth 2020)

2012; Gowan *et al.*, 2016).

During arctic winter, the months of October till May/June, landfast ice is a common feature between Herschel Island and Kay Point and forms a stable cover over most of the Mackenzie Shelf. Pack ice fields can be found about 80 km north of Herschel Island, drifting clockwise in a major offshore surface current along the Beaufort Sea, called the Beaufort Gyre. However, according to Dunton and Carmack, 2006 and Carmack and Macdonald, 2002 the currents effects do not affect the study area. Changing winds and season can, however, have the effect to push the pack ice towards the coast (Klock *et al.*, 2001).

Chapter 3

Material & Methods

3.1 Field work

Fieldwork was performed and samples taken during an expedition led by the Alfred-Wegener-Institut (AWI) Helmholtz Centre for Polar and Marine Research (AWI) in Potsdam, Germany, as part of the EU funded project "Nunataryk", led by Hugues Lantuit. The samples used for this thesis were obtained between the 27th and 29th of April in 2019.
Sea ice and water samples from below ice were collected simultaneously at twelve locations, in two transects which were intersecting and perpendicular to each other (Fig. 3.1). The first

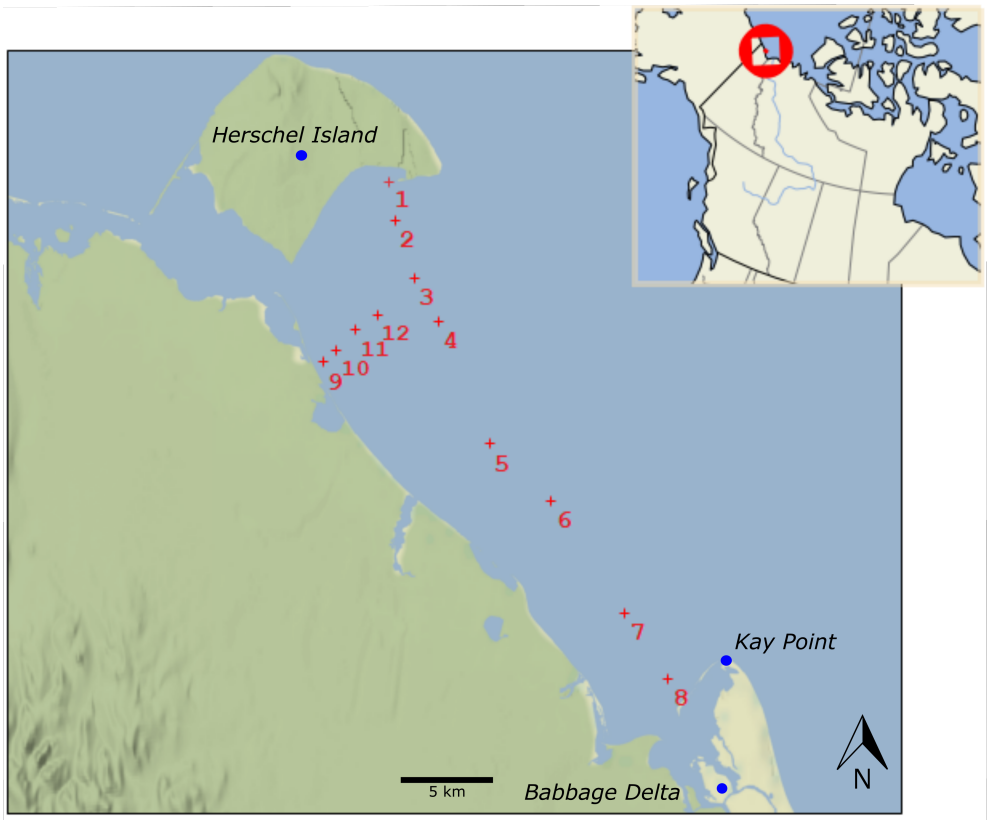

Figure 3.1: Sampling-Locations 2019. Red crosses marked with numbers indicate sampling locations. Transect 1: From 1 to 8. Transect 2: From 9 to 12

transect extends from Herschel Island (Location 01) coast across Herschel Basin towards Kay Point/Philips Bay (Location 08) which is the eastward limit of Herschel Basin and has a length of 36.1 km. The second transect runs from the Yukon mainland coast (Location 09) through Herschel Basin towards Herschel Sill (Location 12) with a lengths of 4.6 km.
Sample locations were visited with a skidoo and a sled. Due to safety reasons the limits of the fast ice edge were not crossed and therefore the station plan was adapted according to fast ice conditions. At each station coordinates were taken with a hand-held GPS. Snow depth was measured, before snow removal with a shovel for ice coring.
Ice cores were retrieved by an engine-powered Kovacs ice corer (Mark II) with an inner diameter of 9 cm and a core barrel length of 100 cm. Ice cores were drilled until sea water was reached. Individual ice core pieces were cleaned with a knife, packed in tube foil and stored frozen in thermoboxes until further processing at the AWI cold lab in Potsdam.
The existing ice hole was enlarged with an engine-powered Jiffiy ice drill of about 30 cm diameter. A CastwayCTD was used for water column profiling of temperature, conductivity and depth until the sea floor. Water samples were taken from surface water directly below the ice, from the middle of the water column and from bottom water with a 2.5 L Niskin bottle with manual trigger and a 2.5 L UWITEC water sampler depending on ice-hole conditions, water depth and trigger success. Water samples were filled up in 2 L Nalgene bottles and stored unfrozen in thermoboxes until further processing in the field camp.
Salinity, electrical conductivity and pH were measured on each sample directly in the field, using a WTW Multi 3430. Thirty milliliters were filled up in narrow-neck LDPE bottles for stable water isotopes and stored under cool (unfrozen) and dark conditions until further processing in the laboratory. Discrete amounts (about 1 L) of water was filtered through pre-weighed and pre-combusted 47 mm glass fibre filters (GF/F 0.7μm) for determining suspended particulate matter (SPM) concentrations. Filters were kept frozen until further processing in the lab.
Gum-free syringes with a syringe filter (23mm, GF/F 0.7 μm) were used for DOC and CDOM filtration. DOC samples were filled up in clear glass vials with screwing lid and acidified with 1μL/ml HCl 30% suprapur, to prevent microbial conversion. CDOM samples were filled into 50 ml amber glass bottles. Both kinds of samples were stored in cool (unfrozen) and dark conditions until further processing at the laboratory.

3.2 Laboratory work

3.2.1 Sample preparation

The the sea ice-cores were cleaned with a knife and cut in half in the cold lab at about -10°C, using a Makita Band-Saw LB1200F, and one half was archived.
Half cores were split, using the same saw, into pieces ranging in sizes between 14 and 43 cm, to obtain enough volume for all analyses. The average length of the segments was 29 cm, depending on already existing cracks or general ice core length. Afterwards the cores were measured and put into labeled whirl-pak bags for further processing (Fig. 3.2). Preexisting, noticeable ice characteristics such as sediment inclusions or ice algae, were noted and the whirl-pak bags with

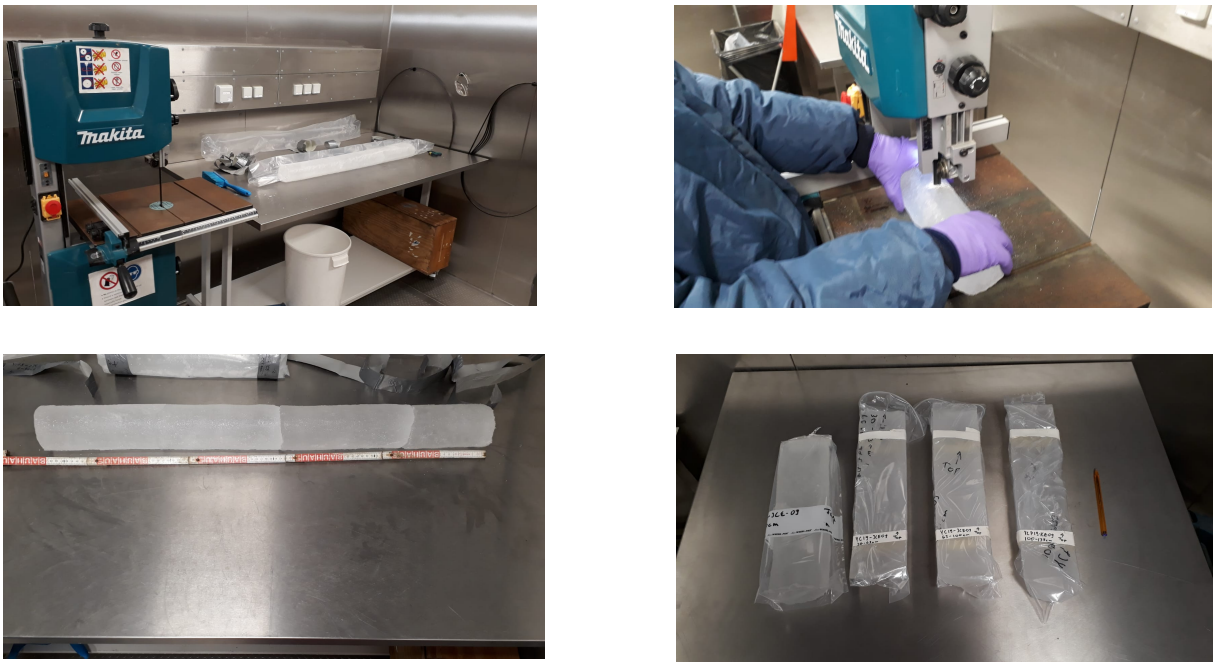

Figure 3.2: Sample preperation at the AWI Cold Chamber; Sea ice sawing, measuring and sampling

the ice- samples were stored again into a freezer at -20°C before further processing.
In the hydrochemistry lab, ice samples were put into 2000 ml clean glass beakers, covered with pre-combusted aluminium foil (550°C), placed in the dark and stored at room temperature to melt. After 48 hours, sea ice samples had melted, and samples were homogenized by stirring with a glass stick. Approximately 90 ml of the melted sea ice was directly filled into narrow-neck bottles (each 30 ml) for stable isotope analysis, brown glass bottles (each 50 ml) for the CDOM-chlorophyll analysis and a miniature glass beaker (each 10 ml) for salinity/electrical conductivity analysis. The remaining meltwater was filtered through pre-weighted and pre-rinsed 47 mm 0.45 μm Sartorius cellulose acetate porefilters for SPM analysis, into a Nalgene^{TM} filtration unit with receiver. The filtrate was split into brown glass bottles (each 50 ml) for CDOM analysis and glass-vials (each 20 ml) for DOC analysis. The DOC samples were acidified with 25 μL HCl suprapur (30 %). Figure 3.3 gives a brief overview on the main sample preparation processes and steps taken.
All sub-samples were stored in the dark at 4°C for further analysis described below. In total a number of 59 ice-core sub-segments out of the twelve ice-cores have been sampled. At the beginning, in the middle and at the end of the sample preperation, "process blanks" were made (from Milli-Q Water) in order to check for any process errors.

3.2.2 Dissolved organic carbon & salinity

The dissolved organic carbon content of the samples was analyzed using high temperature catalytic oxidation (TOC-VCPH, Shimadzu). 20 ml of sample was placed into the auto-sampler of the analyzer. Before the actual measurement of the organic carbon was the inorganic carbon, the inorganic carbon was removed by introducing sparge gas through the samples, along with hydrochloric acid which produced carbon dioxide (CO_2). The remaining organic carbon

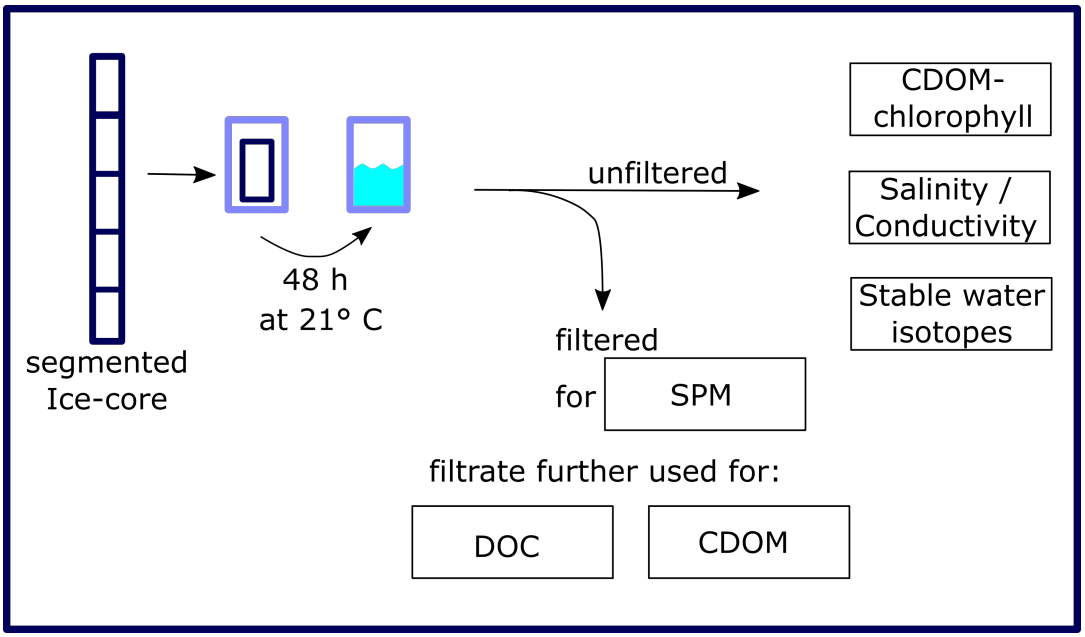

Figure 3.3: Flowchart showing Sample-Workflow preparation for different parameters of analyses. First ice core got sawed and segmented, each segment being brought to melt within 48 h. Afterwards is the melted sample being filtered or not filtered depending on the analysied parameter to be followed.

was measured by catalytic combustion and measuring the CO_2 concentration which converts into a DOC concentration. In order to keep the the accuracy of the measurement high, three replicate measurements of each sample were averaged, after every ten samples, a blank (Milli-Q water) and a standard were measured, using from eight different commercially available certified standards. Covering a range between 0.49 mg L-1 (DWNSVW-15) till up to 100 mg L-1 (Std. US-QC). The results of standards provided an accuracy better than ±5‰.
The salinity and electrical conductivity measurements were conducted with a Multilab 540 (WTW).

3.2.3 Colored dissolved organic matter

CDOM is a subset of DOM, which is coloured and thus shows absorption and fluorescence. Whereas pure water absorbs light in longer wavelengths, CDOM absorbs light in short wavelengths, ranging from 250 to 450 nm, and is therefore optically measurable by spectroscopy and fluorometry (Hoge *et al.*, 1995). This ultra violet (UV) absorbance/fluoroscence acts as one of the primary regulators of light penetrating in the oceanic euphotic zone (Blough, 2002a) and hence also very likely acts as a strong contributor to the dependence of heat storage on depth, potentially directly effecting sea ice build-up (Matsuoka *et al.*, 2011). Furthermore CDOM serves as an important food source for many organisms and bacteria. It also plays an important role in marine ecosystems through its feature of inhibiting light transmittance through the water column (Moran and Zepp, 1997; Blough, 2002b).
As CDOM is a subset of DOM it does positively correlate with it and can therefore be used as a supporting indicator for the general concentrations of DOM and DOC in the waters. The

potential sources of CDOM are: soils, plants, wetlands, phytoplankton, zooplankton, sediments and generally all organic decaying products. In the Arctic the contribution of absorption by CDOM has been stated as remarkably high with over 76 % of the total nonwater absorbers (at 440 nm) (Matsuoka *et al.*, 2007). This strong CDOM absorption in the Arctic Ocean is consistent with the already mentioned fact (Chapter: 2.1) that the AO receives the largest amount of freshwater relative to its volume.

For measuring the light absorption of CDOM different kinds of spectrophotometers exist.

A lamp inside the spectrophotometer provides a source of light. The beam of light strikes a diffraction monochromator, which functions like a prism by separating the light into its wavelengths. This monochromator is rotated so that only a specific wavelength of light reaches the exit slit. Here, the light going out interacts with the sample water placed in a cuvet of specific lengths (Fig. 3.4). From this point, a detector measures the transmittance and absorbance coming through the sample. The detector senses the light being transmitted through the sample, and converts this information into a digital reading. For this work a double-beam spectrophotometer was used, which works the same way as just described but additionally compares the light intensity between the light path of the sample cuvette and one path containing a cuvette with Milli-Q Water to reference the sample against it, and in this way all samples were blank corrected (Fig. 3.4).

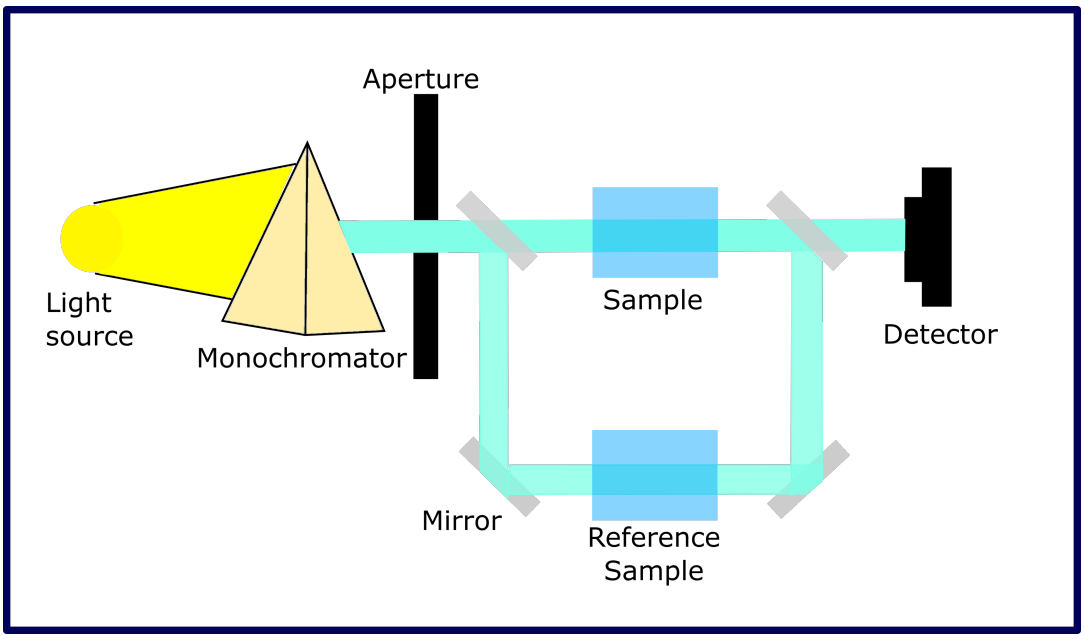

Figure 3.4: General set up and method of a double beam spectrophotometer. Light is transmitted through monochromator where it gets filtered and then after passing the focus of the aperture, it is separated with mirrors into two beams to transmit through the sample and reference sample to be lastly detected by the detector.

For the work of this thesis the CDOM samples were collected in pre-rinsed 50 mL brown glass bottles that were stored in the dark at 4°C until analysis. αCDOM was measured at the at the German Research Center for Geosciences (GFZ), Potsdam, Germany using a LAMBDA 950 UV/Vis (PerkinElmer).

The median absorbance (A_λ) of three replicate measurements was used to calculate the αCDOM$^{(\lambda)}$:

$$\alpha CDOM^{(\lambda)} = \frac{2.303 * A_\lambda}{l} \tag{3.1}$$

where l is the path length, for which a 5 cm cuvette was used.
As mentioned before (Chapter: 3.2.1) two samples from the melted sea ice were taken. One filtered version for the standard CDOM analyses at 254 nm and one additional unfiltered sample. The unfiltered sample was made in order to find out if there were any potential influences on the CDOM spectra by algae growth, measuring the chlorophyll concentration. In order to do so, a subtraction of wavelengths between the filtered and unfiltered sample pair was made, to get a clearer view on the final absorption graphs and to better carve out the chlorophyll peak in the red wavelengths region, explained in Figure 3.5 and the following equation.

$$\alpha(\lambda) = \alpha_w^{(\lambda)} + \alpha_{phyt}^{(\lambda)} + \alpha NAP^{(\lambda)} + \alpha CDOM^{(\lambda)} \tag{3.2}$$

where subscriptions $\alpha, \lambda, w, phyt$, NAP and $CDOM$ indicate: Absorption coefficient, Wavelength, Water, phytoplankton, non-algal particles, and colored dissolved organic matter, respectively.

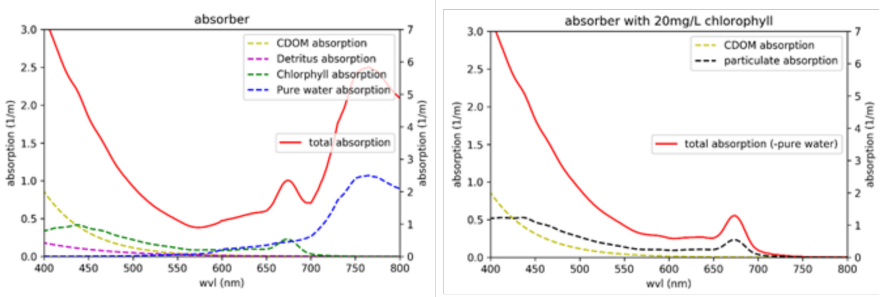

Figure 3.5: Example showing the applied method to detect chlorophyll by distilling out the one significant chlorophyll peak within the red light wavelength (at around 675 nm). After Bennet Juhls.

The absorption coefficient in this equation (Equat. 3.2) is expressed as the sum of the absorption coefficients of the different groups of components within the unfiltered samples. The magnitude of the absorption coefficient varies linearly with the concentration of the absorbing materials.
The absorbance at 254 nm has been shown to be strongly correlated with the hydrophobic organic acid fraction of DOM (Spencer et al. 2012) and is a useful proxy for DOM aromatic content (Weishaar *et al.*, 2003) and molecular weight (Chowdhury, 2013). For that reason it was chosen to also use absorbance at 254 nm on CDOM analysis and to calculate for the specific UV absorbance SUVA (Weishaar *et al.*, 2003). Dissolved organic matter originating from a terrestrial source has a higher aromatic carbon content than autochthonous or altered DOM. This fact is used with the SUVA parameter to search for substances derived from plant or soil organic matter. Since aromtatic substances absorb light more strongly in the UV spectrum, a higher value of SUVA can give indication about increased aromatic content from allochthonous sources, vice versa for lower SUVA values (Battin, 1998).

SUVA values were calculated using the equation:

$$SUVA = (A_{254}/L)/[DOC] \tag{3.3}$$

where $A254$ is the absorbance at 254 nm measured, L is the optical pathlength (0.05 m) and DOC is the dissolved organic carbon concentration in mg/L.

3.2.4 Stable water isotope geochemistry

Oxygen and hydrogen, the elements which bound together to water, in addition to their main and most common stable isotopes ($H_2{}^{16}O$) also exist in other less common isotopes, as such there are: ^{17}O, ^{18}O for oxygen and ^{1}H and D (Deuterium) / ^{2}H for hydrogen. Between these isotopes there is a wide range of combinations and abundances found, which varies in the order of hundreds per mil (Jouzel, 2003).
As water is distributed and redistributed in regions that differ by depth, heights, longitude and latitude, it transitions between phases over and over again. Those phase transitions are strongly temperature dependent and influence the isotopic ratio and signal. These repetitive cycles are called the hydrological cycles (Criss *et al.*, 1999) which lay the foundation of the fractionation processes by stable water isotopes and eventually lead to their characteristic isotopic signatures, formed within different water reservoirs.
Based on these fundamental processes the following method has been applied for this thesis, to be able to assign and differentiate between water sources.
A brief explanation of the basis for this method is as follows. Lighter water isotopes evaporate more easily and accumulate through rain again in freshwater sources such as rivers or lakes, whereas heavier isotopes remain in their regimes, such as snow covers or ocean waters.
The obtained values given in relation to the Vienna standard mean ocean water (V-SMOW), the most widely used standard (defined to be exactly 0 ‰) of the mean ocean water which approximates the bulk isotopic composition of the present-day global ocean reservoirs (Craig, 1961).
Measurements were conducted at the laboratory facility for stable isotopes at AWI Potsdam using a Finnigan MAT Delta-S mass spectrometer equipped with calibration units for the online determination of hydrogen and oxygen isotopic composition. The data is given as δD and $\delta^{18}O$ values, the δ as the per mille difference to standard V-SMOW.
The measurement accuracy for hydrogen and oxygen isotopes was better than ± 0.8‰ for $\delta^{18}O$ and ± 0.1‰ for δD, respectively (Meyer *et al.*, 2000).

3.2.5 Suspended particulate matter

Suspended particulates of matter are microscopic particles of solid or liquid matter suspended in the air or in natural waters. They are commonly defined in relation to a minimum diameter, depending on the pore size of filters used to accumulate them (Loring and Rantala, 1992).
As already mentioned in chapter 3.2.1, in order to filtrate the suspended particulate matters out of the melted sea ice sample, 47 mm 0.45 μm Sartorius cellulose acetate, porefilters were used

in combination with a Nalgene^{TM} reusable filter holders with receiver. Before filtration, each filter was dried at 50°C in an oven, taken out, cooled down to room temperature in a dessicator and weighted directly afterwards to receive a pure filter weight, using a high precision scale by Mettler Toledo with an accuracy of 0,001 g. The filters were then placed into the filter holder and a little amount of the sample water (∼20 ml) used to pre-rinse the filters and to clean of any eventual carbon contents. Afterwards the entire sample was filtered, using an electric vacuum pump. The volumes of the sample waters were noted, for further calculation of the SPM concentrations. After the filtration was completed, the filters were carefully removed from the filter holder, placed in an individual numbered, precleaned petri dish and then put back in the sample-oven for a minimum of 48 hours to dry. After drying the samples were again taken out of the sample-oven, cooled to room temperature in a dessicator and then weighted again, using the same scale as before and receiving the filter weight with particles ($\geq 0.45\mu$m).

Chapter 4

Results

4.1 Overview

In the following chapter the data will be presented resulting from the twelve sea ice cores (YC19-ICE-01 - 12) and complimentary water samples (YC19-WAT-01 - 12) taken from below, on the expedition mentioned in chapter 2.1.
As a first overview, table 4.1 provides the mean values of all measured and calculated parameters of ice core and water samples, from all twelve locations combined and can be used to compare the relative differences between the different samples, locations and types.

Parameter	Ice cores	SD	Water under ice	SD
Salinity ‰	3.05	0.7	33.02	0.49
$\delta^{18}O$ ‰ vs. SMOW	-2.65	2.40	-2.70	0.16
DOC mgL^{-1}	0.61	0.18	1.14	0.12
αCDOM (254) m^{-1}	1.2	0.79	2.78	0.37
SUVA m^2 g C^{-1}	0.86	0.35	1.07	0.12
SPM mgL^{-1}	0.65	0.01	11.28	3.16

Table 4.1: Mean values of ice core and complimentary water parameters. SD = Standard deviation.

Figure 3.1 shows that the samples were taken in two intersecting transects, in order to see if regional differences in the organic matter incorporation exist. All data including those not shown here, can be found in the appendix.
The different ice core lengths range between 120 cm (ICE-07) and 186 cm (ICE-05) with a mean length of 146 cm. The complimentary water samples to the ice cores, were taken at the same locations as each sample. At each location three samples were taken from the water column, at top, mid and bottom. Depending on the bathymetry (Fig.: 2.4) the depths ranged between a minimum of 5.77 until a maximum depth of 59.77 m.

4.2 Salinity

Measurement of salinity gives an indication about the salt or ionic content of seawater and can give information about the water regime, whether or not the sample water has a high or low freshwater content as well as about the structure of the water column. Salinity measurements in sea ice can also reveal information about its growth process.

Generally, when comparing ice cores with water samples, there is to note that the relative range of concentrations is a bit wider for the ice cores than it is with the different water samples. The lowest salinity concentration measured within the ice core was 1.2 ‰and the highest 4.6 ‰. This compares to 31.96 ‰and 34.68 ‰respectively for the water samples. The average salinity value for the ice cores lays at 3.05 ‰and for the water samples 33.01 ‰.

The overall salinity level of all cores plotted over the depths, shows a slight trend towards a higher concentration of salt in the upper sections, closer to the surface (Fig. 4.1), yet with a R^2 of 0.02 and a p-value of >0.05 is the correlation very low. For the water samples a better correlation is observed and the opposite is true, lower concentration at the top and higher concentration in the lower section (Fig. 4.2). Along transect 1 the salinity concentrations for both water and sea-ice samples decrease towards Kay Point, indicating more freshwater input (Fig. 4.3; 4.4). Transect 2 does not show, for the ice cores nor for the water samples (Fig.: 4.5; 4.6), a significant trend ($p > 0.05$), indicating only sea water within its range.

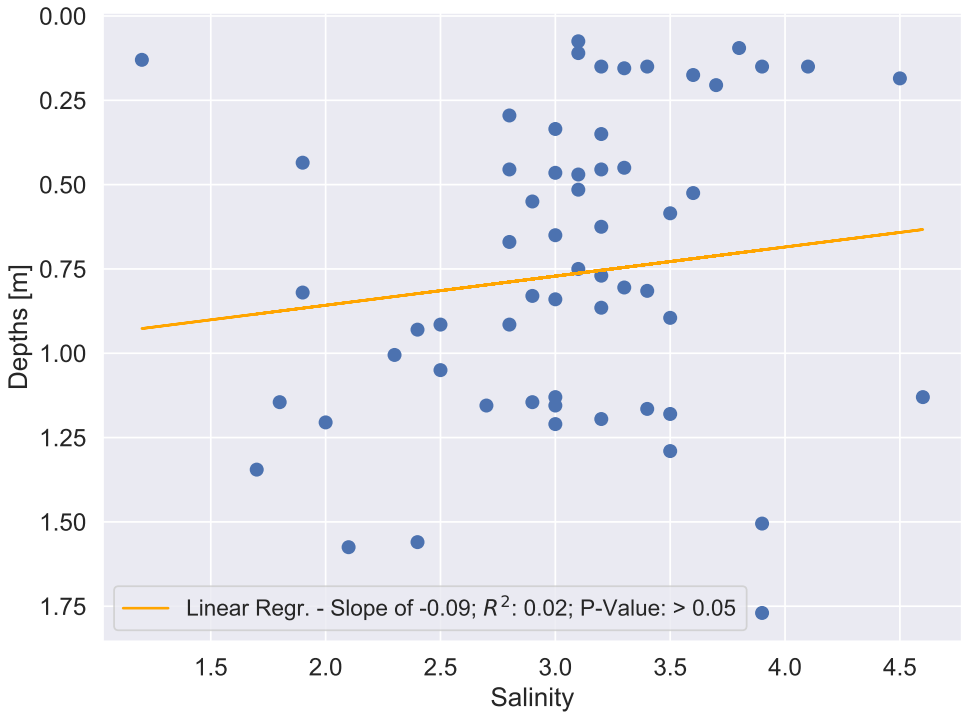

Figure 4.1: Salinity of all twelve ice cores with relation to sampling depth.

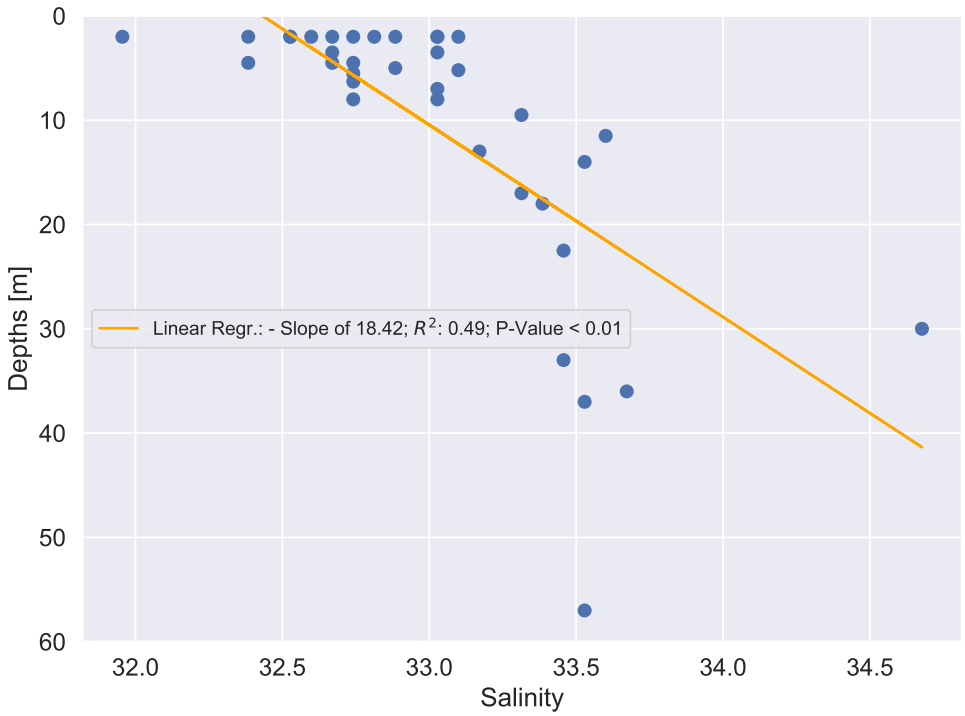

Figure 4.2: Salinity of all twelve water samples with relation to sampling depth.

4.2.1 Transect 1

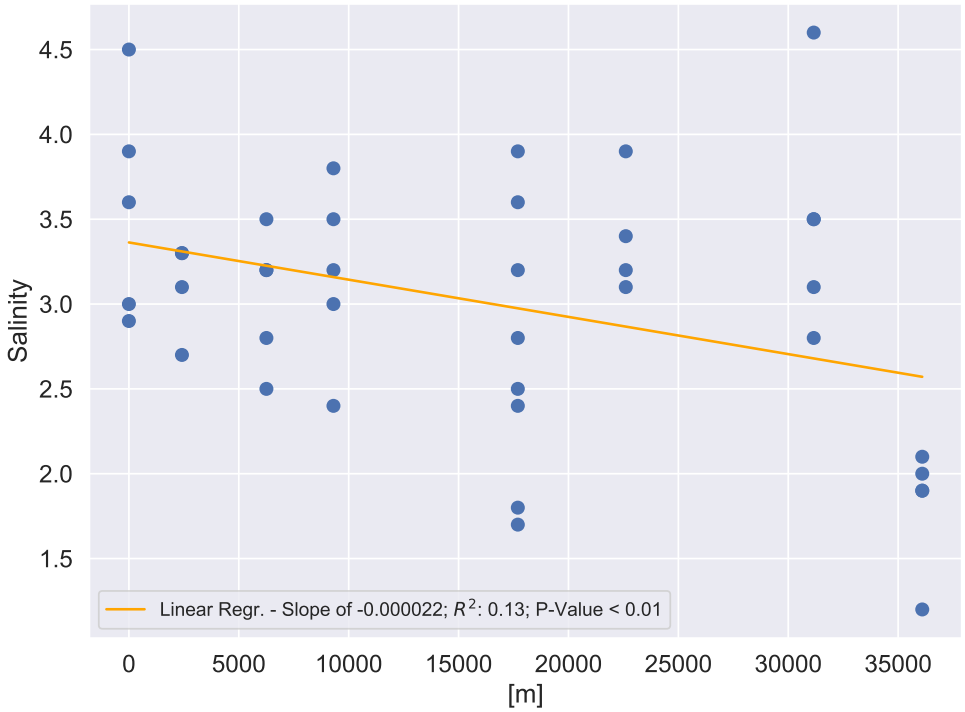

Figure 4.3: Salinity for ice cores along transect 1. From location 01 (0 m) close to Herschel Island until location 08 (36098 m) close to Kay Point.

Figure 4.4: Salinity for water samples along transect 1. From location 01 (0 m) close to Herschel Island until location 08 (36098 m) close to Kay Point.

4.2.2 Transect 2

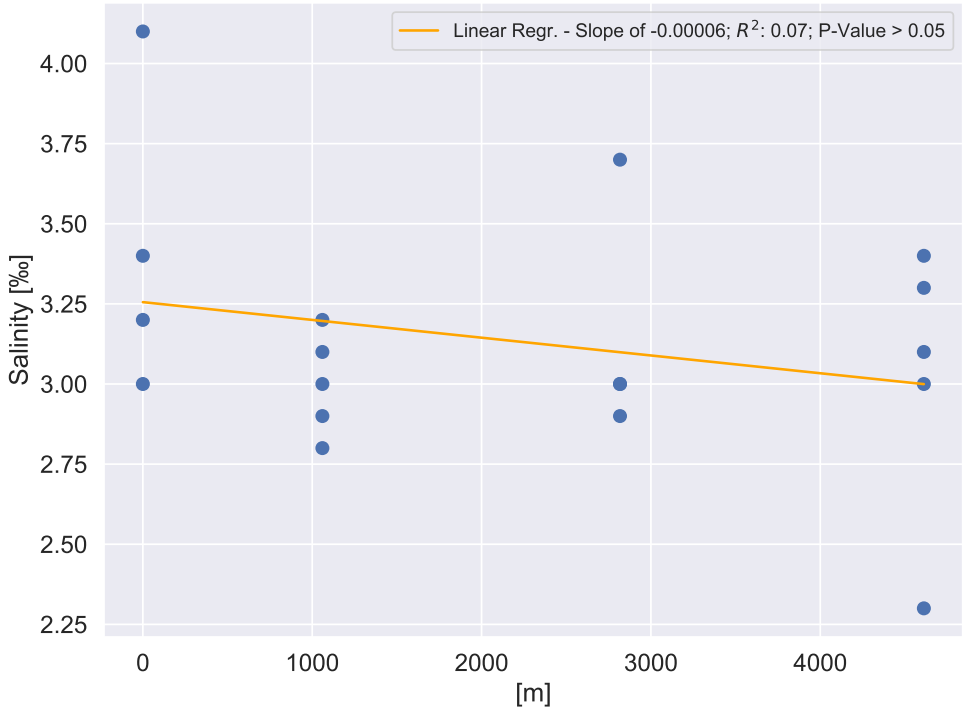

Figure 4.5: Salinity for ice cores along transect 2. From location 09 (0 m) close to Yukon coast until location 12 (4611 m).

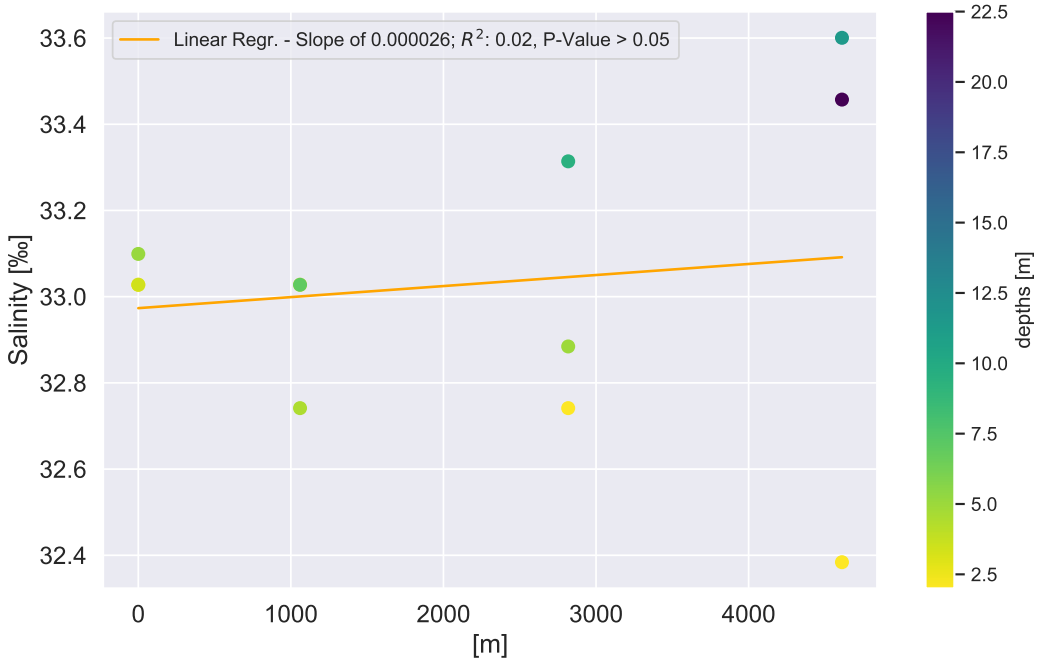

Figure 4.6: Salinity for water samples along transect 2. From location 09 (0 m) close to Yukon coast until location 12 (4611 m).

4.3 Dissolved organic carbon

As one of the main analysis for this study does the dissolved organic carbon analysis contribute to the quantification of the sea ice cores and water samples taken. DOC is the fraction of total organic carbon (TOC), that passes through a filter size range between 0.22 and 0.7 μm. DOC in the coastal waters and in sea ice originates from various autochthonous and allochthonous sources such as dead organic matter, including plants and animals.

The lowest DOC concentration measured within the ice core was 0.36 and the highest 1.43 [mgL^{-1}]. 1.02 and 1.68 [mgL^{-1}] respectively for the water samples. The average DOC value for the ice cores lays at 0.61 [mgL^{-1}] and for the water samples a twofold higher mean concentrations is observed 1.14 [mgL^{-1}].

When comparing the depths of all ice cores against their DOC concentrations, no significant trend or concentration towards a certain depth was found (R^2: 0.00, p $>$ 0.05). The DOC concentration seems equally distributed (Fig. 4.7). In contrast, the water samples show a stronger trend of higher concentrations towards upper water-levels (Fig. 4.8).

When comparing the ice cores with the water samples from below along the transect 1 (Fig.: 4.10) it is noticeable that water and the ice show opposite trends, for the water samples an increase towards Herschel Island and for the ice cores an increase towards Kay Point, with the latter stronger than the water samples. Both show higher concentrations than their respective mean, close to the respective coast (at 0 m and 36098 m).

The crossplot between DOC and Salinity (Fig.: 4.9) for the ice cores shows no strong correlation

(R^2: 0.01, p > 0.05). Some ice cores cluster within a certain area (indicated by the different colors), for example 08 or 10.
Transect 2 does not show, neither for the ice cores nor for the water samples (4.11) a significant trend (R^2: 0.01, p > 0.05), indicating only sea water within its range.

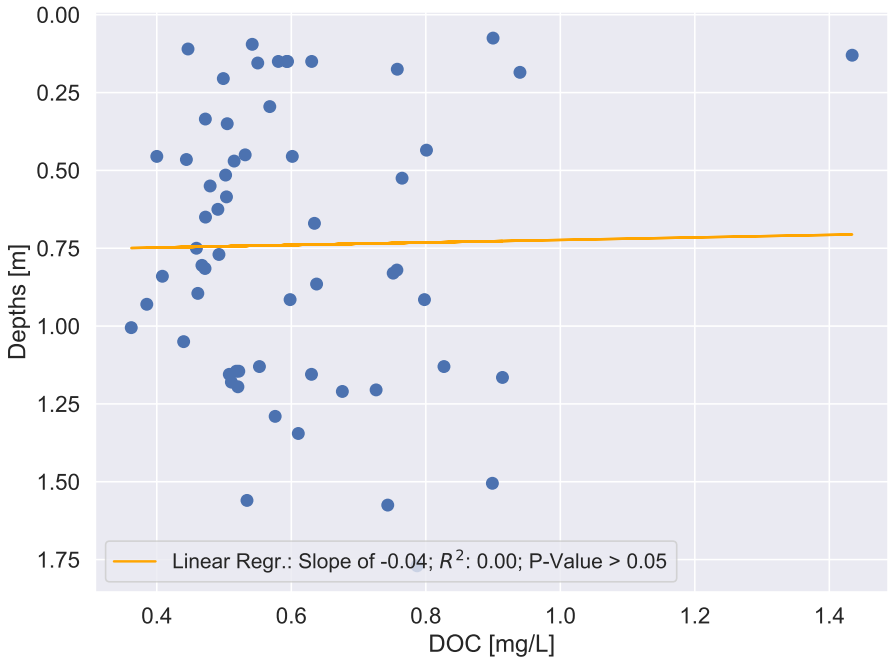

Figure 4.7: DOC concentrations of all twelve ice cores with relation to sampling depth.

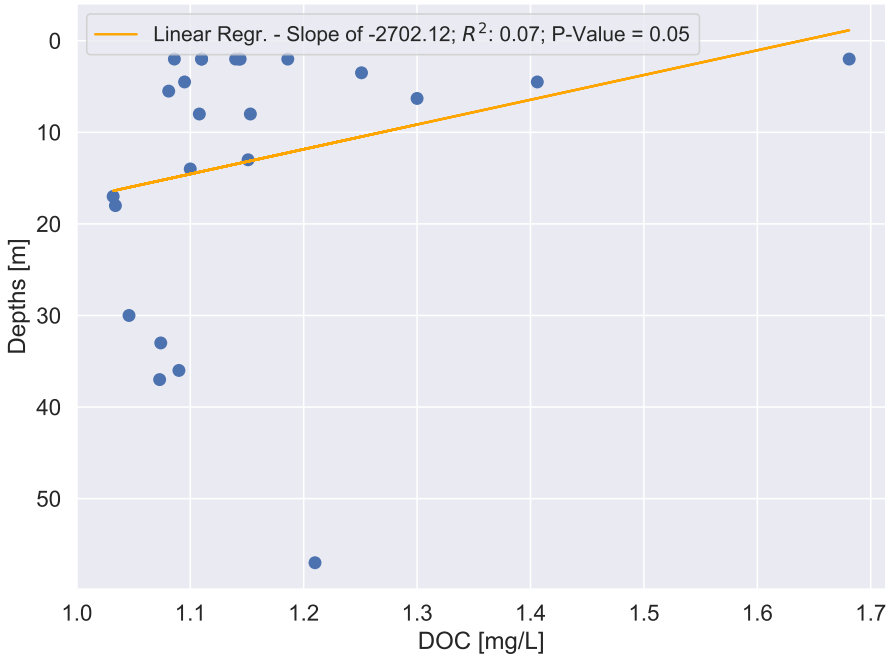

Figure 4.8: DOC concentrations of all twelve water samples with relation to sampling depth.

Figure 4.9: Salinity / DOC crossplot for ice cores. Each color and the corresponding number, stands for one specific ice core sample/location.

4.3.1 Transect 1

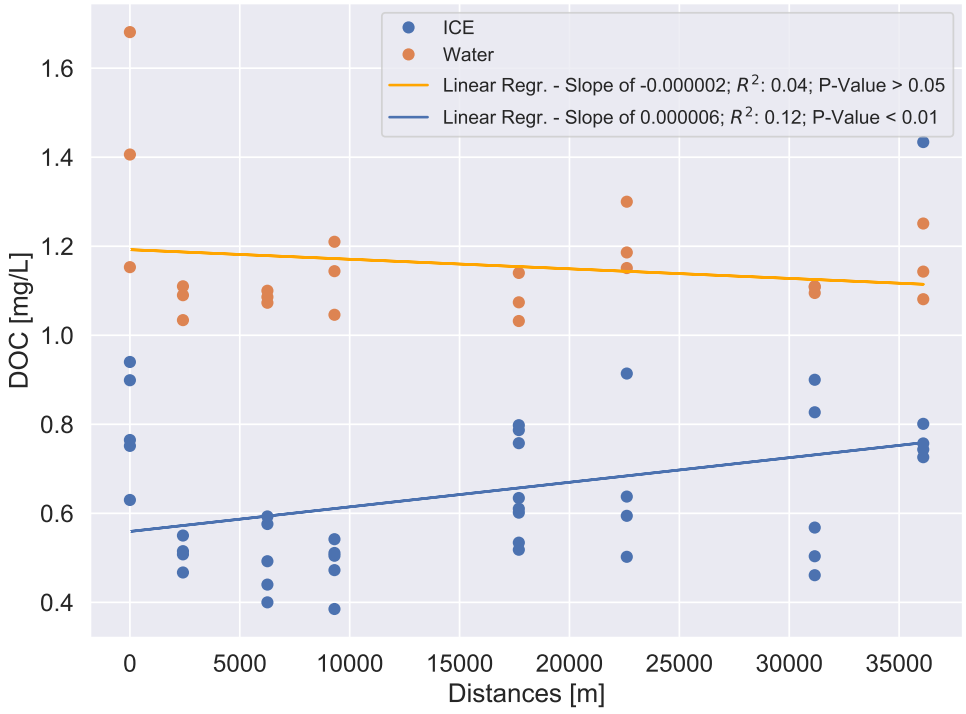

Figure 4.10: DOC concentration for ice cores and water samples along transect 1. From location 01 (0 m) close to Herschel Island till location 08 (36098 m) close to Kay Point

4.3.2 Transect 2

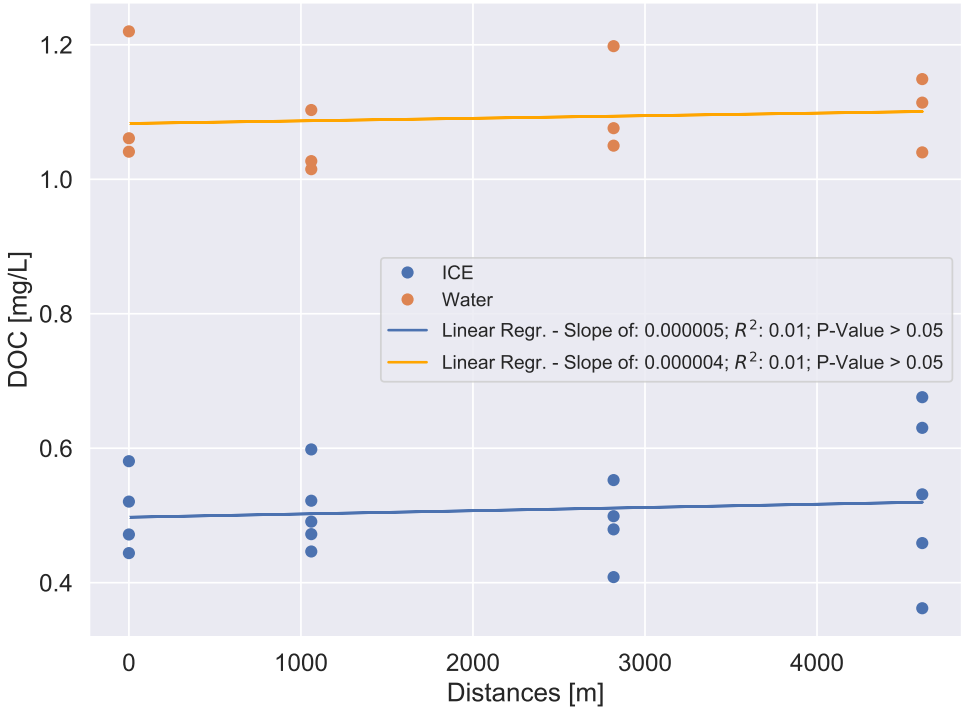

Figure 4.11: DOC concentration for ice cores and water samples along transect 2. From location 09 (0 m) close to Yukon coast until location 12 (4611 m).

4.4 Colored dissolved organic matter

Colored dissolved organic matter CDOM is the optically measurable component of DOM within water.

Hence CDOM is a subset of DOC the two quantities are strongly correlated within the ice and the waters (Fig.: 4.14). Also the general trend over the transect 1 (Fig. 4.15) as well as the concentration distribution over the depths (Fig. 4.12; 4.13) very much align, althoguh a slightly higher concentration within the upper sections is apparent, when compared to the DOC (Fig. 4.7; 4.8). The lowest αCDOM (254) measured within the ice core was 0.85 and the highest 5.76 [m^{-1}]. The highest and lowest were 2.38 and 4.20 [m^{-1}] respectively for the water samples. The average αCDOM (254) value for the ice cores lays at 1.20 [m^{-1}] and for the water samples 2.78 [m^{-1}].

The SUVA along the transect 1 plot (Fig.: 4.16) follows generally the trends of DOC and CDOM. Peaks for the ice cores close to Kay Point at location 08 (36098 m) and for the water samples near the Herschel Island shore, are shown.

The same homogeneous distribution as previously described for the DOC and CDOM distributions over transect 2 is also found here for SUVA on transect 2 (Fig.: 4.17; 4.18).

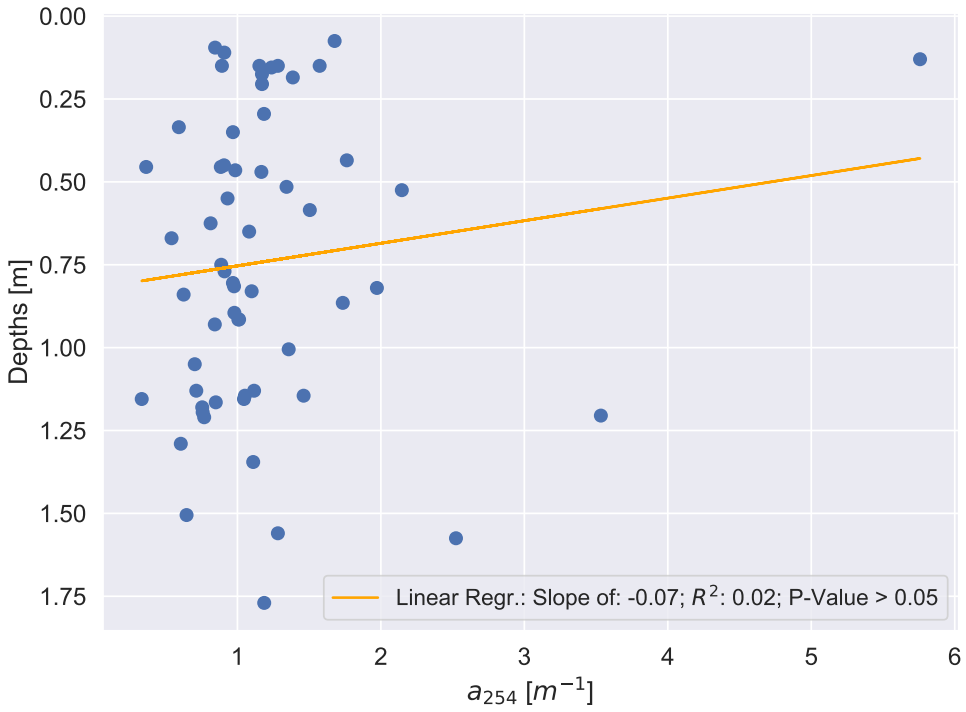

Figure 4.12: CDOM of all twelve ice cores with relation to sampling depth.

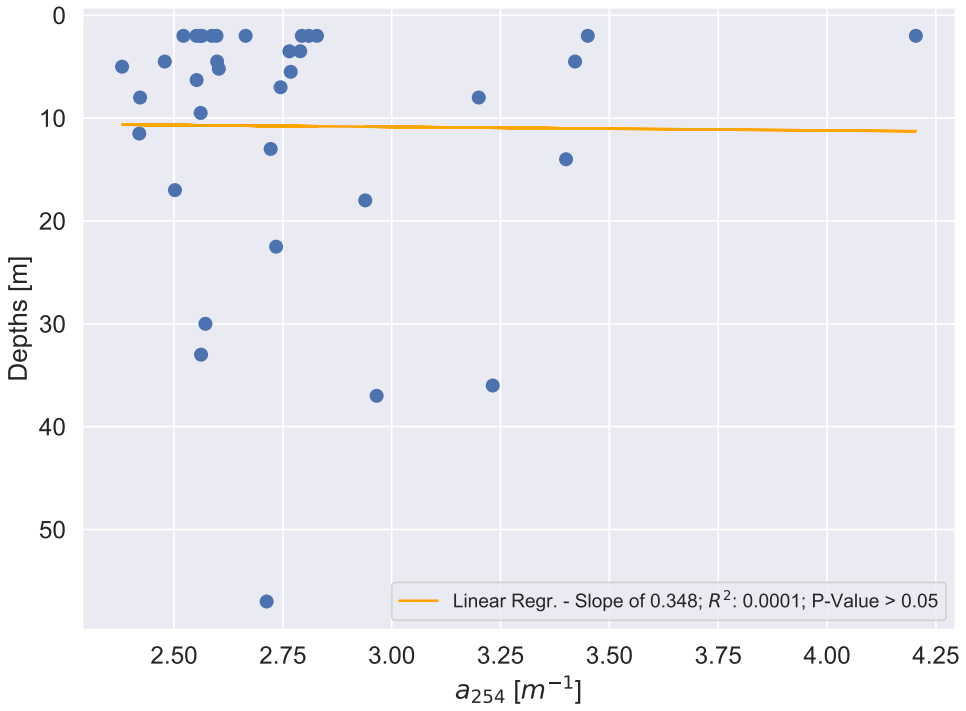

Figure 4.13: CDOM of all twelve water samples with relation to sampling depth.

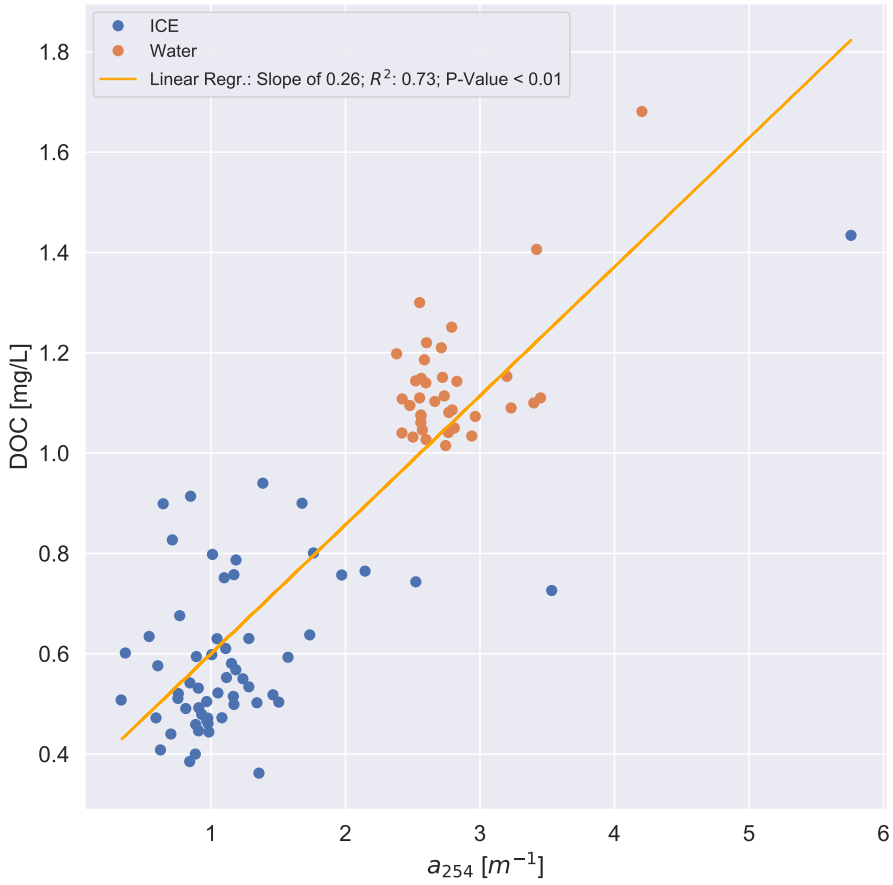

Figure 4.14: CDOM / DOC crossplot of all twelve ice cores and water samples.

4.4.1 Transect 1

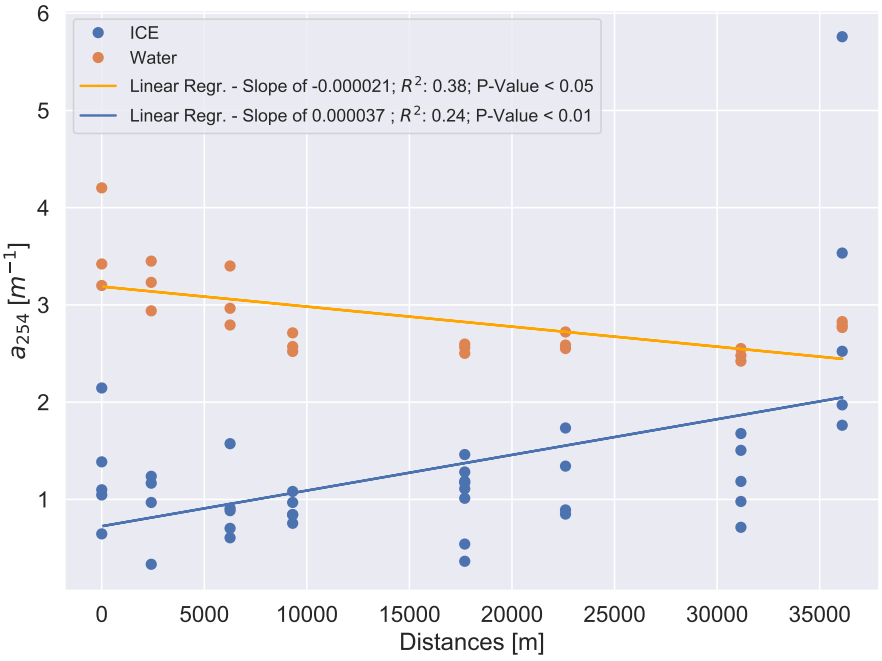

Figure 4.15: CDOM for ice cores and water samples along transect 1. From location 01 (0 m) close to Herschel Island till location 08 (36098 m) close to Kay Point.

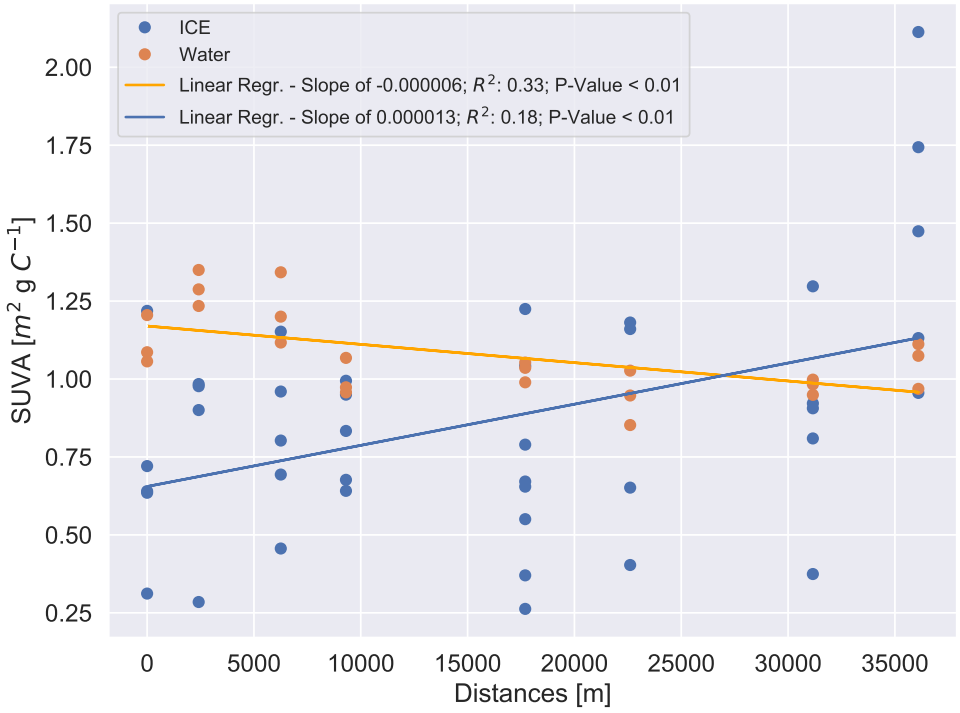

Figure 4.16: SUVA for ice cores and water samples along transect 1. From location 01 (0 m) close to Herschel Island till location 08 (36098 m) close to Kay Point.

4.4.2 Transect 2

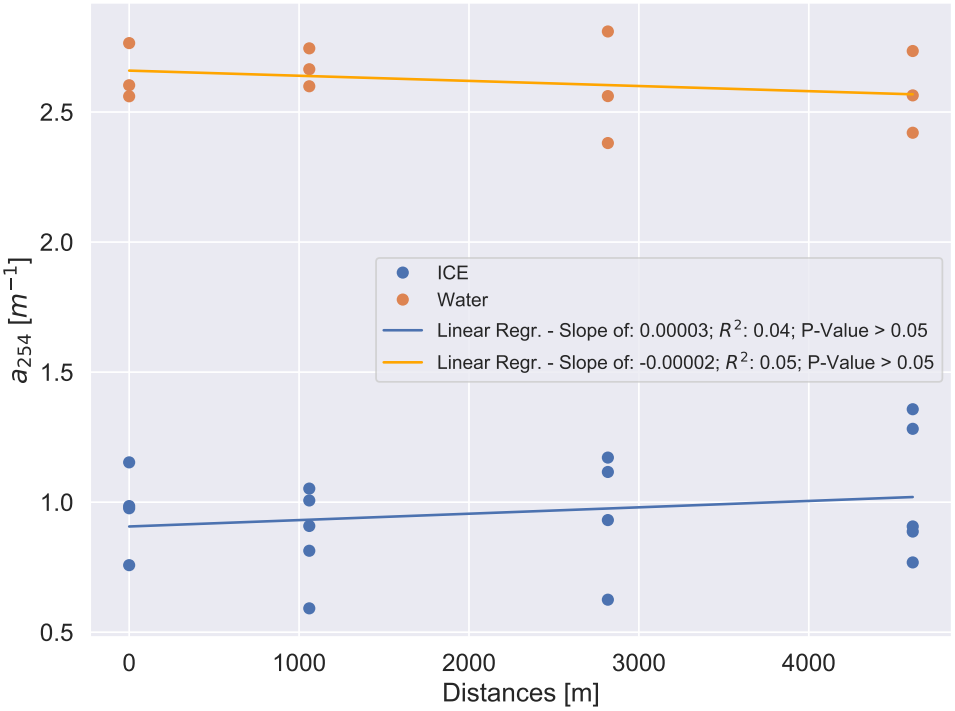

Figure 4.17: CDOM for ice cores and water samples along transect 2. From location 09 (0 m) close to Yukon coast until location 12 (4611 m).

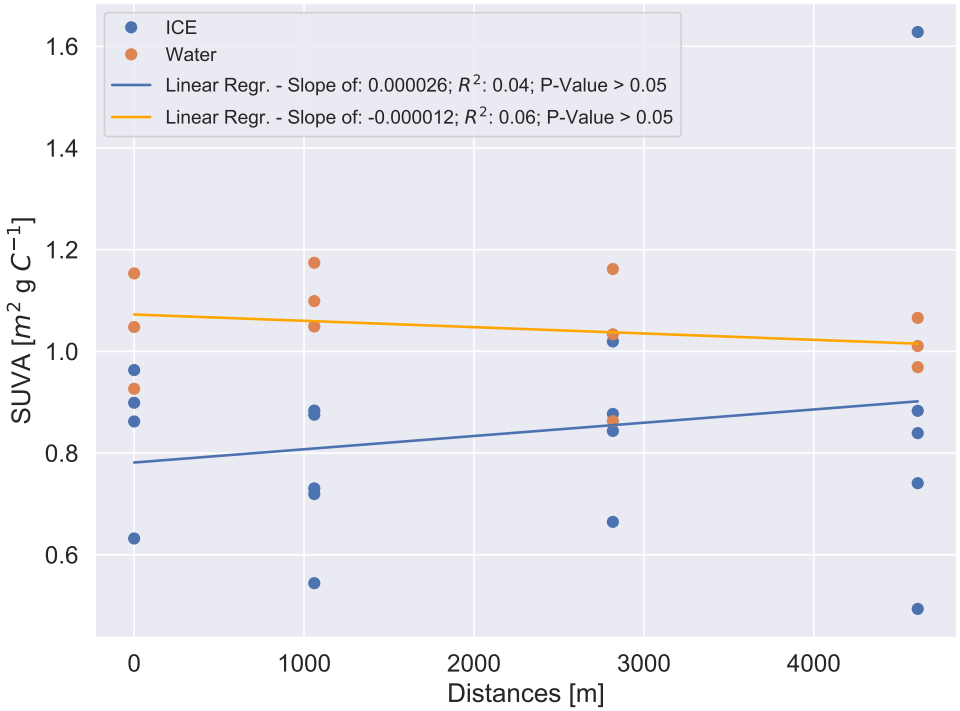

Figure 4.18: SUVA for ice cores and water samples along transect 2. From location 09 (0 m) close to Yukon coast until location 12 (4611 m).

4.5 Stable water - isotopes

To obtain information about the freezing processes and ice build-up (as explained in chapter 3.2.4), δ^{18}O and δD have been analyzed against depths from sea ice surface to the bottom of the underlying ocean. Since δ^{18}O and δD are generally characterized by a strong linear correlation, only $\delta^{18}O$ will be presented here (Fig.: 4.21).

The lowest δ^{18}O concentration measured within the ice core was -14.43 ‰and the highest -0.03 ‰. The range of the δ^{18}O in the water samples is much more narrow with -2.94 and -2.32 ‰respectively. The average δ^{18}O value for the ice cores lays at -2.65 ‰and for the water samples 1.14 ‰.

When looking at Figure 4.19, it is noticeable that the values increase sharply within all cores from a certain depth (∼75cm) upwards towards a more heavier isotopic composition.

In the water column the distribution of the lighter isotopes seems to be clustering within the top ten meters and the heavier isotopes dominating in the lower column (Fig.: 4.20). Two things can be noted when comparing the sea-ice and the water column below along transect 1: Both follow a trend towards Kay Point with lighter isotopes occurring and both also seem to have the heavier isotope signal within their lower or deeper sections (Fig.: 4.23; 4.24).

In Figure 4.21, $\delta^{18}O$ and δD are plotted against each other and brought in comparison with the global meteoric water line (GMWL). The GMWL is a line which correlates with the average hydrogen and oxygen isotope composition of terrestrial waters on a global scale. It is defined as

$$\delta D = 8 \cdot \delta^{18}O + 10‰ \tag{4.1}$$

(Craig, 1961)
With a slope of 8.10 the ice cores align very well with GMWL and the slope of the complimentary water samples is almost the same with 8.09 (Fig.: 4.21), signifiying an isotopic equilibrium with ocean water.
In figure 4.22 $\delta^{18}O$ and salinity are plotted against each other for ice core and water samples, showing a big differences between their values. Both, ice and water, display as well good correlations between isotopes and salinity (R^2: 0.30 / 0.52; $p < 0.01$).
For transect 2 are no significant trends, neither for the ice cores nor for the water samples visible ($p > 0.05$) (Fig.: 4.25; 4.26), indicating a homogeneous sea water mix with no fresh water input to be in its range.

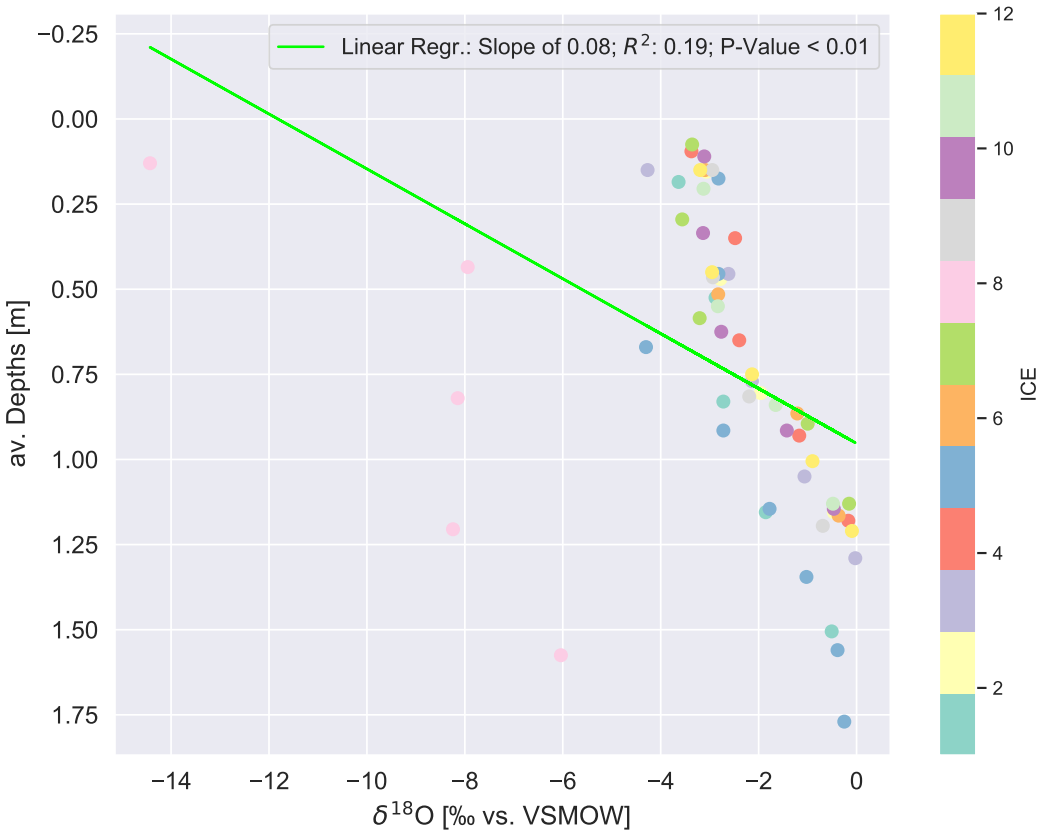

Figure 4.19: Depth over $\delta^{18}O$ of all twelve ice cores. Each color and the corresponding number, stands for one specific ice core sample / location.

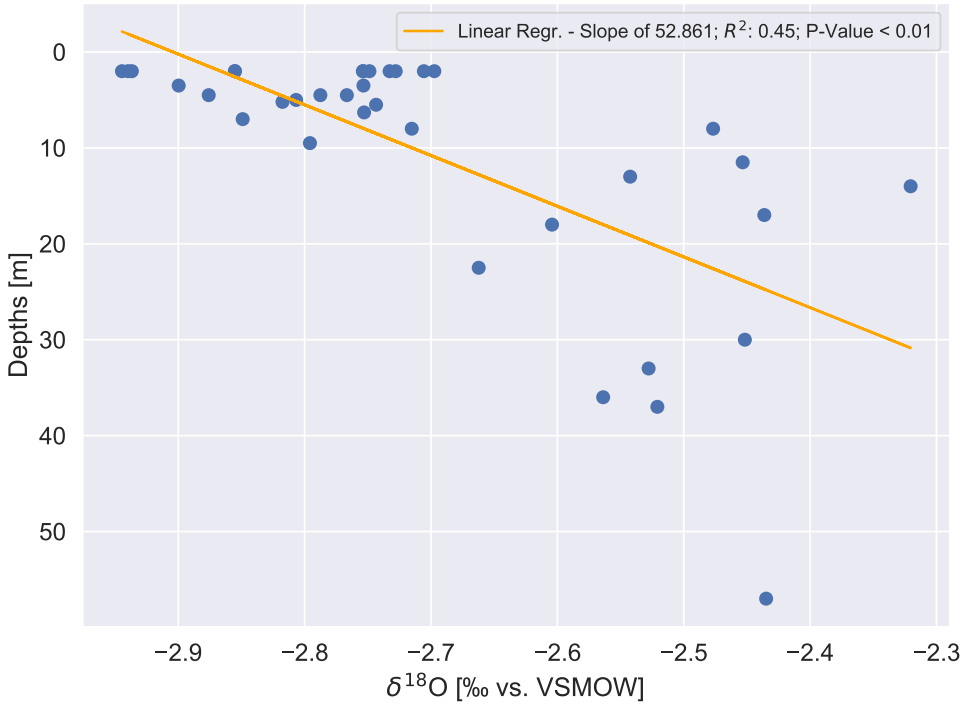

Figure 4.20: Depths over $\delta^{18}O$ of all twelve water samples.

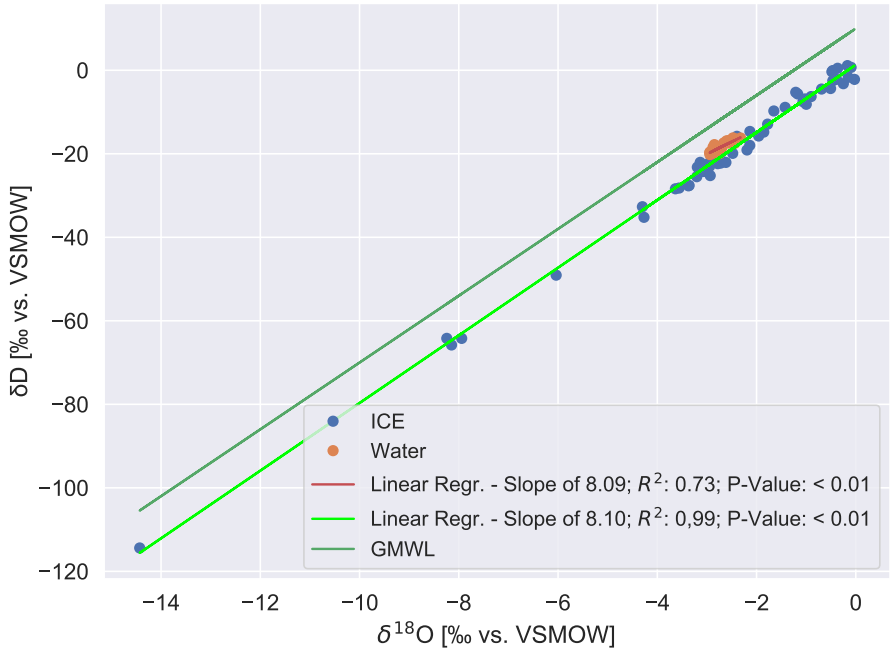

Figure 4.21: A co-isotopic plot of all twelve ice cores - δD against $\delta^{18}O$ in comparison with the GMWL (dark green) line. The red line shows the linear regression from water samples. The green line the linear regression of ice core samples.

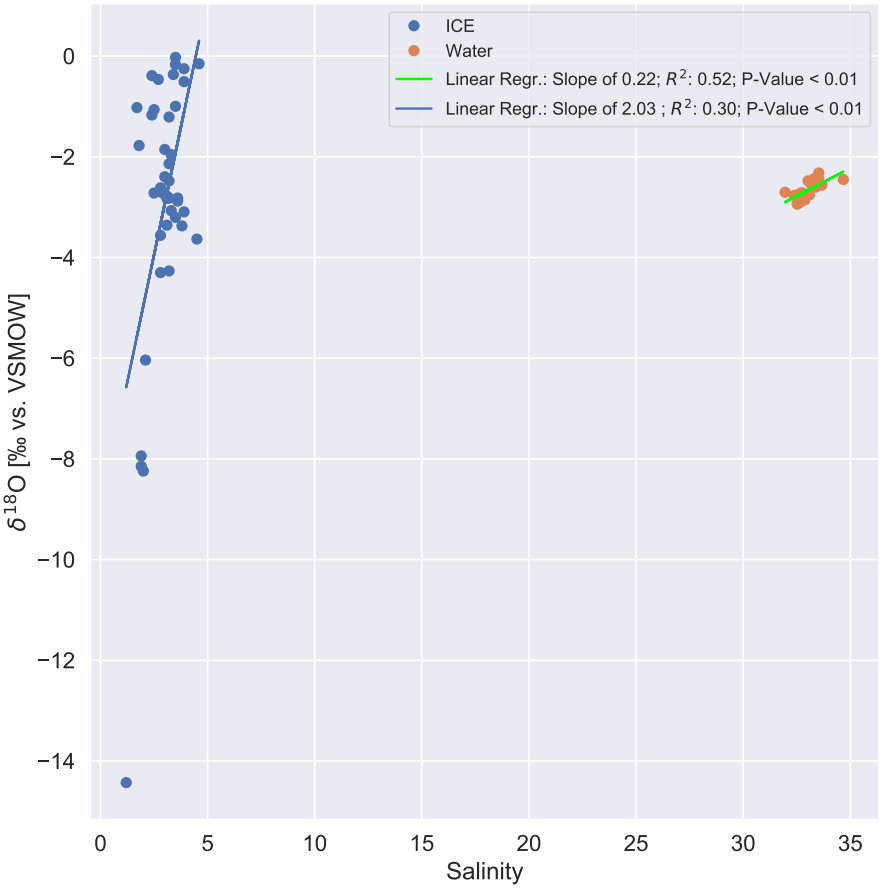

Figure 4.22: $\delta^{18}O$ / Salinity cross plot for ice cores and water- samples.

4.5.1 Transect 1

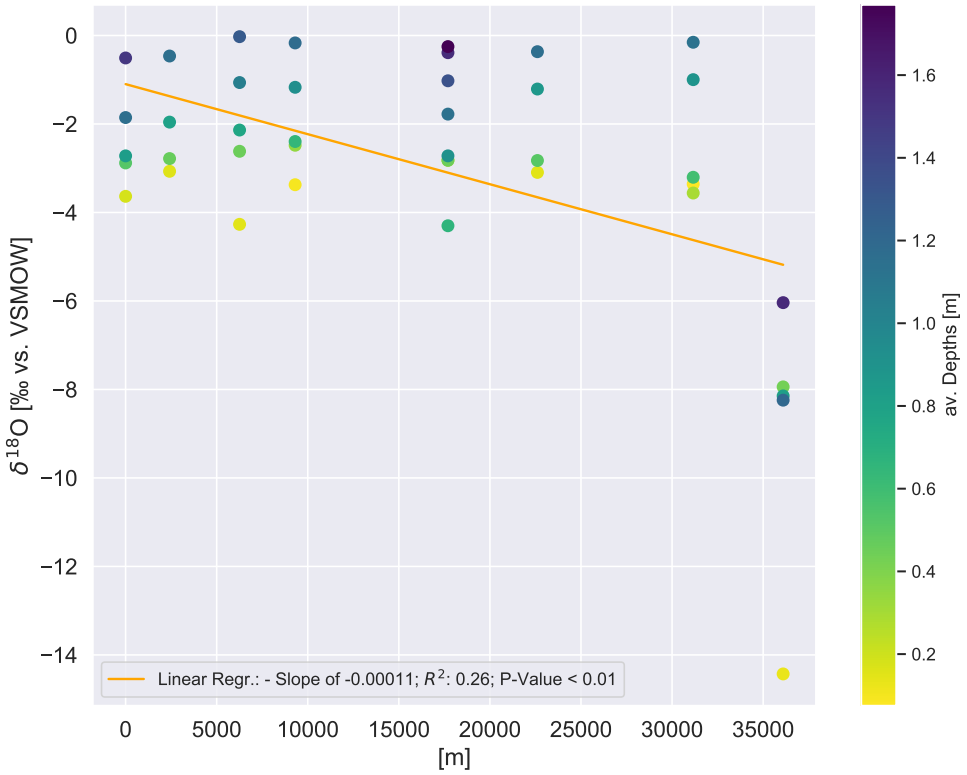

Figure 4.23: $\delta^{18}O$ along transect 1 for ice core samples. From location 01 (0 m) close to Herschel Island till location 08 (36098 m) close to Kay Point

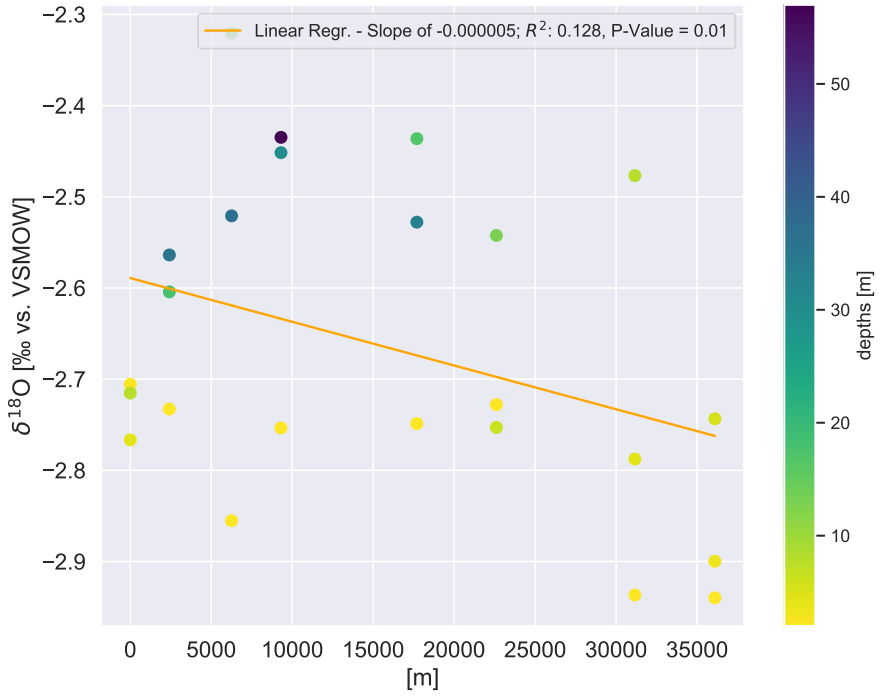

Figure 4.24: $\delta^{18}O$ along transect 1 for water samples. From location 01 (0 m) close to Herschel Island till location 08 (36098 m) close to Kay Point

4.5.2 Transect 2

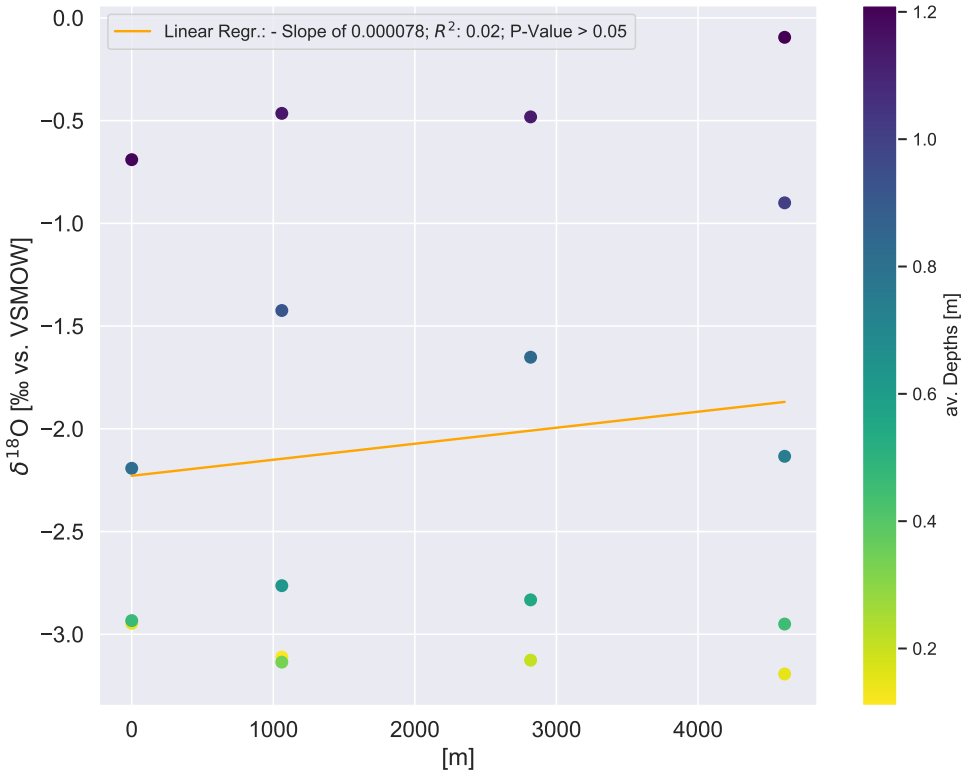

Figure 4.25: $\delta^{18}O$ along transect 2 for ice core samples. From location 09 (0 m) close to Yukon coast until location 12 (4611 m).

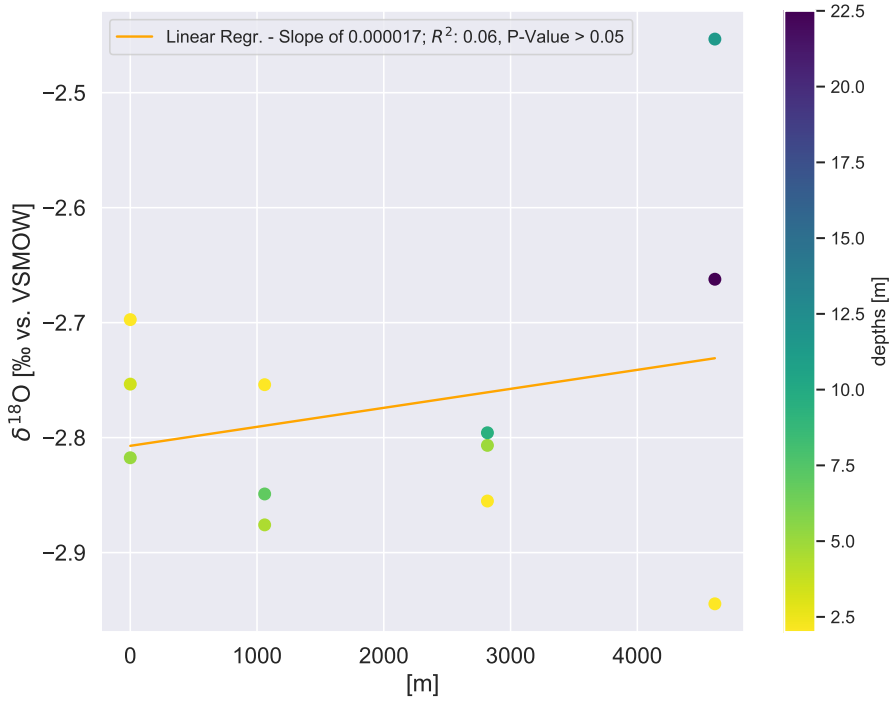

Figure 4.26: $\delta^{18}O$ along transect 2 for water samples. From location 09 (0 m) close to Yukon coast until location 12 (4611 m).

4.6 Suspended particulate matter

Suspended particulate matter consists organic as well as inorganic particles that are autochthonous, e.g. from algae or calcareous organisms or allochthonous and have been either brought into the waters through suspension directly by river transport, through resuspension by currents at the sea floor bottom or through the wind by the air (Pfirman *et al.*, 1995). To examine if and how strong this possible enty by bigger sized particles such as the SPM were, all ice- and water samples have additionally been analyzed for this parameter.

The lowest SPM concentration measured within the ice core was 0.00025 mgL^{-1} and the highest 0.067 mgL^{-1}. 7.38 and 19.17 mgL^{-1} respectively for the water samples. The average SPM value for the ice cores lays at 0.007 mgL^{-1} and for the water samples 11.27 mgL^{-1}.

SPM follow other physical rules on suspension than in comparison for example to DOC and can be a good indicator for turbidity and material transport near the coast and at the point of origin of the particles.

Figure 4.27 shows that the general concentrations of SPM in the cores are quite low, and that their dispersion within the depths of the cores is very much equal (R^2: 0.00; $p > 0.05$). With these small masses for the ice core samples, it must be mentioned that the measurement error plays a major role and that the data should therefore not be overinterpreted. Within the water body below the ice, the concentrations are higher in the upper columns (Figure 4.28). The distribution along transect 1 shows again an increasing trend towards Kay Point (Fig.: 4.29) for both the ice cores and the waters (Fig.: 4.30). The water samples at 0 m at the coast of Herschel Island and between approximately between 1500 and 2500 m show some stronger peaks and the ice cores exhibit as well a peak at the middle sampling site (at approx. 1750 m) and at Kay Point.

For the ice core samples transect 2 shows a significant decreasing trend (R^2: 0.28; $p < 0.01$) from coast towards sea. The complimentary water samples however show no significant trend, indicating a homogeneous water distribution along the water body of the transect 2.

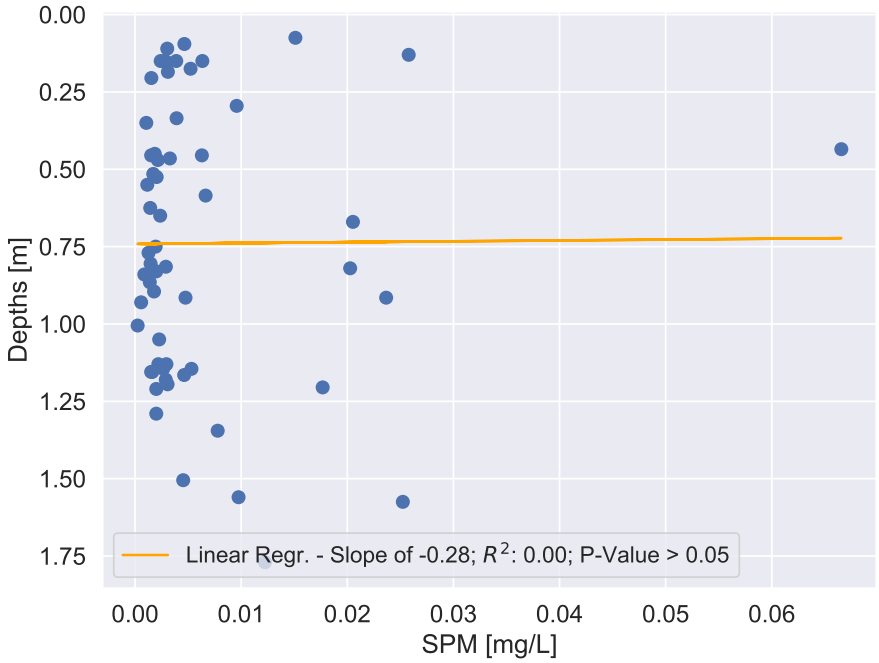

Figure 4.27: SPM concentrations of all twelve ice cores with relation to sampling depth.

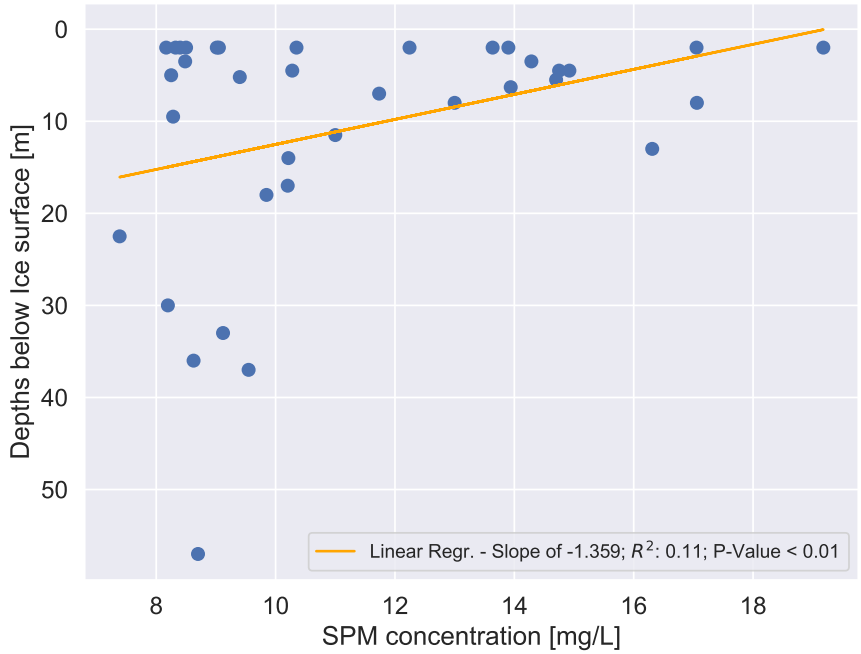

Figure 4.28: SPM concentrations of all twelve water samples with relation to sampling depth.

4.6.1 Transect 1

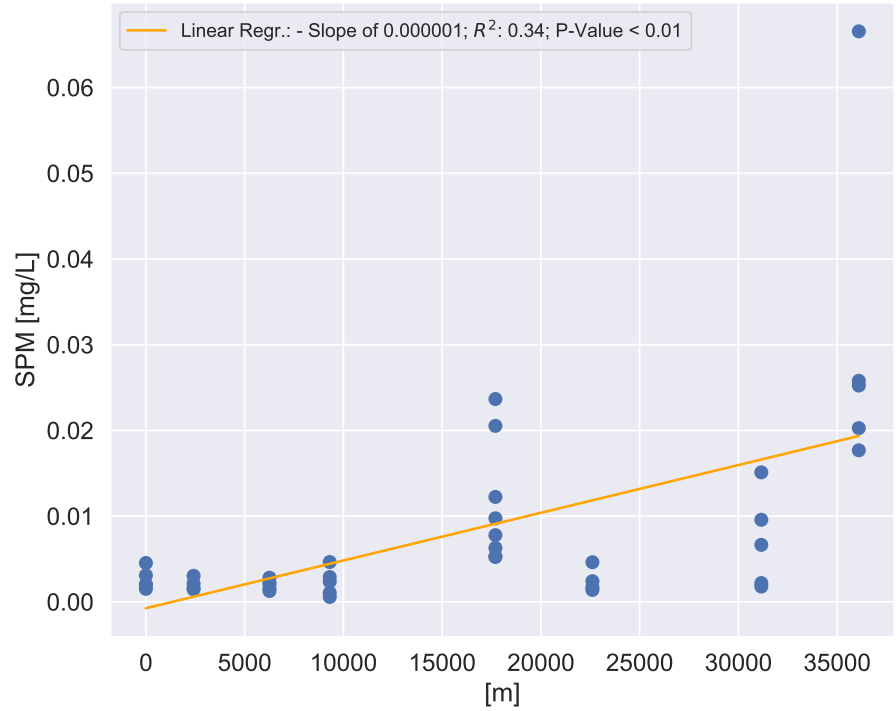

Figure 4.29: SPM concentrations for ice cores along transect 1. From location 01 (0 m) close to Herschel Island till location 08 (36098 m) close to Kay Point

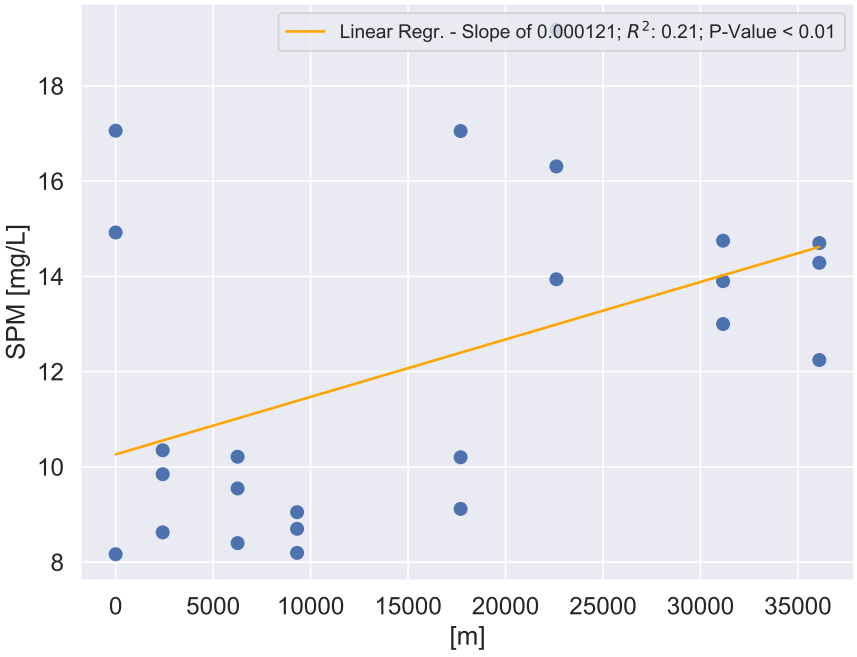

Figure 4.30: SPM concentrations for water samples along transect 1. From location 01 (0 m) close to Herschel Island till location 08 (36098 m) close to Kay Point

4.6.2 Transect 2

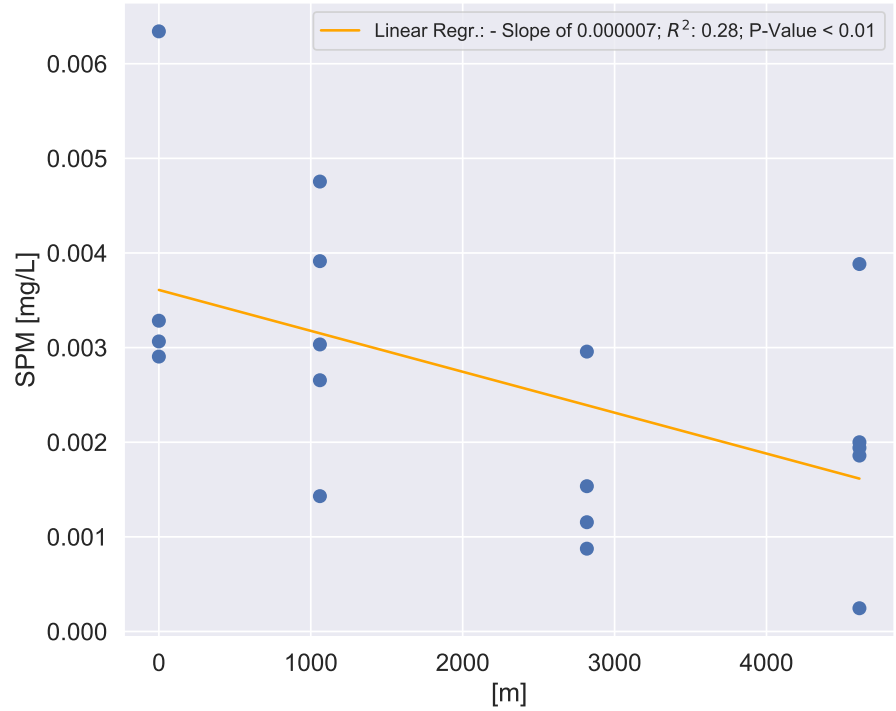

Figure 4.31: SPM along transect 2 for ice core samples. From location 09 (0 m) close to Yukon coast until location 12 (4611 m).

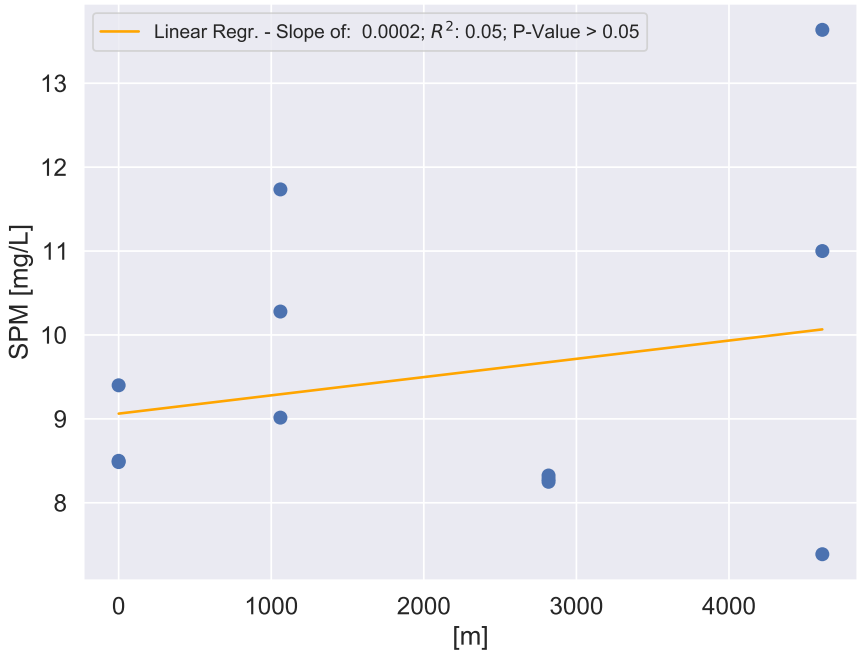

Figure 4.32: SPM along transect 2 for water samples. From location 09 (0 m) close to Yukon coast until location 12 (4611 m).

Chapter 5

Discussion

The following chapter will try to illuminate and discuss the results obtained in the previous chapter (Chapter: 4), based on the hypothesis established at the beginning of this thesis (Chapter: 1). The following chapter is divided into three parts. The first looks at the general formation and destruction processes of the landfast ice, on which this work is based. In the second part, the physical and chemical processes that play a role in the incorporation as well as in the ejection of particles from the sea ice are examined more closely in comparison with the obtained results. Then, for the last part, the organic matter content found within the ice, water samples and along the two transects will be analyzed, discussed and compared to values found within the literature. The aim is to get a better understanding of the organic matter incorporation by potentially accelerating sources of input, like thawing permafrost and eroding arctic coastlines.

5.1 Ice formation and ice break-up

Different kinds of mechanisms for the formation of sea ice exist depending on the environmental conditions. Generally under calm conditions at the beginning of the formation process, randomly orientated and elongated crystals start to form, also referred to as "frazil ice". Those crystals will eventually start to consolidate at the surface and begin to grow in a downward direction. Those first very small sheets of ice are called "Nilas". (Maykut *et al.*, 1992)
Landfast ice grows from the shore towards the sea about the 20 m isobath, reaching by the end of winter a maximum thickness of about 2 m (Stein *et al.*, 2004). The bathymetry within the study area, between Herschel Island and Kay Point, is quite diverse (Chapter: 2.3; Fig.: 2.4). The conditions that make this site ideal for landfast ice to grow, include on the one hand the general bay set up where the ice can find many sites to moor, but on the other hand a sort of natural barrier just 25 to 35 km outside of the bay, the Herschel Sill (Fig.: 2.4 and compare Fig.: 5.1 - 08.10.2018). With an isobath of *circa.* 20 m, the ice is able to anchor, grow and connect from the sea as bedfast ice towards the coast and connect with the landfast ice. Herschel Sill serves also as a protected regime for the growing ice from greater offshore currents.
The formation of the first layers of the studied landfast ice began by the end of October / beginning of November 2018 (Fig.: 5.1), when the monthly average maximum air temperatures

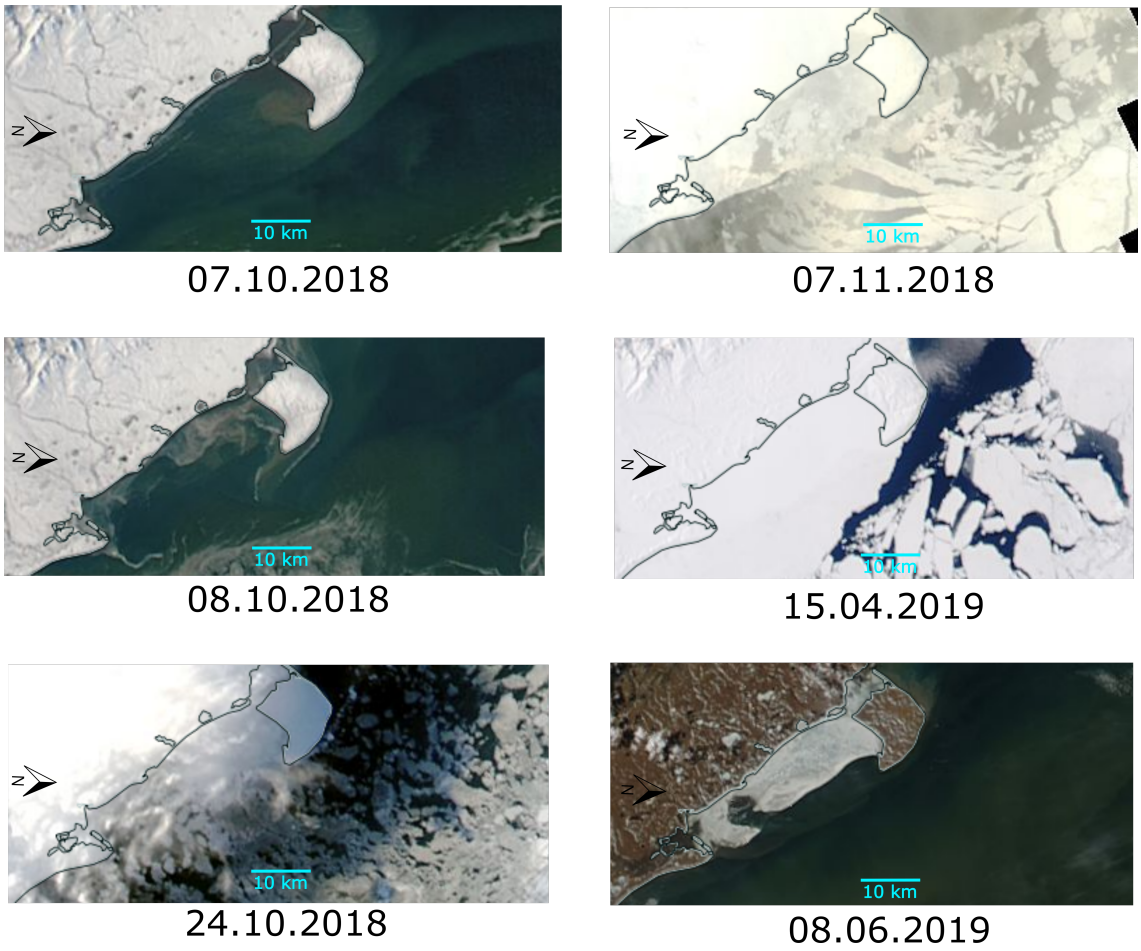

Figure 5.1: Evolution of landfast ice throughout the year 2018-2019 between Herschel Island / Qikiqtaruk and Kay Point at the Beaufort Shelf along the Yukon Coast, Canada. 07.10.2018 = One day before visible ice growing; 08.10.2018 = First major ice fields (Nilas) are starting to form along the coast (as landfast ice) and along Herschel Sill (Bedfast ice). By the end of October / beginning of November the ice shield has covered entire bay area. 15.04.2019 = Ice shield is still stable. Two weeks before core extraction. 08.06.2019 = First visible ice break up at summer. Using Aqua/MODIS satellite provided by www.worldview.earthdata.nasa.gov

dropped from +2.5°C in September down to -2.3°C in October. During the next month, until the days of extraction of the ice-cores by the end of April, the temperatures decreased, reaching minimum values of -35.2°C in December (Gov.Canada, n.d.).

Under these conditions the sea ice was able to grow without disturbances. As is visible on the satellite pictures (Fig.: 5.1) the sea ice developed within the bay between Herschel Island and Kay Point.

In this protected bay the landfast ice consolidates usually until March and usually breaks up in June/July (Fig.: 5.1 - 08.06.2019). Yet two to three months before summer-melt up of the ice starts, the Mackenzie River already increases its river flow discharge (Fig.: 5.2), starting to extend its plume to a widespread lake underneath the ice, also referred to as "Lake Herlinveaux" (Juul-Pedersen *et al.*, 2008; Carmack and Macdonald, 2002). The interactions between the Mackenzie river plume and the spring break-up of the sea ice has already been a matter of investigation (Searcy *et al.*, 1996). The results showed that the river might account for delivering

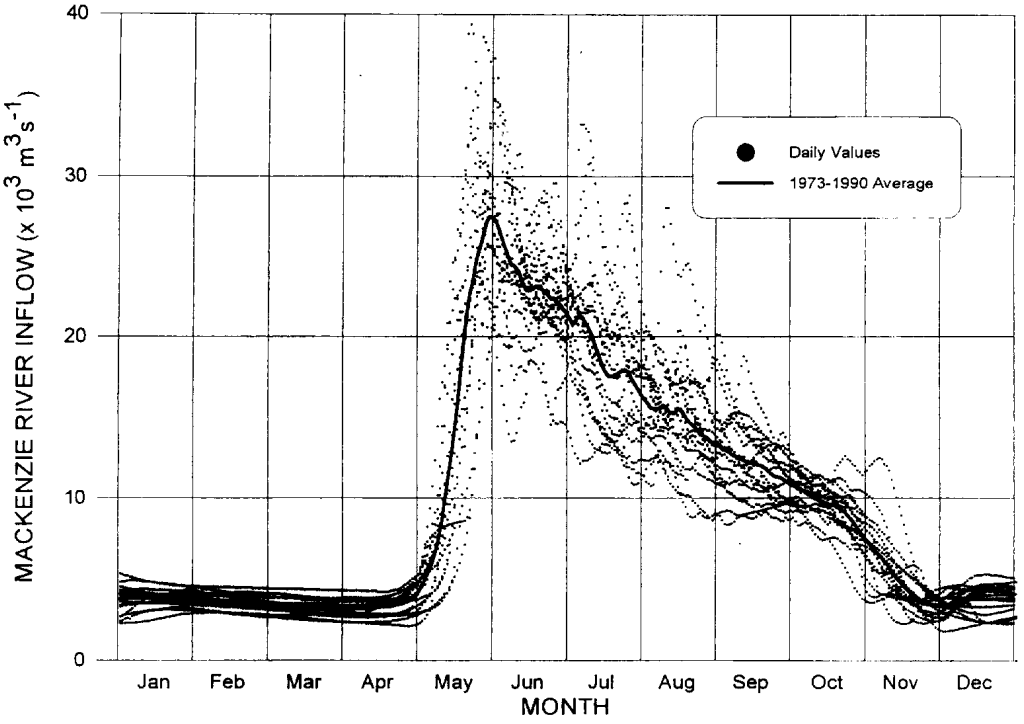

Figure 5.2: The Mackenzie River hydrology for the years 1973-1990 (Watcr Survey of Canada). The solid line shows the averagc daily rate of inflow whereas points show daily values. From R. Macdonald *et al.*, 1998

half of the heat needed to the delta region to melt the ice, resulting in the removal of ice 1-2 weeks prior to the neighbouring coastal areas without significant river inflows.
Due to warming of the Arctic (J. C. Comiso, 2003; Blunden and Arndt, 2012), the lengths of those melting and freezing -seasons, as well the river freshwater input, increase. This results in a longer summer melt up season and a shorter winter freeze-up, with the ice having less time to consolidate and accumulate (Stroeve *et al.*, 2014; Collins *et al.*, 2013) (Fig.: 5.3).
As sea ice naturally limits the interaction between ocean-water and atmosphere as well as between land and ocean-water, the effects on the environment of lower sea ice cover in time and on space are tremendous, especially on the processes of coastal erosion. The direct sediment and organic matter input through coastal erosion is connected to the presence or absence of nearshore- / landfast ice (Barnhart *et al.*, 2014) and thawing of permafrost. Coastal erosion being assumed to have an enormous impact on the nearshore zone (Fritz *et al.*, 2015; Fritz *et al.*, 2017; Wegner *et al.*, 2015). Collapsing coastlines, as an extreme form of degradation, lead directly to a rapid increase and release on large amounts of sediments, organic carbon and nutrients, which then again raises the emission of greenhouse gases (Tanski *et al.*, 2019). Consequently the pollution load to the oceans will increase by everything what was captured before within the collapsed soils, leading to associated greater socio-economic issues within the regions (Irrgang *et al.*, 2018).

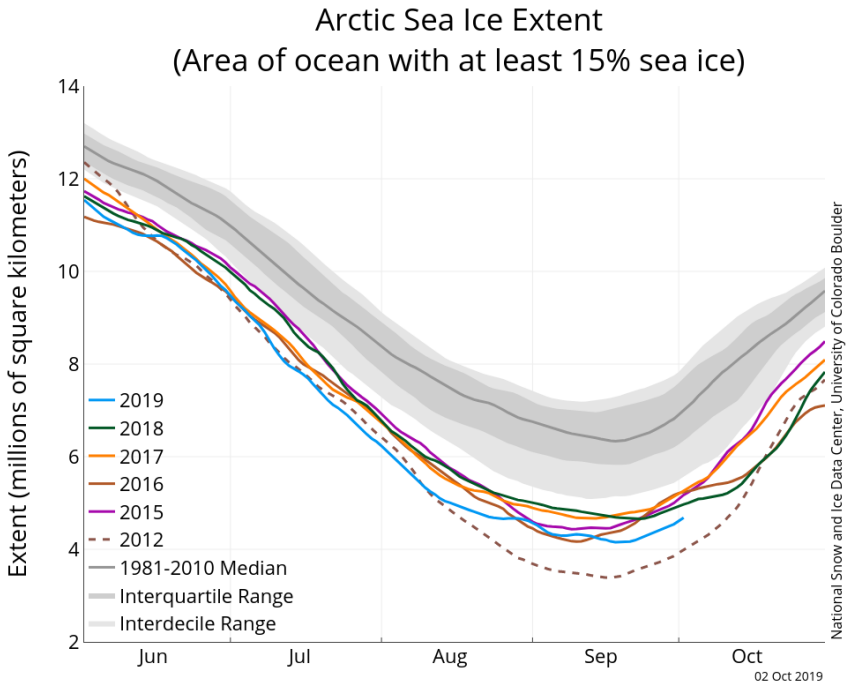

Figure 5.3: The graph above shows Arctic sea ice extent as of October 2, 2019, along with daily ice extent data for four previous years and the record low year (2012). The gray areas around the median line show the interquartile and interdecile ranges of the data collected between 1981 and 2010. From: National Snow and Ice Data Center, University of Colorado Boulder

5.2 Physico-chemical characteristics of sea ice

One of the goals of this work is to quantify the organic content trapped in winter sea ice. Therefore it is necessary to look, and understand some of the processes that are at work during the formation of the ice.

Dissolved organic carbon and inorganic matter are driven out of the crystalline structure of the ice, when sea water freezes and sea ice forms. The concentrate then accumulates in the brine phases. The brines can then either be driven out directly into the sea water, be trapped in the ice or in saline channels and/or pockets (Giannelli *et al.*, 2001; Petrich and Eicken, 2010). How these brines and pockets form shall be briefly described in the following paragraphs:

The salt within the sea water (about 35 ‰, compare Tab.: 5.1) lowers the seawater's freezing point to about -1.9°C. Once the temperatures sink below, the first phase transformation occur and the ice is being formed from the water. When ice grows, the salt is not incorporated into the crystal structure of the ice, but partly remains in the surrounding water, and partly forms brine pockets in the ice. This dependence of the sea ice composition on the temperature is shown in Figure 5.4. Even though the composition of seawater is more complex than displayed in Figure 5.4, it provides an approximation of salt/brine rejection from sea ice during freezing.

As the sea-water, continues to cool, more pure ice forms, causing the remaining sea-water/brine to decrease in volume and become more saline. For example, at -5°C ice coexists with a brine containing 8 wt% NaCl, while at -10°C and -20°C the brine compositions are respectively 14% and 22.5 %.

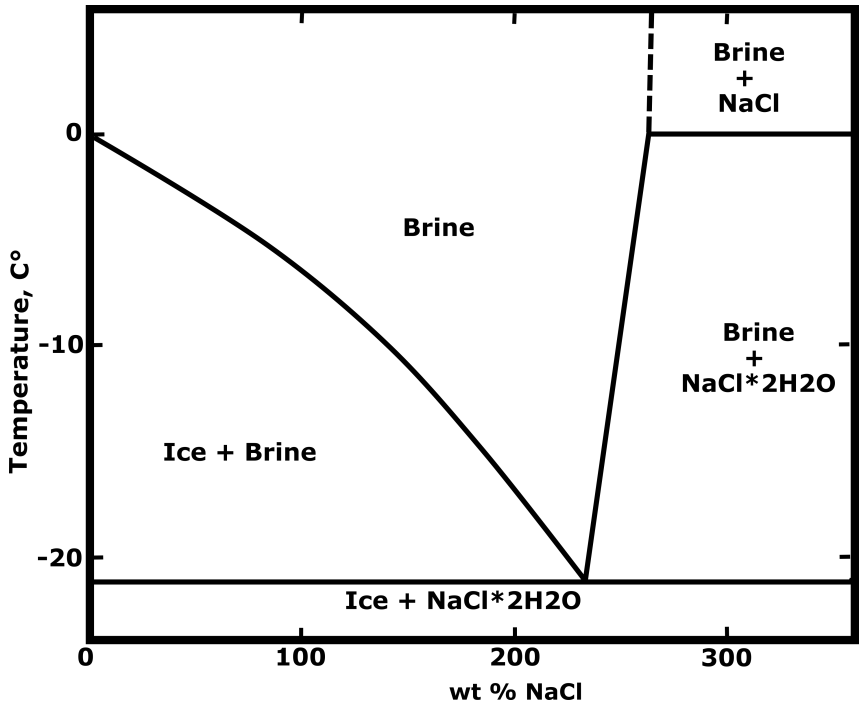

Figure 5.4: A portion of the phase diagram of NaCl-H_2O for the ice and brine separation during freezing. After W. F. Weeks and Ackley, 1986

The above process describes the fractionation of the salt/brines from the ice. The brine, under the influence of gravity, drains out of the ice sheet into the underlying seawater (W. F. Weeks and Ackley, 1986; Lake and Lewis, 1970).
If there is initially no convection, the formation of ice leads to an increase in salinity and density through rejection from the ice to the surrounding sea-water. However, once ice starts to melt again, it acts like an entry of fresh water into the upper ocean layers.
According to the theory described above, the measured salinity values from the ice cores show, a generally low salinity compared to the water column below (Tab.: 4.1). The ice cores also show a lower concentration of organic material (Tab.: 4.1), compared to the water column, which indicate an expulsion during the season. When comparing ice samples to the water samples over transect 1 (Fig.: 4.3; 4.4), it can be seen that the salinity decreases in the direction of Kay Point while water samples had the lowest salinity values positions closest to the coast. For transect 2 no significant trend from shore at location 09 towards the open sea at location 12 can be observed (R^2: 0.07, $p > 0.05$), neither for the ice nor the water samples (Fig.: 4.5; 4.6).
Lower salinity values generally indicate a more fresh water influence. The fact that the ice cores do not show a lower salinity value close to the coast, compared to the relative salinity of water samples close to the coast, could mean that there was no fresh water inflow from this side of the coast at the time the ice was formed, but for transect 1, on the day the water sample was taken, there was. Nevertheless can a significant fresh water influence for example from the Mackenzie River can be ruled out, like the "Lake Herlinveaux" described by Carmack and Macdonald, 2002, since the salinity values are still much to high for any lake regime (Tab.: 5.1). The salinity measurements of the ice-cores and water samples from below, do not display any certain concentration within a certain depths (Fig.: 4.1 + 4.2), but for the ice-cores the

Fresh water	Brackish water	Saline water	Brine
< 0.5 ‰	0.5-30 ‰	30-50 ‰	> 50 ‰
$< 0.05\%$	0.05-3 %	3-5 %	$> 5\%$

Table 5.1: Salinity ranges for different water regimes.

typical "C-shape" can be made out (Nakawo and Sinha, 1981; Eicken *et al.*, 2005). This feature is often found within first year sea ice that can give indication on a stable and continuous ice growth, where salt gets driven out over time at top and bottom, by increasing pressure on the brines, caused by density differences through water-ice phase transformation. Even though the statistical correlations of the linear regression in this Figure 4.2, seem to fit well (R^2: 0.49, $p < 0.01$), the trend has to be considered with care, due to a measuring bias which is implemented: The bathymetry of the basin did not allow measurement everywhere at the same depths. 30% of the values were taken at depths > 10 m and 70% at depths < 10 m, and those at deeper water column show here an expected higher salinity (Fig.: 4.4). However, what can be seen from the water data, especially in Figure 4.4, is that the water basin is clearly stratified, which is an indication that no major external currents have found influence in the bay.
In contrast to salt and salt solutions, the stable water isotopes remain mostly within the ice during equilibrium freezing (Souchez *et al.*, 2000), which means that conclusions can be drawn about the origin of the water in the context of the layer sequences within the ice and relating them to different phases of the water cycle (R. W. Macdonald *et al.*, 1995; Gat, 1996; Eicken *et al.*, 1997; Fritz *et al.*, 2011).
The main fresh water input into the study area is the Babbage River close to Kay Point and the Mackenzie River *circa.* 130 km east of the sampling area. As described by D. Forbes, 1983, the Babbage river runs dry for several months during winter. The isotopic data from the sea ice shows a clear kink towards heavier isotopes at the middle of each core (Fig.: 4.19) with sample Ice-08 standing out. R. W. Macdonald *et al.*, 1995 extracted an ice core in April 1991 in the region, at a location similar to ice core sample 08 (Fig.: 5.6) and used the resulting data to record the sequence of isotopically lighter water within the Mackenzie estuary (R. W. Macdonald *et al.*, 1995). This core shows a similar isotopic pattern and concentration (Fig.: 5.5) with its first layer (0 to 25 cm) incorporating lighter isotopes (< 12 ‰). R. W. Macdonald *et al.*, 1995 states in his work that winter river water inflow for this region comes with a light isotopic composition of around -18.2 for $\delta^{18}O$ and mixes with the nearshore sea water.
To find out more about the formation of the ice and of which water source it came out, plots of oxygen isotopes measurements against salinity found common application in polar ocean regions (Redfield and Friedman, 1969; Östlund and Hut, 1984; R. W. Macdonald *et al.*, 1995) and have also been used here. The measured salinity and the isotopic data in Figure 4.22 correlate well ($p < 0.01$), indicating on the one hand a mixing of seawater with freshwater (Létolle *et al.*, 1993) and showing on the other the strong different isotopic concentrations between sea ice and ocean

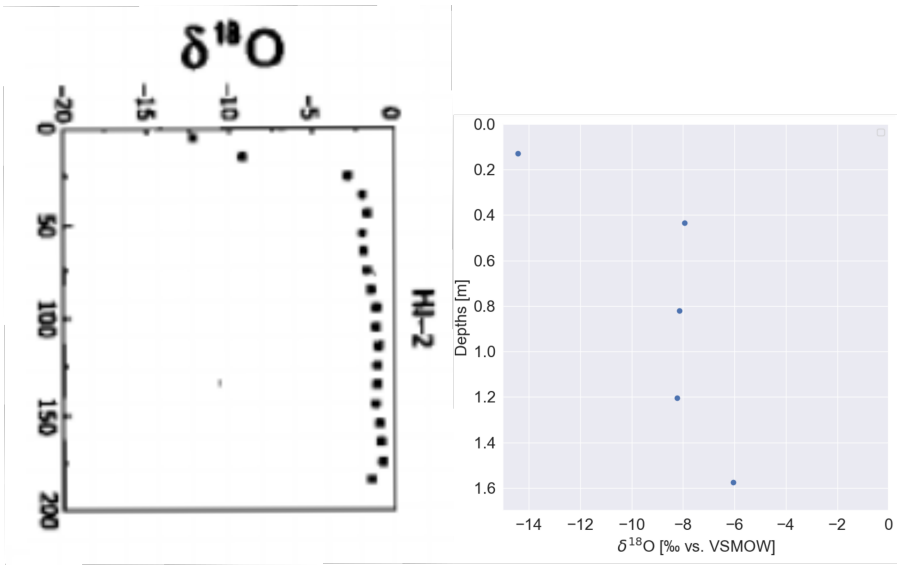

Figure 5.5: $\delta^{18}O$ values from HI-2 from Macdonald 1995 (left) vs. sample Ice-Loc.: 08 (right). Similar low values found within the top section.

water. Some ice-cores in Figure 4.22 show to a greater (bottom left) or lesser degree a direct freshwater input. These observations also stand in good agreement to earlier measurements and observations carried out by Macdonald in 1991 in the same region (R. W. Macdonald *et al.*, 1995). In general for ice and water samples there is notably fewer heavy isotopes found where the salinity is lower and vice versa. If one looks at the isotope data from transect 1 (Fig.: 4.23; 4.24), it is noticeable that these plot in a similar way, as the previously described salinity values along transect 1, and thus also give the indication of a stronger fresh water inflow at the corresponding points. For transect 2, the isotopic data (Fig.: 4.25; 4.26) deliver no significant trend in any direction for ice or water samples and together with the aforementioned salinity measurements along the transect, give indication that towards the coastline of transect 2 no direct fresh water source is nearby or was active during ice formation / day of water sampling. Eicken *et al.*, 2005 researched the origin and incorporated sediment transport of sea ice within the Beaufort Seas. Based on the isotopic analysis of δ^{18}O, for one of their ice-cores, which has a similar mean isotopic concentration (-1.09 $\pm$ 0.9) to the ones of this study (see. Tab.: 4.1), they drew the conclusion that the ice originated over the Mackenzie shelf and formed under "significant influx of river water", since its isotopic values were lower

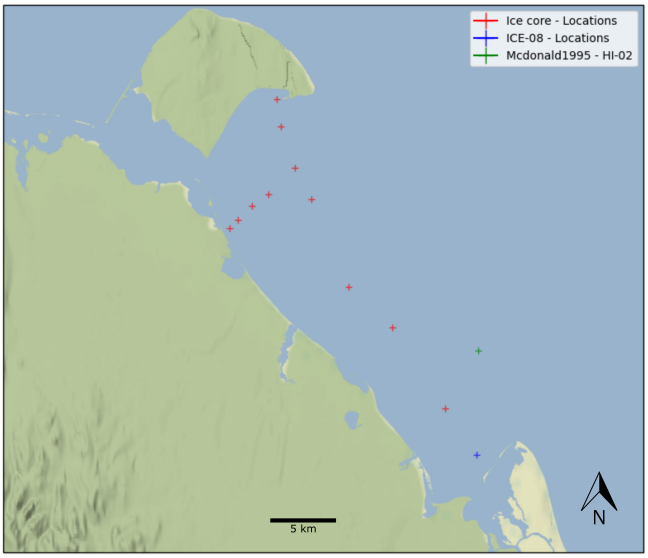

Figure 5.6: Ice-core sampling locations of this study (red crosses) including location 08 (blue cross) and with sample HI-2 from Macdonald 1995 (green cross)

than compared to the other sea ice cores analysed (Eicken *et al.*, 2005).
The complementary sub- ice water samples of all samples, are found to have a much more narrow range in isotopic composition, displaying a quite homogeneous water regime within the bay.
The slope of the linear regression of the ice-core samples is 8.10, which is slightly higher then the one of the GMWL (8.0) (Fig.: 4.21). The water samples plot almost with an identical slope (8.09) and a good R^2 - value of 0.73 along, indicating a steady and similar meteoric source region, throughout the winter season. The isotopes have fractionated in equilibrium, which is to be expected in an open system like this.

5.3 Dissolved and particulate organic matter

One of the key questions to be answered in this thesis is to find out where the organic matter within the ice-cores, comes from. As the previous chapter (Chapter: 4) reveals, organic matter was found in the ice-cores, albeit in a very small amount compared to other studies dealing with sea ice (Thomas *et al.*, 1995; Thomas *et al.*, 2001; C. A. Stedmon *et al.*, 2007; Norman *et al.*, 2011; Longnecker, 2015). The CDOM characteristics broadly followed those for DOC within the ice and the water samples (Fig.: 4.15) and can be seen as significantly related (R^2: 0.73 and p-value: < 0.01).
In order to find out whether the organic matter that was found in the ice had an autochthonous or allochthonous origin, unfiltered samples were also taken. Significant chlorophyll peaks did

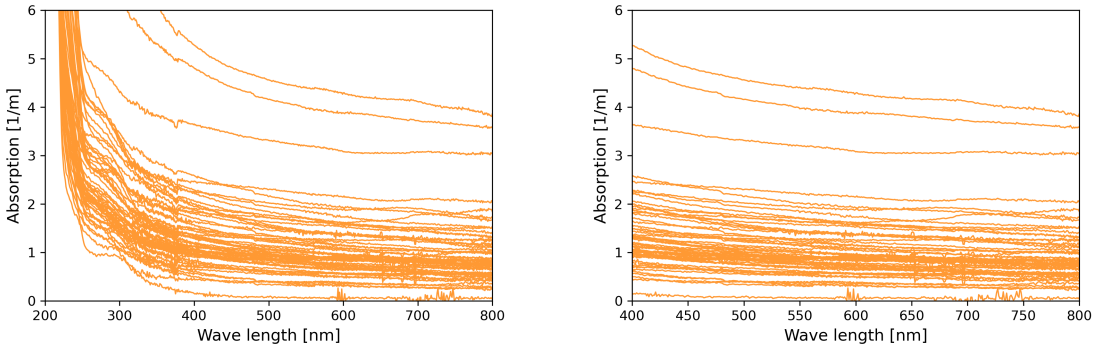

Figure 5.7: CDOM absorption plots of unfiltered ice-core samples for chlorophyll analysis. No significant peak between 500 to 600 nm can be made out. Left: total wave length range. Right: Close up of same plot with close up of wave length range from 400-800.

not occur, therefore an algae bloom etc. as a possible organic matter source can be excluded (Fig.: 5.7 compare Chapter: 3.2.3, Fig.: 3.5).

The dominant sources for DOM within the oceans are terrestrial runoffs (Lobbes *et al.*, 2000; C. Stedmon *et al.*, 2011), like rivers or groundwater discharges. Therefore a strong negative correlation between DOC and salinity is expected, when plotting DOC against salinity (Blough, 2002a). This is not the case for the ice cores (Fig.: 4.9), because the ice grows out of the sea-water, the salt is being driven out (Chapter: 5.2) and the DOC as well, but not in the same way. Some DOC remains enclosed within the sea ice. This assumption is not only supported by the poor correlation between DOC and salinity, but also when the average values between ice and water are compared. In contrast to salinity, the concentration of which decreases tenfold compared to water, the DOC / CDOM concentrations are only half those of water (Tab.: 4.1). The depths against the DOC / CDOM concentration plots by the ice-cores show, just like for the salinity, no specific accumulation in a certain depth (Fig.: 4.7; 4.12) and are widely homogeneously distributed. For the depths against the water samples on the same parameter, the same bias regarding the shown trend, occurs as mentioned before for the depths against salinity with the difference so that, when comparing the R^2 and p-values, the plotted trends have no significance: Neither in the deep nor in the shallower sections can a specific concentration profile for the DOC nor for the CDOM be made out. What does stand out is, when looking along transect 1 (Fig.: 4.10 + 4.15), at location 08 (36098 m), the DOC/CDOM ice-core signal seems here much denser and generally higher, especially for the DOC, indicating a continuous carbon source, over the ice growing period. When one considers the ice growing process (Chapter: 5.1) and a closer look at ice core 08 is taken (Fig.: 5.8), the conclusion can be made that the highest DOC concentration entrained at the beginning of winter and the ice growing process, which agrees well with the before described isotopic data and their lower values found within the upper ice sections (Especially for ice sample 08, Fig.: 4.19; 5.5), in terms of looking for the source of the carbon. When the river is still running (lighter isotopes found), the DOC signal is stronger, when the river peters out (heavier isotopes found), the DOC signal simultaneously becomes lower as well. Hence it can be concluded that the origin of the carbon in this section of ice must be the river, which dries up through the course of winter.

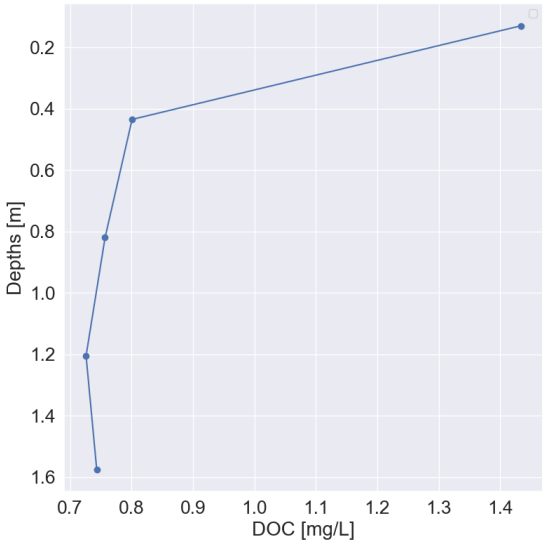

Figure 5.8: Ice core 08: Depths against DOC. Higher concentration within upper [0 - 0.20 m] section of ice measured

For the water samples along transect 1, almost the opposite is true, a carbon peak at location 01/0 m, close to Herschel Island, and therefore some source must be close. Looking at transect 2 on the DOC and CDOM values (Fig.: 4.11; 4.17), just like before for the complimentary salinity and isotopic data, no significant trend is visible along this transect. At this coast side of transect 2, as well as the closest coast side for transect 1 at Herschel Island, no direct river input exists (Fig.: 3.1; 2.4), but other recent studies have found that coastal erosion and thaw streams take place at these and other coasts as well (Fritz *et al.*, 2015). The latter assumption finds extensive support in the global upheavals which coastal regions, in particular permafrost coasts, have been and are exposed to in recent years (Günther *et al.*, 2015). 34% of the world's coastlines consist of permafrost and due to global warming, the erosion rates of those vulnerable coasts are increasing sharply (Lantuit *et al.*, 2012; Fritz *et al.*, 2017). Such erosion brings organic carbon rich sediments, DOC as well as POC (Grotheer *et al.*, 2020) into the sea, to be buried and deposited at the ground, but as well to potentially be matter of resuspension into the upper mixing water column, potentially introducing CO_2 to the atmosphere (Tanski *et al.*, 2019) (Fig.: 5.9). According to estimates, between 4.9 and 14 Tg of organic carbon alone are brought into the near coastal region annually (Wegner *et al.*, 2015), which by far exceeds the amount of POC brought into oceans by river input (McClelland *et al.*, 2016), derived from coastal erosion and permafrost thaw (Jong *et al.*, 2020).

The mean SUVA values of this thesis (Fig.: 4.1) are lower than what Walker *et al.*, 2013, have measured during winter flow for Mackenzie river, but since the ice-cores did not derive directly from river water, those values are in a good agreement. Looking along transect 1 on the SUVA parameter (Fig.: 4.16), peaks are shown for the water samples closer to Herschel Island and for the ice-core at location 08, which are in support of a fresher organic carbon source close to the coast. This indicates that the DOM at those spots are of higher molecular weight and greater aromaticity, compared to the others, which could be the result of a shift in the source of DOM (Neff *et al.*, 2006; C. Stedmon *et al.*, 2011). The SUVA values for transect 2 (Fig.:

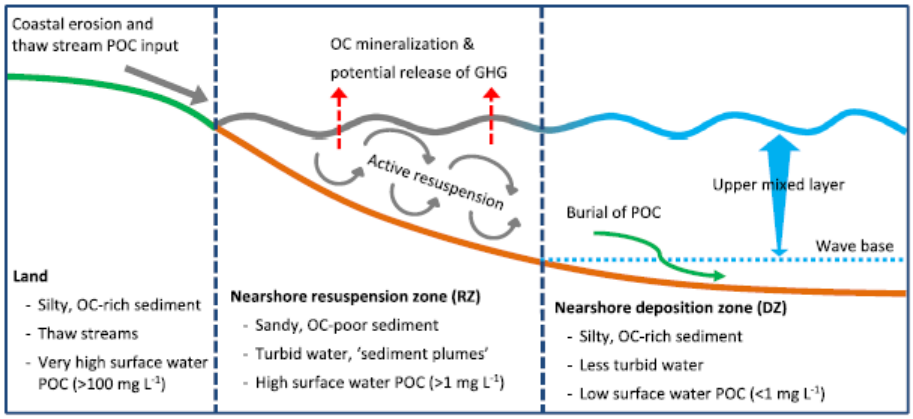

Figure 5.9: Conceptual model of POC pathways at the coast and in the nearshore zone. The nearshore zone is divided in the resuspension zone (RZ) and the deposition zone (DZ).In the upper mixed layer, turbulent mixing by waves and currents is stronger at the surface and decreases with depth (blue arrow). During water column transport, OC can be remineralized and potentially released to the atmosphere as greenhouse gases (GHGs, red arrow) or reach the deposition zone and settle out to the sediment (green arrow). From Jong *et al.*, 2020

4.18), as before for DOC and CDOM, deliver no significant trend towards a direction, neither for the ice-cores nor for the water samples, and support therefore the assumption of no fresh water source near by.

For transect 1 the SPM analysis for ice and water samples go very much along with the before described observations for the DOC/CDOM. No accumulation whatsoever of concentration within any certain depth, but with the same previously described peaks over the transect 1, respectively for ice and water samples (Fig.: 4.29; 4.30). This again could be, even if the supporting evidence is quite weak, a sign that the coastal retreat and erosion are delayed over the colder periods and that the massive ground ice bodies within the permafrost, and also found on Herschel Island (Fritz *et al.*, 2011), show low signs of thaw by late April. With regard to the SPM for the ice core samples along transect 2 a not insignificant downward trend from coast (Location 09 - 0 m) towards open sea (Location 12 - 4611 m) is shown, indicating a higher SPM concentration at the coast (Fig.: 4.31). If a closer look is taken at location 09 (Fig.: 5.10), where the SPM concentration is highest, the ice core shows at its first layers (0 to approx. 20 cm) its highest concentration of SPM. This, just as before for the DOC concentration described for ice core 08 and the ice growing process (Chapter: 5.1), leads to the conclusion that this higher SPM entrainment found at this core was entrained at the beginning of winter and the ice growing process. This same conclusion, an SPM entrainment within the beginning of winter, can be made for the other close coast sea ice cores 07 and 08, towards Kay Point (Fig.: 5.11). Ice core 01 at the coast of Herschel Island shows in contrast its highest entrainment within the lower sections of the core (Fig.: 5.11), giving indication of an SPM entrainment at the end of the ice growing season.

The general SPM concentrations within the ice-cores are low compared to the water-columns below (Tab.: 4.1), nevertheless the entrainment exists and has been described to require a regime of suspension (Eicken *et al.*, 2005). If one sees the latter in connection with the previously de-

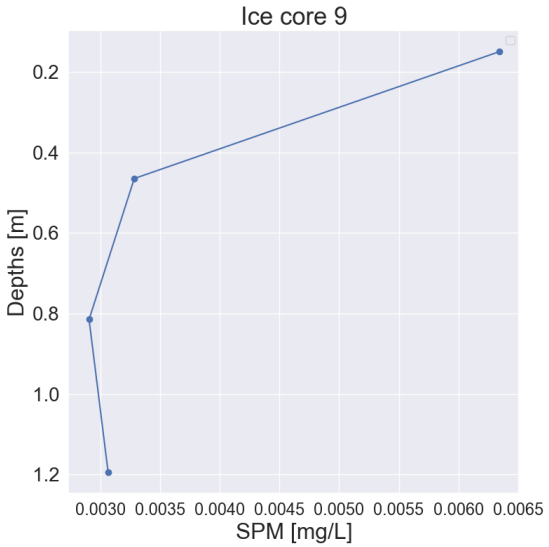

Figure 5.10: Ice core 09: Depth against SPM. Higher concentration within upper [0 - 0.20 m] section of ice measured

scribed values of the salinity (as well as the isotopes) and the stratification of the water column, which suggested a rather calmer water basin, this would only leave open the conclusion that the near coastal SPM entries shown here are due to coastal erosion and maybe to some extent wind flux as well.

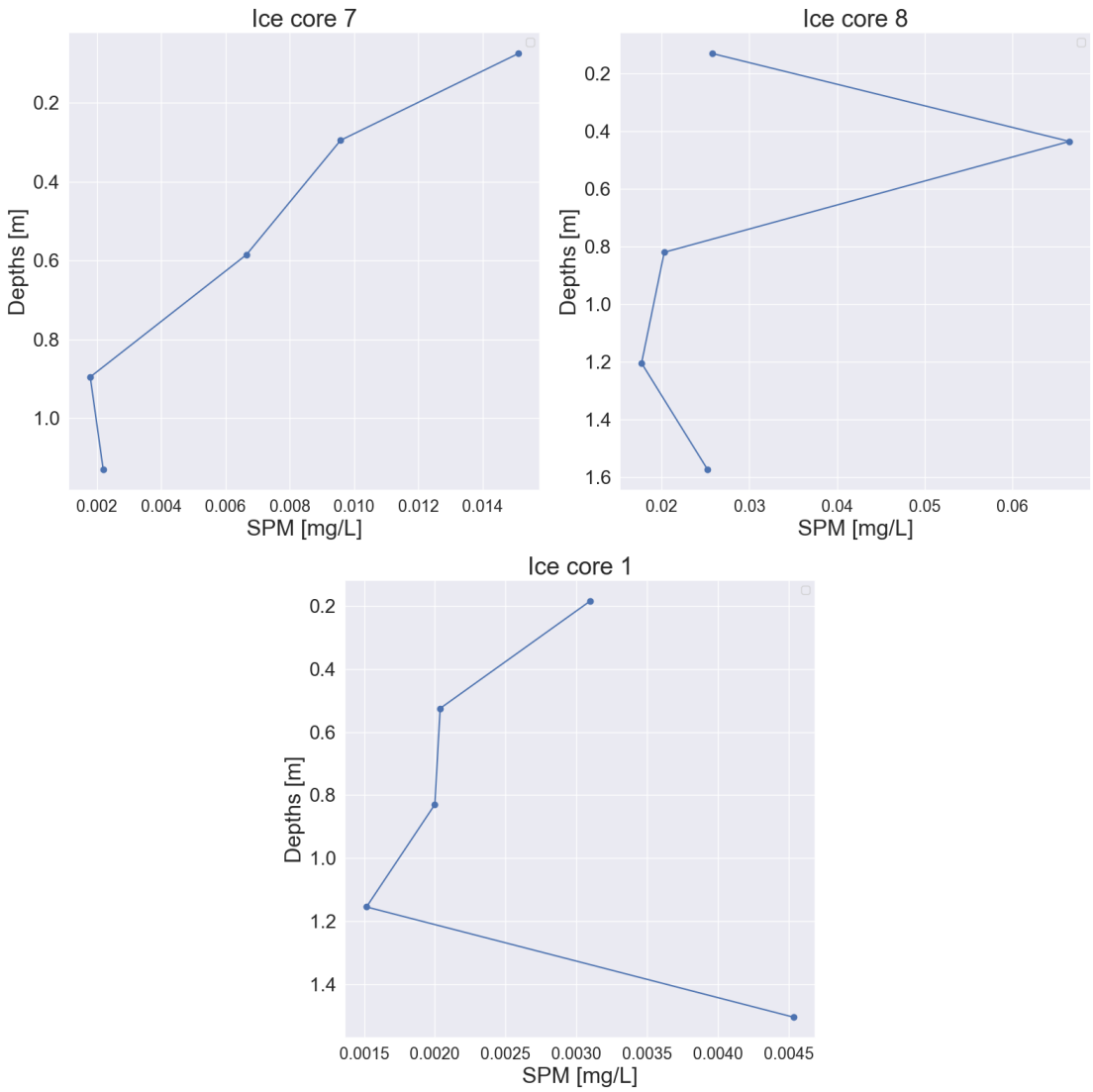

Figure 5.11: Ice core 01, 07 and 08: Depth against SPM. 07 and 08 show a higher concentration within upper section of core, indicating entrainment at the beginning of winter. 01 at the lower section, indicating entrainment at the end of winter.

Chapter 6

Conclusion

When dissolved and particulate organic matter is incorporated into sea ice, the ice only serves as an intermediate medium within its path through the global carbon cycle. The sea ice can temporarily remove the organic matter from the system and thus delay transformation and absorption processes. Furthermore it can serve as a floating transport medium and bring the OM to other places, where it then either becomes directly effective after melting or is deposited. Through this sort of "pause" of the OM along the way, can the ice can serve as a good opportunity to estimate and draw conclusions on the rate of matter transport and from where the matter originates. The aim of this study was to determine the amounts, origin and release of dissolved organic matter contained in winter sea ice, specifically nearshore landfast ice. In addition to the attempt to answer the hypothesis postulated at the beginning of this study in the best possible way, further fundamental questions arose in the course of this work and drove this study forward: What is the distribution of organic matter within the ice cores? Is there a difference in the concentration of organic matter between nearshore and more offshore samples? Can a difference in the distribution and concentration of organic matter between the two transects be determined? Can the deposits in the ice cores be determined in a chronological order? What conclusions can be drawn about the origin of the organic matter trapped in the ice cores?
Based on the measured DOC, CDOM, salinity, water isotopes and SPM concentrations found in different ice cores and the underlying water column (Chapter: 4) four main conclusions can be drawn:

- Matter incorporation within landfast ice takes place but on a fairly low level within this particular study area. However, it can be concluded that if, for a region where no direct major river input over the course of winter exists, matter incorporation takes place on a low level, greater amounts will get incorporated in ice and released for areas of stronger water discharge.

- The analysis of the concentration distribution of organic matter within ice cores is hardly informative about the totality of the samples, in contrast to the regionally differentiated analysis.

- A regional dispersion and concentration trend of matter is observed parallel to the coastline

within the ice and in the water column. Along the long transect 1, at one side (Kay Point near Babbage River) DOM is evident and can most likely be traced back to the river as its origin. At the other side of the bay of transect 1, at Herschel Island, as well as at the Yukon coast side of transect 2, no direct freshwater input is evident, but most likely signals from the beginning and end of winter of coastal erosion can be detected.

- Knowing that the annual organic matter release from the shore ends, or becomes less, by the beginning of winter and starts again over by the end of it, a "point zero" as the annual starting point of matter release into the oceans can be conducted for late winter already, before freshet.

The sampling and analysis of coastal sea ice data poses great challenges, as not all of these regions are accessible in terms of time or location due to the weather and/or local conditions. This can create a statistical regional bias, due to safety standards which have to be observed.
However data on ice composition are not only essential for evaluating the behavior of conservative or non-conservative substances but also for constructing comprehensive budgets on the Arctic environmental conditions in times of global climate warming. Ice-core data have proven many times to be a powerful medium on gaining information of the past earth history and are as well for this study. Quantitative and qualitative insights of the organic matter incorporation and release within sea ice from Arctic regions are a requirement in order to construct further models and forecasts on how strong the thawing of the permafrost, coastal erosion and the matter release into the oceans will be within these vulnerable regions, under increasing global temperatures. Together with newer technologies like e.g. remote sensing, powerful predictions can be made, even for regions that are challenging to access on a regular basis.
With this study indications can be derived of the extent to which the thawing of the permafrost soil, the erosion of the coasts and the entry of organic matter into the water runoff progresses during the course of the winter in the Arctic.

References

Barnhart, K. R., Overeem, I., & Anderson, R. S. (2014). The effect of changing sea ice on the physical vulnerability of arctic coasts. *Cryosphere*, *8*(5), 1777–1799.

Battin, T. J. (1998). Dissolved organic matter and its optical properties in a blackwater tributary of the upper orinoco river, venezuela. *Organic Geochemistry*, *28*(9-10), 561–569.

Blough, N. V. (2002a). Chromophoric dom in the coastal environment. *Biogeochemistry of marine dissolved organic matter*, 509–546.

Blough, N. V. (2002b). Chromophoric dom in the coastal environment. *Biogeochemistry of marine dissolved organic matter*, 509–546.

Blunden, J., & Arndt, D. S. (2012). State of the climate in 2011. *Bulletin of the American Meteorological Society*, *93*(7), S1–S282.

Bowden, W. B. (2010). Climate change in the arctic–permafrost, thermokarst, and why they matter to the non-arctic world. *Geography Compass*, *4*(10), 1553–1566.

Brown, R., & Kupsch, W. (1974). *Permafrost terminology. national resource council of canada* (tech. rep.). Technical Memorandum 111.

Carmack, E. C., & Macdonald, R. W. (2002). Oceanography of the canadian shelf of the beaufort sea: A setting for marine life. *Arctic*, 29–45.

Chadburn, S., Burke, E., Cox, P., Friedlingstein, P., Hugelius, G., & Westermann, S. (2017). An observation-based constraint on permafrost loss as a function of global warming. *Nature Climate Change*, *7*(5), 340–344.

Chowdhury, S. (2013). Trihalomethanes in drinking water: Effect of natural organic matter distribution. *Water Sa*, *39*(1), 1–8.

Christiansen, H. H., Etzelmüller, B., Isaksen, K., Juliussen, H., Farbrot, H., Humlum, O., Johansson, M., Ingeman-Nielsen, T., Kristensen, L., Hjort, J., *et al.* (2010). The thermal state of permafrost in the nordic area during the international polar year 2007–2009. *Permafrost and Periglacial Processes*, *21*(2), 156–181.

Ciais, P., Sabine, C., Bala, G., Bopp, L., Brovkin, V., Canadell, J., Chhabra, A., DeFries, R., Galloway, J., Heimann, M., *et al.* (2014). Carbon and other biogeochemical cycles, In *Climate change 2013: The physical science basis. contribution of working group i to the fifth assessment report of the intergovernmental panel on climate change*. Cambridge University Press.

Collins, M., Knutti, R., Arblaster, J., Dufresne, J.-L., Fichefet, T., Friedlingstein, P., Gao, X., Gutowski, W., Johns, T., G.Krinner, Shongwe, M., Tebaldi, C., Weaver, A., & Wehner, M. (2013). Long-term climate change: Projections, commitments and irreversibility - ipcc 2013. *Cambridge University Press*, 1029–1136.

Comiso, J., Parkinson, C., Gersten, R., & Stock, L. (2007). Accelerated decline in the arctic sea ice cover. *Geophys. Res. Lett.*, *35*(L01703), 1533–1536. https://doi.org/10.1029/2007GL031972

Comiso, J. C. (2003). Warming trends in the arctic from clear sky satellite observations. *Journal of Climate*, *16*(21), 3498–3510.

Craig, H. (1961). Isotopic variations in meteoric waters. *Science*, *133*(3465), 1702–1703.

Criss, R. E. *et al.* (1999). *Principles of stable isotope distribution*. Oxford University Press on Demand.

Dansgaard, W. (1964). Stable isotopes in precipitation. *Tellus*, *16*(4), 436–468.

Dunton, T., & Carmack, E. C. (2006). The nearshore western beaufort sea ecosystem: Circulation and importance of terrestrial carbon in arctic coastal food webs. *Progress in Oceanography*, *71*(2-4), 362–378.

Eicken, H., Reimnitz, E., Alexandrov, V., Martin, T., Kassens, H., & Viehoff, T. (1997). Sea-ice processes in the laptev sea and their importance for sediment export. *Continental Shelf Research*, *17*(2), 205–233.

Eicken, H., Dmitrenko, I., Tyshko, K., Darovskikh, A., Dierking, W., Blahak, U., Groves, J., & Kassens, H. (2005). Zonation of the laptev sea landfast ice cover and its importance in a frozen estuary. *Global and Planetary Change*, *48*(1-3), 55–83.

Fettweis, M. P., & Nechad, B. (2011). Evaluation of in situ and remote sensing sampling methods for spm concentrations, belgian continental shelf (southern north sea). *Ocean Dynamics*, *61*(2-3), 157–171.

Fichot, C. G., Kaiser, K., Hooker, S. B., Amon, R. M., Babin, M., Bélanger, S., Walker, S. A., & Benner, R. (2013). Pan-arctic distributions of continental runoff in the arctic ocean. *Scientific Reports*, *3*, 1053.

Forbes, D. (1983). Morphology and sedimentology of a sinuous gravel-bed channel system: Lower babbage river, yukon coastal plain, canada, In *Modern and ancient fluvial systems*. Inter. Assoc. Sedim. Spec. Publ., 6.

Forbes, D. L. (1981). *Babbage river delta and lagoon: Hydrology and sedimentology of an arctic estuarine system* (Doctoral dissertation). University of British Columbia.

Freeman, C., Evans, C., Monteith, D., Reynolds, B., & Fenner, N. (2001). Export of organic carbon from peat soils. *Nature*, *412*(6849), 785–785.

Freeman, C., Fenner, N., Ostle, N., Kang, H., Dowrick, D., Reynolds, B., Lock, M., Sleep, D., Hughes, S., & Hudson, J. (2004). Export of dissolved organic carbon from peatlands under elevated carbon dioxide levels. *Nature*, *430*(6996), 195–198.

French, H. M., & Williams, P. (1976). *The periglacial environment* (Vol. 341). Wiley Online Library.

Frey, K. E., & Smith, L. C. (2005). Amplified carbon release from vast west siberian peatlands by 2100. *Geophys. Res. Lett.*, *32*(L09401), 195–198. https://doi.org//10.1029/2004GL022025.

Friedlingstein, P., Jones, M., O'sullivan, M., Andrew, R., Hauck, J., Peters, G., Peters, W., Pongratz, J., Sitch, S., Le Quéré, C., *et al.* (2019). Global carbon budget 2019. *Earth System Science Data*, *11*(4), 1783–1838.

Fritz, M., Opel, T., Tanski, G., Herzschuh, U., Meyer, H., Eulenburg, A., & Lantuit, H. (2015). Dissolved organic carbon (doc) in arctic ground ice. *The Cryosphere Discussions*, *9*(1), 77–114. https://doi.org/10.5194/tc-9-737-2015

Fritz, M., Vonk, J. E., & Lantuit, H. (2017). Collapsing arctic coastlines. *Nature Climate Change*, *7*(1), 6–7.

Fritz, M., Wetterich, S., Meyer, H., Schirrmeister, L., Lantuit, H., & Pollard, W. H. (2011). Origin and characteristics of massive ground ice on herschel island (western canadian arctic) as revealed by stable water isotope and hydrochemical signatures. *Permafrost and Periglacial Processes*, *22*(1), 26–38.

Fritz, M., Wetterich, S., Schirrmeister, L., Meyer, H., Lantuit, H., Preusser, F., & Pollard, W. H. (2012). Eastern beringia and beyond: Late wisconsinan and holocene landscape dynamics along the yukon coastal plain, canada. *Palaeogeography, Palaeoclimatology, Palaeoecology*, *319*, 28–45.

Gat, J. R. (1996). Oxygen and hydrogen isotopes in the hydrologic cycle. *Annual Review of Earth and Planetary Sciences*, *24*(1), 225–262.

Giannelli, V., Thomas, D. N., Haas, C., Kattner, G., Kennedy, H., & Dieckmann, G. S. (2001). Behaviour of dissolved organic matter and inorganic nutrients during experimental sea-ice formation. *Annals of Glaciology*, *33*, 317–321.

GISTEMP, T. (2016). Giss surface temperature analysis (gistemp). *NASA Goddard Institute for Space Studies. Dataset accessed*, 06–16.

Gov.Canada. (n.d.). *Weather, climate and hazard*. https://climate.weather.gc.ca/ (accessed: 20.08.2020)

Gowan, E. J., Tregoning, P., Purcell, A., Montillet, J.-P., & McClusky, S. (2016). A model of the western laurentide ice sheet, using observations of glacial isostatic adjustment. *Quaternary Science Reviews*, *139*, 1–16.

Grotheer, H., Meyer, V., Riedel, T., Pfalz, G., Mathieu, L., Hefter, J., Gentz, T., Lantuit, H., Mollenhauer, G., & Fritz, M. (2020). Burial and origin of permafrost-derived carbon in the nearshore zone of the southern canadian beaufort sea. *Geophysical Research Letters*, *47*(3), e2019GL085897.

Günther, F., Overduin, P. P., Yakshina, I. A., Opel, T., Baranskaya, A. V., & Grigoriev, M. N. (2015). Observing muostakh disappear: Permafrost thaw subsidence and erosion of a ground-ice-rich island in response to arctic summer warming and sea ice reduction. *The Cryosphere*, *9*(1), 151–178.

Hansell, D., & Carlson, C. (2001). Marine dissolved organic matter and the carbon cycle. *Oceanography*, *14*(4), 41–49. https://doi.org/10.5670/oceanog.2001.05

Hansen, J., Ruedy, R., Sato, M., & Lo, K. (2010). Global surface temperature change. *Rev. Geophys.*, *48*(RG4004), 1–29. https://doi.org/10.1029/2010RG000345

Harper, J. R. (1990). Morphology of the canadian beaufort sea coast. *Marine Geology*, *91*(1-2), 75–91.

Hjort, J., Karjalainen, O., Aalto, J., Westermann, S., Romanovsky, V. E., Nelson, F. E., Etzelmüller, B., & Luoto, M. (2018). Degrading permafrost puts arctic infrastructure at risk by mid-century. *Nature Communications*, *9*(1), 1–9.

Hoge, F. E., Vodacek, A., Swift, R. N., Yungel, J. K., & Blough, N. V. (1995). Inherent optical properties of the ocean: Retrieval of the absorption coefficient of chromophoric dissolved organic matter from airborne laser spectral fluorescence measurements. *Applied Optics*, *34*(30), 7032–7038.

Holmes, R. M., McClelland, J. W., Peterson, B. J., Shiklomanov, I. A., Shiklomanov, A. I., Zhulidov, A. V., Gordeev, V. V., & Bobrovitskaya, N. N. (2002). A circumpolar perspective on fluvial sediment flux to the arctic ocean. *Global Biogeochemical Cycles*, *16*(4), 45–1.

Holmes, R. M., McClelland, J. W., Peterson, B. J., Tank, S. E., Bulygina, E., Eglinton, T. I., Gordeev, V. V., Gurtovaya, T. Y., Raymond, P. A., Repeta, D. J., *et al.* (2012). Seasonal and annual fluxes of nutrients and organic matter from large rivers to the arctic ocean and surrounding seas. *Estuaries and Coasts*, *35*(2), 369–382.

Irrgang, A., Lantuit, H., Gordon, R., Piskor, A., & Manson, G. K. (2018). Impacts of coastal dynamics on the socio-economic component of the yukon coast, western canadian arctic.

Jong, D., Bröder, L., Tanski, G., Fritz, M., Lantuit, H., Tesi, T., Haghipour, N., Eglinton, T. I., & Vonk, J. E. (2020). Nearshore zone dynamics determine pathway of organic carbon from eroding permafrost coasts. *Geophysical Research Letters*, e2020GL088561.

Jouzel, J. (2003). Water stable isotopes: Atmospheric composition and applications in polar ice core studies. *Treatise on Geochemistry*, *4*, 347.

Juhls, B., Stedmon, C. A., Morgenstern, A., Meyer, H., Hölemann, J., Heim, B., Povazhnyi, V., & Overduin, P. P. (2020). Identifying drivers of seasonality in lena river biogeochemistry and dissolved organic matter fluxes. *Frontiers in Environmental Science*, *8*, 53.

Juul-Pedersen, T., Michel, C., & Gosselin, M. (2008). Influence of the mackenzie river plume on the sinking export of particulate material on the shelf. *Journal of Marine Systems*, *74*(3-4), 810–824.

Klock, R., Hudson, E., Aihoshi, D., & Mullock, J. (2001). Seasonal weather and local effects northern yukon including the yukon coast and herschel island. *Graphic Area Forecast*, *35*, 83–135.

Köchy, M., Hiederer, R., & Freibauer, A. (2015). Global distribution of soil organic carbon–part 1: Masses and frequency distributions of soc stocks for the tropics, permafrost regions, wetlands, and the world. *Soil*, *1*(1), 351–365.

Lake, R., & Lewis, E. (1970). Salt rejection by sea ice during growth. *Journal of Geophysical Research*, *75*(3), 583–597.

Lantuit, H., Overduin, P. P., Couture, N., Wetterich, S., Aré, F., Atkinson, D., Brown, J., Cherkashov, G., Drozdov, D., Forbes, D. L., *et al.* (2012). The arctic coastal dynamics database: A new classification scheme and statistics on arctic permafrost coastlines. *Estuaries and Coasts*, *35*(2), 383–400.

Larsen, J. N., & Fondahl, G. (2015). *Arctic human development report: Regional processes and global linkages*. Nordic Council of Ministers.

Lenssen, N. J., Schmidt, G. A., Hansen, J. E., Menne, M. J., Persin, A., Ruedy, R., & Zyss, D. (2019). Improvements in the gistemp uncertainty model. *Journal of Geophysical Research: Atmospheres*, *124*(12), 6307–6326.

Létolle, R., Martin, J., Thomas, A., Gordeev, V., Gusarova, S., & Sidorov, I. (1993). 18o abundance and dissolved silicate in the lena delta and laptev sea (russia). *Marine Chemistry*, *43*(1-4), 47–64.

Lewis, E., Jones, E., Lemke, P., Prowse, T., & Wadhams, P. ((2000). *Introduction. in: Lewis el (ed) the freshwater budget of the arctic ocean*. Berlin, Heidelberg, © Springer-Verlag.

Li, J., Chen, X., Tian, L., Huang, J., & Feng, L. (2015). Improved capabilities of the chinese high-resolution remote sensing satellite gf-1 for monitoring suspended particulate matter (spm) in inland waters: Radiometric and spatial considerations. *ISPRS Journal of Photogrammetry and Remote Sensing*, *106*, 145–156.

Lobbes, J. M., Fitznar, H. P., & Kattner, G. (2000). Biogeochemical characteristics of dissolved and particulate organic matter in russian rivers entering the arctic ocean. *Geochimica et Cosmochimica Acta*, *64*(17), 2973–2983.

Longnecker, K. (2015). Dissolved organic matter in newly formed sea ice and surface seawater. *Geochimica et Cosmochimica Acta*, *171*, 39–49.

Loring, D. H., & Rantala, R. T. (1992). Manual for the geochemical analyses of marine sediments and suspended particulate matter. *Earth-Science Reviews*, *32*(4), 235–283.

Macdonald, R. W., Paton, D. W., Carmack, E. C., & Omstedt, A. (1995). The freshwater budget and under-ice spreading of mackenzie river water in the canadian beaufort sea based on salinity and 18o/16o measurements in water and ice. *Journal of Geophysical Research: Oceans*, *100*(C1), 895–919.

Macdonald, R., Carmack, E., & Paton, D. (1999). Using the $\delta 18o$ composition in landfast ice as a record of arctic estuarine processes. *Marine Chemistry*, *65*, 3–24. https://doi.org//10.1016/S0304-4203(99)00007-9

Macdonald, R., Solomon, S., Cranston, R., Welch, H., Yunker, M., & Gobeil, C. (1998). A sediment and organic carbon budget for the canadian beaufort shelf. *Marine Geology*, *144*(4), 255–273.

Mackay, J. R. (1959). Glacier ice-thrust features of the yukon coast. *Geographical Bulletin*, *13*(5), 21.

Maslanik, J., Fowler, C., Stroeve, J., Drobot, S., Zwally, J., Yi, D., & Emery, W. (2007). A younger, thinner arctic ice cover: Increased potential for rapid, extensive sea-ice loss. *Geophys. Res. Lett.*, *34*(L24501), 1533–1536. https://doi.org/10.1029/2007GL032043

Matsuoka, A., Boss, E., Babin, M., Karp-Boss, L., Hafez, M., Chekalyuk, A., Proctor, C., Werdell, P. J., & Bricaud, A. (2017). Pan-arctic optical characteristics of colored dissolved organic matter: Tracing dissolved organic carbon in changing arctic waters using satellite ocean color data. *Remote Sensing of Environment*, *200*(L09401), 89–101. https://doi.org//10.1016/j.rse.2017.08.009

Matsuoka, A., Bricaud, A., Benner, R., Para, J., Sempéré, R., Prieur, L., Bélanger, S., & Babin, M. (2012). Tracing the transport of colored dissolved organic matter in water masses of the southern beaufort sea: Relationship with hydrographic characteristics. *Biogeosciences*, *9*. https://doi.org//10.5194/bg-9-925-2012

Matsuoka, A., Hill, V., Huot, Y., Babin, M., & Bricaud, A. (2011). Seasonal variability in the light absorption properties of western arctic waters: Parameterization of the individual components of absorption for ocean color applications. *Journal of Geophysical Research: Oceans*, *116*(C2).

Matsuoka, A., Huot, Y., Shimada, K., Saitoh, S.-I., & Babin, M. (2007). Bio-optical characteristics of the western arctic ocean: Implications for ocean color algorithms. *Canadian Journal of Remote Sensing*, *33*(6), 503–518.

Maykut, G., Grenfell, T., & Weeks, W. (1992). On estimating spatial and temporal variations in the properties of ice in the polar oceans. *Journal of Marine Systems*, *3*(1-2), 41–72.

McClelland, J., Holmes, R., Peterson, B., Raymond, P., Striegl, R., Zhulidov, A., Zimov, S., Zimov, N., Tank, S., Spencer, R., *et al.* (2016). Particulate organic carbon and nitrogen export from major arctic rivers. *Global Biogeochemical Cycles*, *30*(5), 629–643.

Meehl, G., Stocker, T., Collins, W., Friedlingstein, P., Gaye, A., Knutti, J. G. A. K. R., Murphy, J., Noda, A., Raper, S., Watterson, I., Weaver, A., & Zhao, Z.-C. (2007). Global climate projections - ipcc 2007. *Cambridge University Press*, 747–845.

Meyer, H., Derevyagin, A. Y., S., C., & Hubberten, H.-W. (2002). Paleoclimate studies on bykovsky peninsula, north siberia-hydrogen and oxygen isotopes in ground ice. *Polarforschung*, *70*, 37–51.

Meyer, H., Schönicke, L., Wand, U., Hubberten, H.-W., & Friedrichsen, H. (2000). Isotope studies of hydrogen and oxygen in ground ice-experiences with the equilibration technique. *Isotopes in Environmental and Health Studies*, *36*(2), 133–149.

Moran, M. A., & Zepp, R. G. (1997). Role of photoreactions in the formation of biologically labile compounds from dissolved organic matter. *Limnology and Oceanography*, *42*(6), 1307–1316.

Mulligan, R. P., Perrie, W., & Solomon, S. (2010). Dynamics of the mackenzie river plume on the inner beaufort shelf during an open water period in summer. *Estuarine, Coastal and Shelf Science*, *89*(3), 214–220.

Nakawo, M., & Sinha, N. K. (1981). Growth rate and salinity profile of first-year sea ice in the high arctic. *Journal of Glaciology*, *27*(96), 315–330.

Neff, J., Finlay, J. C., Zimov, S., Davydov, S., Carrasco, J., Schuur, E., & Davydova, A. (2006). Seasonal changes in the age and structure of dissolved organic carbon in siberian rivers and streams. *Geophysical Research Letters*, *33*(23).

Nghiem, S., Hall, D., Rigor, I., Li, P., & Neumann, G. (2014). Effects of mackenzie river discharge and bathymetry on sea ice in the beaufort sea. *Geophysical Research Letters*, *41*(3), 873–879.

Norman, L., Thomas, D. N., Stedmon, C. A., Granskog, M. A., Papadimitriou, S., Krapp, R. H., Meiners, K. M., Lannuzel, D., van der Merwe, P., & Dieckmann, G. S. (2011). The characteristics of dissolved organic matter (dom) and chromophoric dissolved organic matter (cdom) in antarctic sea ice. *Deep Sea Research Part II: Topical Studies in Oceanography*, *58*(9-10), 1075–1091.

O'brien, M., Macdonald, R., Melling, H., & Iseki, K. (2006). Particle fluxes and geochemistry on the canadian beaufort shelf: Implications for sediment transport and deposition. *Continental Shelf Research*, *26*(1), 41–81.

Östlund, H. G., & Hut, G. (1984). Arctic ocean water mass balance from isotope data. *Journal of Geophysical Research: Oceans*, *89*(C4), 6373–6381.

Pepin, N., Bradley, R. S., Diaz, H., Baraër, M., Caceres, E., Forsythe, N., Fowler, H., Greenwood, G., Hashmi, M., Liu, X., *et al.* (2015). Elevation-dependent warming in mountain regions of the world. *Nature Climate Change*, *5*(5), 424–430.

Petit, J., Jouzel, J., & Raynaud, D. e. a. (1999). Climate and atmospheric history of the past 420,000 years from the vostok ice core, antarctica. *Nature*, *399*, 429–436. https://doi.org/10.1038/20859

Petrich, C., & Eicken, H. (2010). Growth, structure and properties of sea ice. *Sea ice*, *2*, 23–77.

Pfirman, S., Eicken, H., Bauch, D., & Weeks, W. (1995). The potential transport of pollutants by arctic sea ice. *Science of the Total Environment*, *159*(2-3), 129–146.

Rachold, V., Eicken, H., Gordeev, V., Grigoriev, M. N., Hubberten, H.-W., Lisitzin, A. P., Shevchenko, V., & Schirrmeister, L. (2004). Modern terrigenous organic carbon input to the arctic ocean, In *The organic carbon cycle in the arctic ocean*. Springer.

Radosavljevic, B., Lantuit, H., Pollard, W., Overduin, P., Couture, N., Sachs, T., Helm, V., & Fritz, M. (2016). Erosion and flooding—threats to coastal infrastructure in the arctic: A case study from herschel island, yukon territory, canada. *Estuaries and Coasts*, *39*(4), 900–915.

Rampton, V. N. (1982). Quaternary geology of the yukon coastal plain.

Raymond, P., McClelland, J., Holmes, R., Zhulidov, A., Mull, K., Peterson, B., Striegl, R., Aiken, G., & Gurtovaya, T. (1999). Flux and age of dissolved organic carbon exported to the arctic ocean: A carbon isotopic study of the five largest arctic rivers. *Glob. Biogeochem. Cycles*, *21*(GB4011), 3–24. https://doi.org//10.1029/2007GB002934

Redfield, A. C., & Friedman, I. (1969). The effect of meteoric water, melt water and brine on the composition of polar sea water and of the deep waters of the ocean.

Reimnitz, E., Toimil, L., & Barnes, P. (1978). Arctic continental shelf morphology related to sea-ice zonation, beaufort sea, alaska. *Marine Geology*, *28*(3-4), 179–210.

Romanovsky, V., Gruber, S., Instanes, A., Jin, H., Marchenko, S., Smith, S., Trombotto, D., & Walter, K. (2007). Frozen ground. *Global outlook for ice and snow*, 181–200.

Rudels, B., Anderson, L., & Jones, E. (1996). Formation and evolution of the surface mixed layer and halocline of the arctic ocean. *Journal of Geophysical Research: Oceans*, *101*(C4), 8807–8821.

Sathyendranath, S. ((2000). Remote sensing of ocean colour in coastal, and other optically-complex, waters. *IOCCG*, *3*.

Schaefer, K., Lantuit, H., Romanovsky, V. E., Schuur, E. A., & Witt, R. (2014). The impact of the permafrost carbon feedback on global climate. *Environmental Research Letters*, *9*(8), 085003.

Schuur, E., McGuire, A., Schädel, C., & et al. (2015). Climate change and the permafrost carbon feedback. *Nature*, *520*, 170–179. https://doi.org//10.1038/nature14338

Screen, J. A., & Simmonds, I. (2010). The central role of diminishing sea ice in recent arctic temperature amplification. *Nature*, *464*(7293), 1334–1337.

Searcy, C., Dean, K., & Stringer, W. (1996). A river-coastal sea ice interaction model: Mackenzie river delta. *Journal of Geophysical Research: Oceans*, *101*(C4), 8885–8894.

Serreze, M., Barrett, A., Stroeve, J., Kindig, D., & Holland, M. (2009). The emergence of surface-based arctic amplification. *The Cryosphere*, *3*(1), 11.

Serreze, M., Holland, M., & Stroeve, J. (2007). Perspectives on the arctic's shrinking sea-ice. *Science*, *315*, 1533–1536. https://doi.org/10.1126/science.1139426

Shiklomanov, I. (1993). World fresh water resources, water in crisis: A guide to the world's fresh water resources. Oxford University Press, New York.

Slater, T., Hogg, A. E., & Mottram, R. (2020). Ice-sheet losses track high-end sea-level rise projections. *Nature Climate Change*, 1–3.

Souchez, R., Jouzel, J., Lorrain, R., Sleewaegen, S., Stiévenard, M., & Verbeke, V. (2000). A kinetic isotope effect during ice formation by water freezing. *Geophysical Research Letters*, *27*(13), 1923–1926.

Stedmon, C., Amon, R., Rinehart, A., & Walker, S. (2011). The supply and characteristics of colored dissolved organic matter (cdom) in the arctic ocean: Pan arctic trends and differences. *Marine Chemistry*, *124*(1-4), 108–118.

Stedmon, C. A., Thomas, D. N., Granskog, M., Kaartokallio, H., Papadimitriou, S., & Kuosa, H. (2007). Characteristics of dissolved organic matter in baltic coastal sea ice: Allochthonous or autochthonous origins? *Environmental Science & Technology*, *41*(21), 7273–7279.

Stein, R., Macdonald, R. W., Stein, R., & MacDonald, R. W. (2004). *The organic carbon cycle in the arctic ocean*. Springer.

Stroeve, J., Markus, T., Boisvert, L., Miller, J., & Barrett, A. (2014). Changes in arctic melt season and implications for sea ice loss. *Geophysical Research Letters*, *41*(4), 1216–1225.

Tanski, G., Wagner, D., C., K., Fritz, M., & Sachs T. & Lantuit, H. (2019). Rapid co_2 release from eroding permafrost in seawater. *Geophysical Research Letters*, *46*(11), 244–11, 252. https://doi.org/10.1029/2019GL084303

Thomas, D. N., Kattner, G., Engbrodt, R., Giannelli, V., Kennedy, H., Haas, C., & Dieckmann, G. S. (2001). Dissolved organic matter in antarctic sea ice. *Annals of Glaciology*, *33*, 297–303.

Thomas, D. N., Lara, R. J., Eicken, H., Kattner, G., & Skoog, A. (1995). Dissolved organic matter in arctic multi-year sea ice during winter: Major components and relationship to ice characteristics. *Polar Biology*, *15*(7), 477–483.

Van Everdingen, R. (2005). Multi-language glossary of permafrost and related ground-ice terms. national snow and ice data center/world data center for glaciology, boulder, co. *World Wide Web Address: http://nsidc. org/fgdc/glossary*.

Vieira, G., Bockheim, J., Guglielmin, M., Balks, M., Abramov, A. A., Boelhouwers, J., Cannone, N., Ganzert, L., Gilichinsky, D. A., Goryachkin, S., *et al.* (2010). Thermal state of permafrost and active-layer monitoring in the antarctic: Advances during the international polar year 2007–2009. *Permafrost and Periglacial Processes*, *21*(2), 182–197.

Walker, S. A., Amon, R. M., & Stedmon, C. A. (2013). Variations in high-latitude riverine fluorescent dissolved organic matter: A comparison of large arctic rivers. *Journal of Geophysical Research: Biogeosciences*, *118*(4), 1689–1702.

Weeks, W. F., & Ackley, S. F. (1986). The growth, structure, and properties of sea ice, In *The geophysics of sea ice*. Springer.

Weeks, W. (2010). *On sea ice*. University of Alaska Press.

Wegner, C., Bennett, K. E., de Vernal, A., Forwick, M., Fritz, M., Heikkilä, M., Łacka, M., Lantuit, H., Laska, M., Moskalik, M., *et al.* (2015). Variability in transport of terrigenous material on the shelves and the deep arctic ocean during the holocene. *Polar Research*, *34*(1), 24964.

Weise, O. (1983). *Das periglazial: Geomorphologie und klima in gletscherfreien, kalten regionen; mit 6 tabellen*. Borntraeger.

Weishaar, J. L., Aiken, G. R., Bergamaschi, B. A., Fram, M. S., Fujii, R., & Mopper, K. (2003). Evaluation of specific ultraviolet absorbance as an indicator of the chemical composition and reactivity of dissolved organic carbon. *Environmental Science & Technology*, *37*(20), 4702–4708.

Woo, M., & Thorne, R. (2003). Streamflow in the mackenzie basin, canada. *Arctic*, 328–340.

Acknowledgements

Foremost, I would like to express my sincere gratitude to Hugues Lantuit and Michael Fritz for giving me the chance of participating in their workgroup and to let me make this extremely interesting study with them and at the Alfred-Wegener-Institute for the period of one whole year.
In particular I would like to pay my special regards to Michael Fritz who served as the first advisor of this thesis project. The door to Dr. Fritz's office was always open whenever I ran into a trouble spot or had a question about my research or writing and this even through, the troubled times of a pandemic. He consistently allowed this paper to be my own work, but steered me in the right direction whenever he thought I needed it. Thank you for your invested time, your help all along the different parts of the project, from the first briefing and working together in the various laboratories, to the many joint meetings (online and offline) and to the great support during the writing process. Without your knowledge, brought in thoughts and hints, your patience and your friendly character, this thesis would have not been possible.
I wish to show my gratitude as well to Bennet Juhls who served as my second supervisor for this thesis. I appreciated very much the many hours you spent on introducing to me Python programming as well as the work in the hydrochemistry laboratories.
I would also like to thank the experts who were involved in the validation survey for this research project: Prof. Dr. Liane Benning from the Freie Universität Berlin / German Research Centre for Geosciences Potsdam and Prof. Dr. Hugues Lantuit from the University of Potsdam / Alfred-Wegener-Institute.
I would also like to acknowledge to the technical assitance of the PERMA research team by Antje Eulenberg and the invaluable introductions to the different apparatus and machines the assistance that she provided during the many weeks I spent at her labortory.
Thanks also for Dr. Hanno Meyer and his team for processing the samples of this study at his labortory, tank you also for your interesting introduction to your laboratory and the talk and advises afterwards.

I am also indebted to Dr. Patrick Littlewood and his invested time at the very end of this process and providing me with such a great feedback.
I would also like to say thanks to my parents for believing in me and keeping up with me on these not always conventional paths I have taken. Finally, I must express my very profound gratitude to Alixia for providing me with unfailing support and continuous encouragement throughout the years of my study and through the process of researching and writing this thesis. This accomplishment would not have been possible without you. Thank you.

Appendix A

Ice samples

Sample ID	Depths [m]	Meltw. [L]	Salinity [g/L]	δ18O	δD	D-excess	DOC [mg/L]	CDOM [254]	SUVA [$m^2 gC^{1}$]	SPM [mg/L]
ICE-01_0-37	0,185	1,03	4,5	-3,6	-28,4	0,70	0,94	1,39	0,64	0,0031
ICE-01_133-168	1,505	0,89	3,9	-0,5	-4,4	-0,31	0,90	0,65	0,31	0,0045
ICE-01_37-68	0,525	0,85	3,6	-2,9	-19,4	3,69	0,76	2,15	1,22	0,0020
ICE-01_68-78-98	0,83	0,975	2,9	-2,7	-22,2	-0,45	0,75	1,10	0,64	0,0020
ICE-01_98-133	1,155	0,91	3	-1,9	-14,8	0,03	0,63	1,05	0,72	0,0015
ICE-02_0-25-31	0,155	0,865	3,3	-3,1	-24,2	0,31	0,55	1,24	0,98	0,0030
ICE-02_31-63	0,47	1,03	3,1	-2,8	-22,4	-0,12	0,52	1,17	0,98	0,0021
ICE-02_63-98	0,805	0,95	3,3	-2,0	-15,7	-0,08	0,47	0,97	0,90	0,0015
ICE-02_98-109-133	1,155	0,96	2,7	-0,5	-2,5	1,20	0,51	0,33	0,28	0,0016
ICE-03_0-30	0,15	0,88	3,2	-4,3	-35,2	-1,07	0,59	1,57	1,15	0,0028
ICE-03_117-141	1,29	0,94	3,5	0,0	-2,2	-1,97	0,58	0,61	0,46	0,0020
ICE-03_30-42-61	0,455	0,9	2,8	-2,6	-22,1	-1,12	0,40	0,88	0,96	0,0015
ICE-03_61-93	0,77	0,715	3,2	-2,1	-18,0	-0,90	0,49	0,91	0,80	0,0013
ICE-03_93-117	1,05	0,59	2,5	-1,1	-7,5	0,99	0,44	0,70	0,69	0,0023
ICE-04_0-19	0,095	0,625	3,8	-3,4	-27,7	-0,69	0,54	0,84	0,68	0,0046
ICE-04_107-129	1,18	0,93	3,5	-0,2	1,1	2,46	0,51	0,75	0,64	0,0029
ICE-04_19-51	0,35	0,83	3,2	-2,5	-19,9	-0,05	0,50	0,97	0,83	0,0011
ICE-04_51-79	0,65	0,85	3	-2,4	-15,8	3,36	0,47	1,08	0,99	0,0024
ICE-04_79-107	0,93	0,665	2,4	-1,2	-5,7	3,70	0,39	0,84	0,95	0,0006

Sample ID	Depths [m]	Meltw. [L]	Salinity [g/L]	δ18O	δD	D-excess	DOC [mg/L]	CDOM [254]	SUVA [$m^2 gC^{1}$]	SPM [mg/L]
ICE-05_0-35	0,175	0,82	3,6	-2,8	-18,9	3,70	0,76	1,17	0,67	0,0052
ICE-05_105-124	1,145	0,56	1,8	-1,8	-12,9	1,32	0,52	1,46	1,22	0,0053
ICE-05_124-145	1,345	0,615	1,7	-1,0	-6,9	1,32	0,61	1,11	0,79	0,0078
ICE-05_145-167	1,56	0,74	2,4	-0,4	-2,2	0,94	0,53	1,28	1,04	0,0098
ICE-05_167-187	1,77	0,495	3,9	-0,3	-3,2	-1,21	0,79	1,19	0,65	0,0122
ICE-05_35-56	0,455	0,57	3,2	-2,8	-18,9	3,65	0,60	0,36	0,26	0,0063
ICE-05_56-78	0,67	0,58	2,8	-4,3	-32,7	1,72	0,63	0,54	0,37	0,0205
ICE-05_78-105	0,915	0,5	2,5	-2,7	-21,5	0,27	0,80	1,01	0,55	0,0237
ICE-06_0-30	0,15	0,87	3,9	-3,1	-23,8	0,91	0,59	0,89	0,65	0,0024
ICE-06_100-133	1,165	0,97	3,4	-0,4	0,5	3,41	0,91	0,85	0,40	0,0046
ICE-06_30-73	0,515	0,93	3,1	-2,8	-21,4	1,23	0,50	1,34	1,16	0,0017
ICE-06_73-100	0,865	0,86	3,2	-1,2	-5,3	4,41	0,64	1,73	1,18	0,0014
ICE-07_0-15	0,075	0,46	3,1	-3,4	-27,6	-0,72	0,90	1,68	0,81	0,0151
ICE-07_106-120	1,13	0,85	4,6	-0,2	-1,7	-0,46	0,83	0,71	0,37	0,0022
ICE-07_15-44	0,295	0,895	2,8	-3,6	-28,2	0,28	0,57	1,19	0,91	0,0096
ICE-07_44-73	0,585	0,96	3,5	-3,2	-25,5	0,15	0,50	1,50	1,30	0,0067
ICE-07_73-106	0,895	0,4	3,5	-1,0	-8,1	-0,16	0,46	0,98	0,92	0,0018
ICE-08_0-26	0,13	0,8	1,2	-14,4	-114,4	1,04	1,43	5,76	1,74	0,0258
ICE-08_103-117-138	1,205	0,95	2	-8,2	-64,2	1,73	0,73	3,53	2,11	0,0177

Sample ID	Depths [m]	Meltw. [L]	Salinity [g/L]	δ18O	δD	D-excess	DOC [mg/L]	CDOM [254]	SUVA [$m^2 gC^{1}$]	SPM [mg/L]
ICE-08_138-156-177	1,575	0,98	2,1	-6,0	-49,1	-0,76	0,74	2,52	1,47	0,0252
ICE-08_26-61	0,435	0,87	1,9	-7,9	-64,2	-0,68	0,80	1,76	0,96	0,0666
ICE-08_61-97-103	0,82	0,995	1,9	-8,1	-65,8	-0,62	0,76	1,97	1,13	0,0203
ICE-09_0-30	0,15	0,85	4,1	-2,9	-23,0	0,53	0,58	1,15	0,86	0,0063
ICE-09_100-139	1,195	0,97	3,2	-0,7	-4,5	1,02	0,52	0,76	0,63	0,0031
ICE-09_30-63	0,465	1,04	3	-2,9	-25,2	-1,75	0,44	0,98	0,96	0,0033
ICE-09_63-100	0,815	1,02	3,4	-2,2	-19,1	-1,55	0,47	0,98	0,90	0,0029
ICE-10_0-22	0,11	0,715	3,1	-3,1	-23,0	1,89	0,45	0,91	0,88	0,0030
ICE-10_103-126	1,145	0,67	2,9	-0,5	-0,1	3,64	0,52	1,05	0,88	0,0027
ICE-10_22-45	0,335	0,95	3	-3,1	-22,1	3,03	0,47	0,59	0,54	0,0039
ICE-10_45-80	0,625	0,62	3,2	-2,8	-18,9	3,21	0,49	0,81	0,72	0,0014
ICE-10_80-103	0,915	0,67	2,8	-1,4	-8,9	2,51	0,60	1,01	0,73	0,0048
ICE-11_0-23-41	0,205	1,08	3,7	-3,1	-23,4	1,61	0,50	1,17	1,02	0,0015
ICE-11_41-69	0,55	0,94	2,9	-2,8	-21,2	1,44	0,48	0,93	0,84	0,0012
ICE-11_69-99	0,84	0,9	3	-1,7	-9,7	3,46	0,41	0,62	0,66	0,0009
ICE-11_99-108-127	1,13	0,8	3	-0,5	-0,3	3,52	0,55	1,12	0,88	0,0030
ICE-12_0-30	0,15	0,88	3,4	-3,2	-23,2	2,34	0,63	1,28	0,88	0,0039
ICE-12_111-131	1,21	0,94	3	-0,1	0,7	1,45	0,68	0,77	0,49	0,0020
ICE-12_30-60	0,45	0,93	3,3	-3,0	-22,2	1,43	0,53	0,91	0,74	0,0019

Sample ID	**Depths [m]**	**Meltw. [L]**	**Salinity [g/L]**	**δ18O**	**δD**	**D-excess**	**DOC [mg/L]**	**CDOM [254]**	**SUVA [$m^2 gC^{1}$]**	**SPM [mg/L]**
ICE-12_60-90	0,75	0,66	3,1	-2,1	-14,7	2,42	0,46	0,89	0,84	0,0019
ICE-12_90-111	1,005	0,55	2,3	-0,9	-6,3	0,90	0,36	1,36	1,63	0,0002
Blank_01	-	1,8	0	-	-	-	0,22	0,01	0	-0,0001
Blank_02	-	1,8	0	-	-	-	0,23	0,00	0	-0,0003
Blank_03	-	1,8	0	-	-	-	0,25	0,00	0	-0,0001

Appendix B

Water samples

Sample ID	**Depths [m]**	**Salinity [g/L]**	$\delta 18O$	δD	**D-excess**	**DOC [mg/L]**	**cDOM [254]**	**SUVA** $[m^2 gC^{1}]$	**SPM [mg/L]**
YC19-WAT-01	2	32,0	-2,7	-18,4	3,2	1,68	4,20	1,09	8,17
YC19-WAT-01	4,5	32,4	-2,8	-18,7	3,4	1,41	3,42	1,06	14,92
YC19-WAT-01	8	32,7	-2,7	-18,1	3,6	1,15	3,20	1,21	17,06
YC19-WAT-02	2	32,8	-2,7	-18,4	3,4	1,11	3,45	1,35	10,35
YC19-WAT-02	18	33,4	-2,6	-16,9	3,9	1,03	2,94	1,23	9,85
YC19-WAT-02	36	33,7	-2,6	-16,8	3,7	1,09	3,23	1,29	8,63
YC19-WAT-03	2	32,9	-2,9	-18,8	4,1	1,09	2,79	1,12	8,40
YC19-WAT-03	14	33,5	-2,3	-16,2	2,3	1,10	3,40	1,34	10,21
YC19-WAT-03	37	33,5	-2,5	-17,1	3,1	1,07	2,97	1,20	9,55
YC19-WAT-04	2	33,1	-2,8	-18,9	3,1	1,14	2,52	0,96	9,05
YC19-WAT-04	30	34,7	-2,5	-17,5	2,1	1,05	2,57	1,07	8,20
YC19-WAT-04	57	33,5	-2,4	-17,5	2,0	1,21	2,71	0,97	8,70
YC19-WAT-05	2	32,6	-2,7	-19,4	2,6	1,14	2,60	0,99	17,05
YC19-WAT-05	17	33,3	-2,4	-16,8	2,7	1,03	2,50	1,05	10,20
YC19-WAT-05	33	33,5	-2,5	-17,3	3,0	1,07	2,56	1,04	9,12
YC19-WAT-06	2	32,7	-2,7	-19,0	2,8	1,19	2,59	0,95	19,18
YC19-WAT-06	6,3	32,7	-2,8	-19,4	2,7	1,30	2,55	0,85	13,94
YC19-WAT-06	13	33,2	-2,5	-17,4	2,9	1,15	2,72	1,03	16,31
YC19-WAT-07	2	32,5	-2,9	-19,6	3,9	1,11	2,55	1,00	13,90

Sample ID	**Depths [m]**	**Salinity [g/L]**	$\delta 18O$	δD	**D-excess**	**DOC [mg/L]**	**cDOM [254]**	**SUVA** $[m^2 gC^{1}]$	**SPM [mg/L]**
YC19-WAT-07	4,5	32,7	-2,8	-19,7	2,6	1,10	2,48	0,98	14,75
YC19-WAT-07	8	33,0	-2,5	-16,2	3,6	1,11	2,42	0,95	13,00
YC19-WAT-08	2	32,5	-2,9	-20,2	3,3	1,14	2,83	1,07	12,24
YC19-WAT-08	3,5	32,7	-2,9	-20,0	3,2	1,25	2,79	0,97	14,29
YC19-WAT-08	5,5	32,7	-2,7	-19,9	2,0	1,08	2,77	1,11	14,70
YC19-WAT-09	2	33,0	-2,7	-18,5	3,1	1,06	2,56	1,05	8,50
YC19-WAT-09	3,5	33,0	-2,8	-18,6	3,4	1,04	2,77	1,15	8,48
YC19-WAT-09	5,2	33,1	-2,8	-18,5	4,1	1,22	2,60	0,93	9,40
YC19-WAT-10	2	33,0	-2,8	-18,8	3,2	1,10	2,66	1,05	9,01
YC19-WAT-10	4,5	32,7	-2,9	-18,4	4,6	1,03	2,60	1,10	10,28
YC19-WAT-10	7	33,0	-2,8	-17,8	5,0	1,02	2,74	1,17	11,73
YC19-WAT-11	2	32,7	-2,9	-18,8	4,1	1,05	2,81	1,16	8,32
YC19-WAT-11	5	32,9	-2,8	-19,2	3,2	1,20	2,38	0,86	8,25
YC19-WAT-11	9,5	33,3	-2,8	-18,7	3,7	1,08	2,56	1,03	8,28
YC19-WAT-12	2	32,4	-2,9	-19,8	3,8	1,15	2,56	0,97	13,64
YC19-WAT-12	11,5	33,6	-2,5	-16,3	3,3	1,04	2,42	1,01	11,00
YC19-WAT-12	22,5	33,5	-2,7	-17,4	3,9	1,11	2,73	1,07	7,39